Master Thesis

Sound propagation through Australian forest land

With special regards to noise generated by wind turbines

Alexandra Gronberg

Division of Machine Design • Department of Design Sciences
Faculty of Engineering LTH • Lund University • 2015

LUND UNIVERSITY

GE

Sound propagation through Australian forest land

With special regards to noise generated by wind turbines

Alexandra Gronberg

Division of Machine Design • Department of Design Sciences

Faculty of Engineering LTH • Lund University • 2015

Division of Machine Design, Department of Design Sciences
Faculty of Engineering LTH, Lund University
P.O. Box 118
SE-221 00 Lund
Sweden

ISRN LUTMDN/TMKT XX/5XXX SE (you will receive this number from Cilla)

Preface

I would like to express warm thanks to the following people, without the help of which this thesis project would not have been possible.

David Lian, Peter Cowling & Greg Politakis at GE Power & Water Asia Pacific

Christophe Delaire at Marshall Day Acoustics

David Axup & Alf at Skyhigh Solutions

Markus Koschinsky, Roger Drobietz & Benoit Petitjean at GE Power & Water

Kerryn McTaggart at the Department of Environment and Primary Industries

Rachel Briggs at HVP Plantations

Helen Barker, Senior Ranger at Parks Victoria

Shane Bowen, who has assisted me during sound measurements

And my thesis counsellor Delphine Bard, Division of Engineering Acoustics, Lund University

Lund, January 2015

Alexandra Gronberg

Abstract

Wind has become an increasingly accepted source of renewable energy and is currently exploited worldwide. Wind energy has the advantage of close to zero greenhouse gas emissions, however one of the key concerns the public has about wind farm development is noise emissions. To address these local governments have introduced noise regulations, which limit noise levels at residential buildings located near wind farms. Failure to comply with these limits can lead to turbines being forced to be shut off, with associated loss of revenue. There is therefore a strong motivation to ensure compliance with current noise regulations. This is typically checked in the development stage via noise modelling. Australia has seen an escalation of wind energy projects in recent years and as a result many of the best sites for wind farm development have been utilised, thus forcing companies into more complex regions where noise modelling can be difficult. Such areas commonly comprise a complex topography or surrounding barriers, such as vegetation. The effects of forestry on sound propagation is difficult to predict, trees and shrubs generally have a dampening effect on noise, however the sound reduction rate often depends on the forest type and characteristics. Attenuation by vegetation is commonly divided into two parts; foliage as well as trunks and branches. The sound attenuation caused by foliage is largely dependent on the tree canopy and leaf characteristics, furthermore the attenuation rate generally increases with frequency. Sound attenuation by trunks and branches is also frequency dependent. Sound with wavelengths that are large in comparison with the tree diameter, i.e. low frequency sound, will be transmitted through tree trunks during interference, whereas sound within the high frequency range will scatter at the surface.

Many of the noise prediction models employed by wind farm developers have been designed for sound sources close to the ground surface. Although these models are often capable of incorporating the effects of forestry in noise predictions, they assume that the sound source is positioned below the tree canopy, which is generally not the case for wind turbines. A series of noise measurements have been conducted to study the difference in attenuation caused by vegetation for a sound source positioned below and above the canopy of an Australian forest. The measurements were performed at three separate occasions, during which a loudspeaker was employed to emit white noise which was recorded with three sound pressure level meters located at equal distance from each other. In total 21 noise measurements were recorded, three of which were performed with the loudspeaker elevated to 26 m, thus exceeding the average tree height. The results indicated that the attenuation by vegetation curve with frequency is comparable in both situations, with a low attenuation within the low frequency range and high attenuation with increasing frequency, which coincided with the expected behaviour of the curve. A portion of the sound energy was reflected at the forest edge when the sound source was positioned close to the ground surface, this sound level decline was however not observed when the source was elevated above the tree canopy.

A sound level calculation model was also constructed with the use of Microsoft Excel, which is an established software within engineering as well as other business sectors. The model comprises attenuation by geometrical divergence, atmospheric absorption, ground interaction and vegetation. It also incorporates the ambient weather conditions present at the particular site and enables implementation of noise restrictions. The particular wind turbine used at the site may be selected from a range provided by GE Power & Water or entered manually. Sound level prediction are made in 1/3 octaves for the frequency range 25 Hz to 20,000 Hz. The results are presented as the A-weighted noise level detected at the receiver point for mean wind speeds ranging from 3 m/s to 10 m/s.

Keywords:

Sound propagation, wind turbine noise, forestry, measurements, calculation model.

Sammanfattning

Vind har blivit en alltmer accepterad källa till förnyelsebar energi och utnyttjas idag världen över. Vindenergi har fördelen av nästintill inga utsläpp av växthusgaser, men allmänheten har i vissa uttryckt oro över det buller som associeras med vindkraftverk. For att möta detta missnöje har kommuner infört föreskrifter som begränsar ljudnivåerna vid bostadshus belägna i närheten av vindkraftverk. Underlåtelse av att uppfylla dessa krav kan leda till att vindturbiner tvingas stängas av, med tillhörande förlust av intäkter. Det finns därför en stark motivation för att säkerställa att gällande ljud restriktioner uppfylls. Detta kontrolleras normalt i utvecklingsstadiet med hjälp av ljudmodellering. Australien har sett en upptrappning av vindenergiprojekt under de senaste åren och många av de områden som anses lämpliga for utveckling av vindkraft har således blivit upptagna, vilket har tvingat företag in i regioner där ljudmodellering kan vara besvärligt. Sådana områden omfattar vanligtvis en oregelbunden topografi eller omgivande barriärer, såsom vegetation. Effekterna av ljudutbredning genom skogsområden är svåra att förutspå, träd och buskar har generellt en dämpande effekt på ljud, men reduktionsgraden beror ofta på vilken typ av skog som avses. Ljuddämpning på grund av växtlighet delas allmänt upp i två delar; bladverk samt stammar och grenar. Den ljuddämpning som orsakas av bladverk är till stor del beroende på trädkronans samt bladens dimensioner, dessutom ökar dämpningsgraden generellt med ljudets frekvens. Även ljuddämpning på grund av skogens stammar och grenar är beroende av frekvensen. Ljud med våglängder som är stora i jämförelse med trädets diameter, det vill säga lågfrekvent ljud, kommer transmitteras genom trädstammarna, medan ljud inom högfrekvensområdet kommer reflekteras vid ytan.

Många av de beräkningsmodeller som används inom vindkraftsindustrin har utformats för ljudkällor placerade nära markytan. Även om dessa modeller ofta har förmågan att integrera effekterna av skog på ljudutbredning vid beräkningar av vindkraftsbuller, antar dessa att ljudkällan är placerad nedanför trädkronorna, vilket ofta inte är fallet för vindkraftverk. En serie ljudmätningar har genomförts för att studera skillnaden i dämpning orsakad av vegetation för en ljudkälla placerad ovanför respektive nedanför trädkronorna i en australiensisk skog. Mätningarna utfördes vid tre skilda tillfallen och en högtalare användes for att avge vitt ljud, vilket spelades in

med tre ljudnivåmätare placerade på lika avstånd från varandra. Totalt registrerades 21 ljudmätningar, varav tre utfördes med högtalaren förhöjd till 26 m ovanför marken, vilket översteg den genomsnittliga trädhöjden. Resultaten klargjorde att den frekvensberoende ljuddämpning som uppstår på grund av vegetation är jämförbar i båda situationerna, med låg dämpning inom det låga frekvensområdet och hög ljuddämpning for höga frekvenser, vilket överensstämde med det förväntade beteendet av reduktionskurvan. En del av ljud energin reflekterades vid skogens rand då ljudkällan var placerad nära markytan, denna ljudnivå minskning observerades dock inte i fallet då källan höjdes ovanför trädkronorna.

En beräkningsmodell konstruerades även med hjälp av Microsoft Excel, vilket är en etablerad programvara inom både ingenjörsbranschen och andra verksamhetssektorer. Modellen innefattar dämpning genom geometrisk divergens, atmosfärisk absorption, markeffekt samt vegetation. Den inbegriper även väderförhållandena i området samt möjliggör tillämpning av ljudrestriktioner. De vindkraftverk som används i området kan väljas från ett antal modeller tillhandahållna ifrån GE Power & Water eller införas manuellt. Ljudnivån vid en mottagarpunkt beräknas i 1/3 oktaver för frekvensområdet 25 Hz till 20 000 Hz. Resultatet presenteras som den upplevda A-viktade ljudnivån hos mottagaren för gensnittliga vindhastigheter från 3 m/s till 10 m/s.

Table of Contents

1 Introduction 1

1.1 Background 1

1.2 Objectives...2

1.3 Method 3

1.3.1 Literature study...3

1.3.2 Sound measurements...3

1.3.3 Interpretation of data 3

1.3.4 Formulation of a model 3

1.4 Limitations 4

2 Fundamentals in sound propagation 5

2.1 General theory 5

2.1.1 Frequency, wavelength and speed of sound..6

2.1.2 Sound pressure level..7

2.1.3 Sound power and intensity 9

2.1.4 Specific impedance 10

2.1.5 Sound absorption, reflection and transmission....................................10

2.1.6 Sound refraction, scattering and attenuation..12

2.1.7 Tonality 13

2.2 Indoor sound propagation 14

3 Chapter heading..14

3.1 Sound source 15

3.1.1 Wind turbine noise characteristics 16

3.1.2 Directivity...18

3.1.3 Noise regulations in Australia 19

3.2 Speed of sound 21

3.2.1 Wind speed...21

3.2.2 Atmospheric temperature 24

3.2.3 Refraction due to wind and temperature 26
3.3 Sound attenuation 30
3.3.1 Atmospheric absorption 31
3.3.2 Ground attenuation 34
3.3.3 Atmospheric turbulence 42
3.3.4 Effects of topography 45
3.4 Sound propagation in forest areas 47
3.4.1 Australian forest configuration 47
3.4.2 Wind speed in forests 49
3.4.3 Atmospheric temperature in forests 55
3.4.4 Ground attenuation in forests 56
3.4.5 Attenuation caused by vegetation 63
4 Sound measurements 69
4.1 Site description 69
4.2 Hypothesis 72
4.3 Measurements 74
4.3.1 Methodology 74
4.3.2 Treatment of data 78
4.3.3 Results 84
4.3.4 Combined results 93
5 Sound propagation model 97
5.1 Current prediction models 97
5.1.1 ISO 9613-2 Model 97
5.1.2 CONCAWE Model 103
5.1.3 Nord 2000 Model 109
5.2 Calculation model 119
5.2.1 Calculations 119
5.2.2 Interaction design 126
6 Discussion 129
7 References 133
8 Abbreviations 141
Appendix A: A- and C-filters 147
Appendix B: Surface roughness length 149
Appendix C: Atmospheric absorption coefficient 151

Appendix D: Effective flow resistivity **153**
Appendix E: Ground attenuation derivation **155**
Appendix F: Effective flow resistivity in forests **157**
F.1 Granular surfaces 157
F.2 Organic root layers 158
F.3 Low flow resistivity outdoor surfaces 158
F.4 Grassland 159
Appendix G: Fresnel function derivation **161**
Appendix H: Noise measurement results **163**
Appendix I: Meteorological data **173**
Appendix J: Sound attenuation factors **177**
Appendix K: ISO 9613-2 ground attenuation **189**
Appendix L: Nord2000 scattering zones **191**
Appendix M: Distribution of labour **193**
M.1 Distribution of work between final thesis students 193
M.2 Assumed timetable and actual outcomes 193
Appendix N: Model interface **196**

1 Introduction

This chapter provides some contextual information into the objectives of the thesis presented in this report. Furthermore, the basic steps undertaken during the project are described briefly as well as the limitations encountered.

1.1 Background

Due to development escalations in recent years, wind power is currently the fastest growing energy source in Australia with an annual increase of almost 27.3 % between 2000 and 2010. Although Australia represents only 1 % of the globally installed wind power capacity, sanctioning of the Renewable Energy Target (RET) scheme in 2009 has allowed for the expansion of wind farms to increase further. During 2013 six wind farm project were commenced, which corresponds to 655 MW wind energy capacity, an 80 % increase compared to the previous year. The RET scheme was implemented to ensure 20 % of Australian electricity demand will be met by renewable energy sources by 2020. The target is however currently under review [5] [30].

Wind power is generated by converting the kinetic energy contained within the wind into electrical power, by the use of wind turbines. Although there are numerous advantages of exploiting the power in the wind as a source of energy, such as a decreased dependence on fossil fuels and greenhouse gas emissions, the development of wind farms has encountered some criticism from the public. A key issue with generating wind power is the noise emissions it entails. Current scientific evidence has not been able to confirm a definite relationship between wind turbine noise and adverse health effects, however research suggests that the generated noise may cause annoyance for surrounding residents [17]. Annoyance due to noise exposure, although being an acknowledged health issue, is not viewed as an adverse health effect and is closely related to the individual perception of sound. The sensitivity to noise varies between individuals and continued exposure to noise may consequently decrease the noise sensitivity of some individuals, hence lessening the annoyance of the sound. However, it may also have the reversed effect and annoyance could increase the sensitivity of noise. In a very few cases, this has been found to cause sleep disturbance [25] [26] [18].

To decrease the levels of annoyance experienced due to wind turbine noise emissions as well as abide with the local noise limits set by government regulations, developers employ models to predict the sound levels detected at various receiver points, prior to commencing the construction of wind farms. The precision of such noise prediction models is largely dependent on the complexity of the particular site. For wind turbines positioned on levelled ground with no surrounding obstacles, which may redirect the noise propagation path, the predicted sound levels will be similar to those measured after the completion of the wind farm. However, at sites with a complex topography and surrounding barriers, such as vegetation, or irregular meteorological conditions, the calculated values are generally less precise. Due to the recent increase in wind energy projects, many of the sites suitable for wind farm developments have become unavailable. As a result, developing companies are forced into regions that may meet many of the key siting objectives, such as reliable wind resources and access to transmission lines, but at which noise emissions may be difficult to control. An example is sites that includes forestry. Australia has approximately 125 million hectares of various forest types, which covers 16 % of the land area. In consequence, Australian wind farm projects are increasingly being commenced in areas that comprise some vegetation. The behaviour of noise propagating through forest areas varies from that over open ground. Trees and shrubs generally have a dampening effect on noise, however the sound reduction rate commonly depends on the forest type and characteristics. Furthermore, many of the noise prediction models employed by wind farm developers have been designed for sound sources close to the ground surface. Although these models are often capable of incorporating the effects of forestry in noise predictions, they assume that the sound source is positioned below the tree canopy, which may make them unsuitable for wind turbines [4] [74].

1.2 Objectives

The objective of this master thesis is to investigate the effect a native Australian forest has on the propagation of sound. The thesis will explore eventual differences in sound propagation through a forest with the source positioned close to the ground surface and elevated above the forest canopy. The aim is to better understand the behaviour of sound in Australian forests, in order for prediction to be made more accurately.

In addition, the objective is to design a prediction model, which is capable of calculating the sound levels detected at any receiver points in the vicinity of a wind farm in Australia. The model will incorporate the effects of forests previously examined.

1.3 Method

The thesis was conducted according to the following five steps. Each part was not chronologically succeeded by the next, but often several steps were managed simultaneously. For instance, large parts of the literature study was performed alongside the formulation of the model, as this simplified the process. A brief description of each step may be found below.

1.3.1 Literature study

A thorough literature study was initially performed. The study included fundamental definitions in acoustics, sound propagation in indoor and outdoor conditions as well as an explanation of the influencing variables. Furthermore, current research into the effects of forestry on sound propagation was reviewed and some calculation models commonly employed for wind turbine noise predictions were examined.

1.3.2 Sound measurements

Noise measurements were performed at three separate occasions, two of which were conducted at ground level and one using an elevated sound source. The measurements were performed in the Wombat State forest, in the north western part of Victoria, Australia. Since there were no wind turbines installed at the site, a loudspeaker was employed to generate white noise. Between three and four sound pressure level meters were utilized to measure the emitted noise at various distances into the forest.

1.3.3 Interpretation of data

The measured sound was treated with dBTrait, a software developed for handling of environmental noise. With the use of dBTrait, the equivalent sound pressure level for the particular measuring time period could be obtained and corrected for background noise. The sound level reduction rate could thus be studied and compared with previously conducted research.

1.3.4 Formulation of a model

With the use of information obtained in the literature study as well as the results from the sound measurements, a calculation model was developed. The aim of the model was not merely to provide accurate noise predictions, but also to offer a satisfactory user experience. Considerations were thus taken into creating a model interface that incorporates several interaction design features. Comparisons were also made with the interface of existing prediction models. However, the model was developed using the software Excel, which limited the design of the interface and thus the usability of the model to some extent.

1.4 Limitations

The work presented in this report is a study of the behaviour of sound during propagation through a native Australian forest. Many miscellaneous factors that influence the propagation of sound have also been taken into account, with the exception of topography. The effects of topography on sound propagation is difficult to predict and implementing it would thus decrease the accuracy and reliability of the study. The noise measurements that were performed in the Wombat State forest were conducted over reasonably flat grounds and the effects of complex terrain could thus be excluded from the results. Although not incorporated in the calculation model, it important to acknowledge the dampening or amplifying effects of hills and valleys when analysing the results.

Due to the strict time frame of this work as well as restricted access to equipment, noise measurements could not be performed to the extended period of time recommended by standard IEC 61400-11. Measurements are generally conducted over a period of several weeks or months, in order to include a wide variety of wind speeds, temperatures and other meteorological conditions. However, this was not possible with the time frame that was provided.

A major limiting factor in this master thesis was the absence of wind turbines during the noise measurements. White noise was instead generated by a loudspeaker, which was elevated to a maximum height of 26 m with the use of a boom lift. Although not corresponding to the height of a wind turbine hub, this exceeded the average tree height thus allowing for measurements to be performed with a sound source elevated above the forest canopy.

2 Fundamentals in sound propagation

As an introduction to the topic of sound propagation, this chapter presents a brief description of some fundamental definitions within acoustics.

2.1 General theory

Sound is generated by pressure fluctuations caused by the vibration or turbulence of a medium. The oscillations of pressure creates sound waves, which propagates through the specific medium. The transmission of sound waves causes a displacement of the medium particles from an equilibrium state. In air sound pressure varies above and below the ambient atmospheric pressure level, causing areas of particle compressions and rarefactions respectively. Such particle displacements creates longitudinal waves within the medium. Sound propagation through solid materials also generates transverse sound waves, causing the medium particles to deviate in a direction perpendicular to the path of transmission. Sound waves may be illustrated as a cosine curve, as shown in figure 2.1 [31].

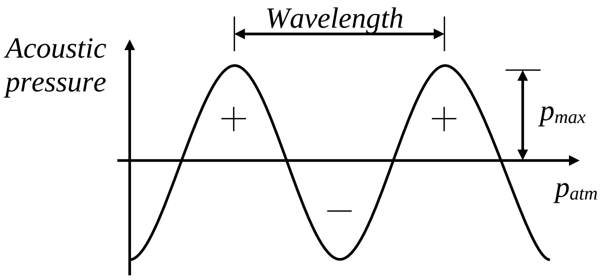

Figure 2.1. Representation of a sound wave in air, pressure variations above and below atmospheric pressure [31].

The sound wave presented in figure 2.1 is characterized as plane, i.e. propagating in a straight line. The sound pressure variations of a one-dimensional plane wave that is transmitted in a positive direction may be expressed with the complex relationship below [8] [60].

$$p(x,t) = \hat{p}\cos(kx - \omega t) = \mathrm{Re}\left[p_c(x)e^{-i\omega t}\right] \quad (2.1)$$

Where $p_c(x) = \hat{p}e^{ikx}$

p_c	the complex pressure amplitude [Pa]
p	the sound pressure dependent on time and position [Pa]
$\hat{p}$	the pressure amplitude of the sound wave [Pa]
x	a given location on the x-axis [m]
t	a given point in time [s]

The *complex pressure amplitude* is a function of the sound pressure with position on the x-axis, i.e. the propagation distance from the source. Equation (2.1) demonstrates the sound pressure dependence on the time and position, during calculations the real part of the complex relationship is generally used.

As the fluctuations in sound pressure causes a displacement of fluid particles, the speed by which the particles are transferred is related to the pressure variations. At maximum sound pressure amplitude, the particle velocity will also obtain a peak value. Consequently, the particle velocity variations for a one-dimensional plane wave is expressed with an equation similar to that of sound pressure [8] [60].

$$v(x,t) = \hat{v}\cos(kx - \omega t) = Re\left[v_c(x)e^{-i\omega t}\right] \quad (2.2)$$

Where $v_c(x) = \hat{v}e^{ikx}$

v_c	the complex velocity amplitude [m/s]
v	the particle velocity dependent on time and position [m/s]

2.1.1 Frequency, wavelength and speed of sound

Sound is perceptible to humans when the generated sound waves have frequencies within the audible range, hence between 20 Hz and 20 kHz [39]. The audible range is generally divided into frequency segments, known as octave and one-third octave bands.

Frequency is defined as the number of oscillations a sound wave performs each second. For a pure tone, the sound waves have a constant frequency and an amplitude that varies periodically. This rarely occurs in nature, but may be fabricated through an artificial source such as loudspeaker. A sound wave with constant frequency will also have a constant wavelength, assuming fixed ambient conditions. *Wavelength* is the distance the wave travels in one cycle. For noise, however, frequency and amplitude varies irregularly with distance, hence also causing the wavelength to fluctuate. Such irregularities are often experienced as unpleasant. The relationship between frequency and wavelength is expressed in equation (2.3) [39].

$$\lambda = \frac{c}{f} = \frac{2\pi c}{\omega} = \frac{2\pi}{k} \tag{2.3}$$

Where λ the wavelength [m]
c the speed of sound [m/s]
f the frequency [Hz]
ω $= 2\pi f$, the angular frequency [rad/s]
k $= \omega/c$, the wave number [rad/m]

Sound propagates with a specific speed, depending on the medium and ambient conditions of transmission. The speed of sound through a gas is determined using the following equation [39] [31].

$$c = \sqrt{K_S/\rho} = \sqrt{\gamma p_o/\rho} = \sqrt{\gamma R T_K/M} \tag{2.4}$$

Where ρ the equilibrium density of the medium [kg/m^3]
γ the adiabatic index (= 1.402 for air) [-]
p_o the static pressure [Pa]
T_K the absolute temperature [K]
M the molecular weight (= 0.029 for air) [kg/mole]
R = 8.314, the universal gas constant [J/K]
K_S $= \gamma p_o$, the adiabatic bulk modulus [Pa]

2.1.2 Sound pressure level

The audibility of sound also requires a sufficient level of sound pressure deviation, as the pressure amplitude of sound waves determines the loudness of noise. The range of audible sound varies between 20×10^{-6} Pa to 60 Pa, above which human ears generally experience pain [31]. Due to the wide perceptible range, sound pressure is measured on a logarithmic scale in unit decibel. The conversion is performed with equation (2.5) [8].

$$L_p = 10 \log\left(\frac{\tilde{p}^2}{p_{ref}^2}\right) = 20 \log\left(\frac{\tilde{p}}{p_{ref}}\right) \tag{2.5}$$

Where L_p the sound pressure level [dB]
p_{ref} the reference sound pressure (= 2×10^{-5} for air) [Pa]
$\tilde{p}$ $= \hat{p}/\sqrt{2}$, the effective (rms) sound pressure [Pa]

Doubling the sound pressure would hence result in a 6 dB increase of sound pressure level.

The noise detected at a receiver point is often the result of many sound emitting sources. The combined sound pressure level from several independent sources is calculated with the following equation [8].

$$L_{p,tot} = 10 \log \left(\sum_{n=1}^{N} 10^{L_{p,n}/10} \right) \tag{2.6}$$

The sensitivity of the human ear varies with frequency. For instance, sound pressure levels at very low frequencies are generally perceived as quieter than actuality, whereas sound levels at mid-range frequencies are considered amplified. To account for the perceived loudness, sound pressure levels are generally weighted with A-, B-, C- or D-filters, of which A- and C-filters are most common. In case of infrasound explained in section 3.1.1, a special G-filter is commonly used, which emphasizes the sound within the infrasound frequency range and excludes any frequency components above this limit. Sound levels are denoted L_Z if no weighting is applied [39]. Sound pressure levels may be transformed into filtered octave and one-third octave band values with equation (2.7) below. Values for A- and C-filters in 1/3 octave band may be found in appendix A [8].

$$L_{Weighted} = 10\log \left(\sum 10^{(L_n + Weighting)/10} \right) \tag{2.7}$$

In order to obtain reliable results, sound is commonly measured over a long period of time. The *equivalent sound pressure level* is the average sound level of a specific time period and thus expressed as a single value. It is calculated with equation (2.8) [39].

$$L_{eq,T} = 10 \log \left(\sum_i \frac{t_i}{T} 10^{L_i/10} \right) \tag{2.8}$$

Where $L_{eq,T}$ the equivalent sound pressure level [dB]
L_i the sound pressure level of time interval i [dB]
T the total time period [s]
t_i the time period i [s]

2.1.3 Sound power and intensity

The vibration or turbulence of a medium that generates sound also causes a conversion of energy into sound energy. The *sound power* is the rate of the sound energy transformation, thus a measurement of the energy that is transmitted by the sound wave per unit time.

The energy contained within the sound wave decreases with distance from the source. *Sound intensity* is the power transmitted by the sound wave per unit area. It is hence related to the geometrical shape of the sound propagation as well as the distance from the sound source to the receiver. Most sources emit sound uniformly from a point, thus generating a spherically shaped area of propagation. The relationship between sound power and intensity for such sources is presented below [31].

$$W = 4\pi r^2 I \tag{2.9}$$

Where W the sound power [W]
I the sound intensity [W/m^2]
r the radial distance from sound source to receiver [m]

As with sound pressure, sound power and intensity is generally measured logarithmically. The transformation is performed with equations (2.10) and (2.11) [8].

$$L_W = 10 \log\left(\frac{W}{W_{ref}}\right) \tag{2.10}$$

Where L_W the sound power level [dB]
W_{ref} $=10^{-12}$, the reference power [W]

$$L_I = 10 \log\left(\frac{I}{I_{ref}}\right) \tag{2.11}$$

Where L_I the sound intensity level [dB]
I_{ref} $=10^{-12}$, the reference intensity [W/m^2]

2.1.4 Specific impedance

The *specific sound impedance* is defined as the ratio of the sound pressure and particle velocity, i.e. the speed that medium particles possesses during the transmission of a sound wave. As previously mentioned, both the sound pressure and particle velocity are expressed as complex numbers. However for a one-dimensional wave, the variables are in phase and thus independent of the propagation distance. The definition may thus be derived to the following equation [44] [75].

$$Z_s = \frac{\hat{p}}{\hat{v}} = c\rho \tag{2.12}$$

Where Z_s the specific impedance [Pa ·m/s]

Specific impedance may be described as a resistance to movement, a medium with high impedance require high sound pressure in order to achieve a particular particle velocity.
Equation (2.12) is primarily employed during sound propagation through a fluid medium.

2.1.5 Sound absorption, reflection and transmission

When a sound wave intersects normal to the surface of a separate medium, some of the sound energy within the wave will be *absorbed*. The fraction of absorbed energy is determined by the absorption coefficient α of the medium.

$$\alpha = I_a/I_i \qquad 0 \le \alpha \le 1 \tag{2.13}$$

Where I_a the absorbed sound intensity [W/m^2]
I_i the incident sound intensity [W/m^2]

The sound energy that is absorbed by the intersecting medium is partially transformed into heat, while the remaining part is *transmitted* through the medium. The sound energy that is not absorbed will be *reflected* by the intersected medium.
The reflection and transmission coefficients, ρ and τ respectively, of the incident sound wave is determined by the specific sound impedance of the exiting and entering medium. A sound wave that is transmitted through a medium with specific impedance $Z_1 = \rho_1 c_1$ and incidents with a medium with specific impedance $Z_2 = \rho_2 c_2$ behave according to the following equations.

$$\rho = \frac{|\rho_2 c_2 - \rho_1 c_1|^2}{(\rho_2 c_2 + \rho_1 c_1)^2} = \frac{|Z_2 - Z_1|^2}{(Z_2 + Z_1)^2} \tag{2.14}$$

$$\tau = \frac{4\rho_2 c_2 \times \rho_1 c_1}{(\rho_2 c_2 + \rho_1 c_1)^2} = \frac{4Z_2 Z_1}{(Z_2 + Z_1)^2} \tag{2.15}$$

Equation (2.15) assumes that no energy is converted into heat, i.e. $\tau = \alpha$. Consequently, the following relationship applies [44].

$$\tau + \rho = 1$$

Reflection occurs solely for sound waves that incidents normal to the surface of the intersected medium. However, the behaviour of the reflected sound wave depends on the medium surface conditions. Reflection is thus classified as either specular or diffuse.

Specular reflection occurs for sound that incidents with large uniform surfaces, resulting in a reflected sound wave that propagates in a singular direction. In contrast, sound waves that intersect with a soft or porous material will cause a diffuse reflection, hence sound waves are reflected in different directions due to the uneven surface of such materials [27].

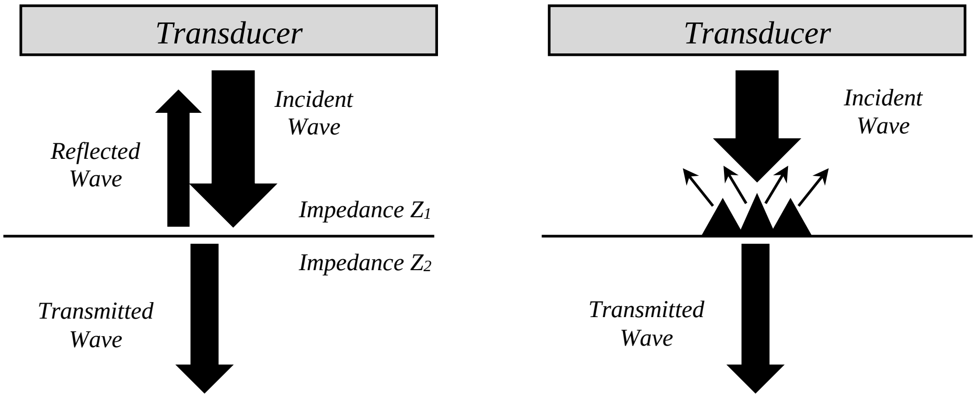

Figure 2.2. Specular vs. Diffuse Reflection [27].

2.1.6 Sound refraction, scattering and attenuation

Refraction is defined as the reflection and transmission that a sound wave will experience when colliding with a tilted surface. The transmitted sound wave behaves differently depending on whether the medium is a fluid or a solid, as is illustrated in figure (2.3).

During refraction, the properties of the intersected medium will cause the transmitted wave to bend towards regions where the speed of sound is low. For example, the speed of sound is higher in water than in air which causes the transmitted wave to bend away from the normal when moving from one to the other, respectively. In consequence the transmitted angle will be large, which is the case in figure 2.3 (a).

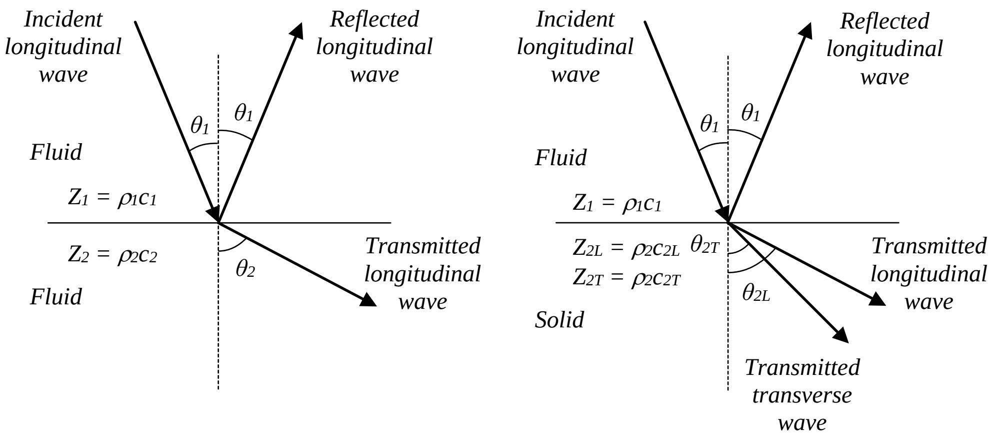

Figure 2.3. Reflection and refraction at the boundary (a) between two fluids and (b) between a fluid and a solid medium. The incident and transmitted angle as well as the transmitted angle are denoted θ_1 and θ_2, respectively. The speed of sound of the exiting and entering medium is represented by c_1 and c_2, respectively. Based on [43].

A sound wave that collides with a medium of small dimensions will experience *scattering* and hence be reflected in various directions. Scattering generally occurs for sound with a wavelength that is longer than the incident medium [27].

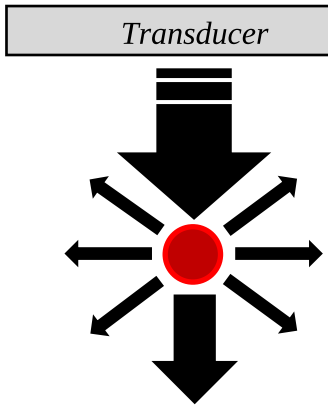

Figure 2.4. Scattering [27].

Attenuation is the intensity decrease that a sound wave experience when passing through a medium. It is dependent on the absorbing properties of the medium as well as the reflection or scattering at the medium surface. The attenuation coefficient is a measurement of the attenuating effect with distance, it is influenced by the properties of the exiting and entering medium as well as the frequency of the specific sound wave [27].

2.1.7 Tonality

As mentioned in section 2.1.1, sole pure tones are rarely generated naturally. However, they often occur as a part of noise and are thus distinguished as dominant frequencies within the noise. This is known as *tonality* and may be detected as a peak in sound pressure level at a specific frequency.
The presence of tonality is generally perceived as disturbing, both for low frequency and high frequency tones [25] [26].

2.2 Indoor sound propagation

Predicting the propagation of sound in an enclosed environment such as a room, is much facilitated by the virtually invariable ambient conditions. Indoors, there are no wind or weather fluctuations and a close to constant temperature profile, hence no parameters that influence the speed or direction of sound. Consequently sound is assumed to spread evenly indoors.
As mentioned in section 2.1.3, sound is often emitted uniformly from a point source. The sound intensity at variable distance from such as source was expressed in equation (2.9), but sound intensity may also be expressed in terms of sound pressure and impedance, resulting in the following relationship.

$$I = \frac{\tilde{p}^2}{\rho c} = \frac{W}{4\pi r^2}$$

By employing equations (2.10) and (2.11) the relationship above can be further developed and expressed in terms of sound pressure level and power level [42].

$$\begin{aligned} L_p &= 10\log\left(\frac{\tilde{p}^{\,2}}{{p_{ref}}^2}\right) \\ &= 10\log\left(\frac{W\rho c}{{p_{ref}}^2 \times 4\pi r^2}\right) \\ &= 10\log W - 20\log r + 10\log\left(\frac{\rho c}{{p_{ref}}^2 \times 4\pi}\right) \\ &= L_W - 20\log r + 10\log\left(\frac{W_{ref} \times \rho c}{{p_{ref}}^2 \times 4\pi}\right) \\ &= L_W - 20\log r + 10\log(2 \times 10^{-4} \times \rho c) \end{aligned} \tag{2.16}$$

The two latter terms are known as the *geometrical divergence*, i.e. the sound attenuation that occur due to the geometrical shape of the sound propagation. For standard ambient conditions (15^{o}C and 101.325 kPa) equation (2.16) may be simplified to that shown below.

$$L_p = L_W - 20\log r - 11 \tag{2.17}$$

The sound attenuation that occur with increasing distance from source will thus behave logarithmically, with a rapid sound pressure level decrease close to the source and smaller variations ensuing at great distances.

3 Outdoor sound propagation

Sound propagation in outdoor conditions is generally more difficult to predict than that in an enclosed environment. The propagation is affected by numerous variables including wind speed, wind direction and other meteorological conditions that influence the speed of sound, atmospheric absorption as well as various causes for sound attenuation, such as ground interaction and surrounding obstructions (e.g. buildings or vegetation). This chapter will explain the impact of these factors on sound propagation for open ground conditions as well as in forested areas.

3.1 Sound source

The sound that is generated by wind turbines is a result of two combined noise sources; aerodynamic and mechanical noise. *Aerodynamic noise* is created by the rotational movement of the turbine blades. The intensity of the noise is determined by the shape and speed of the blades as well as the air turbulence. Aerodynamic noise possess similar characteristics to the sound of the wind and hence may be masked by the natural background noise at high wind speeds. It is audible within a wide frequency spectrum, ranging from 63 Hz to 4,000 Hz.
Mechanical noise originates from the motion of mechanical and electrical parts inside the turbine. The most common noise emitting components are the gearbox, generator, yaw drives and auxiliary equipment such as hydraulics [58]. Mechanical noise is generally less prominent than aerodynamic, however it is often perceived as more aggravating due to the distinctive characteristics of the noise. Modern wind turbines rarely generate mechanical noise and if it occurs the cause is usually a construction error [15].

Although the location of each sound source within a wind turbine may vary, the combined noise is generally regarded a single point source deriving from the centre of the hub. Equation (2.16) from section 2.2, which is used for predicting the attenuating effect of geometrical divergence, is thus also applicable for wind turbine sound sources [76]. It is however advisable that this method is employed primarily at distances greater than 100 m, as the uniform shape of propagation emerges first at such distances from the sound source [15].

3.1.1 Wind turbine noise characteristics

Depending on the origin of the various noise sources within a wind turbine, different types of sound is emitted with varying impact on humans. The combined turbine noise may thus be divided into four categories; tonal, broadband, low frequency and infrasound as well as impulsive sound.

Tonal sound was defined in section 2.1.7 as noise containing pure tones, i.e. a distinct peak in the sound pressure level at a specific frequency. It is generally audible in mechanical noise and is thus primarily caused by components such as meshing gears, but also by unstable wind flow over holes and slits in the turbine design or by a blunt trailing edge. Tonal sound is often experienced as unpleasant, since pure tones are clearly detectable even in the presence of other noise and can thus not be masked by the natural background noise [15] [65].

Wind turbines predominantly emit sound pressure levels within the 200 to 1,000 Hz range. Frequencies above 100 Hz is characterized as *broadband* sound and is generated by the interaction of turbulent wind and the trailing edge of the turbine blades, it is hence classified as aerodynamic noise. Broadband noise generally increases at higher wind speeds as this causes an acceleration of the rotational velocity [65] [25] [26].

Sound of frequencies within the range of 20 to 100 Hz is characterized as *low frequency*, while frequencies below 20 Hz are associated with *infrasound*. Low frequency sound is partly generated by the wind turbine blades interacting with the tower wake, a phenomenon that occur in downwind machines, i.e. in wind turbines for which the rotor is positioned on the shaded side of the tower. However, low frequency sound may also be caused by aerodynamic loading of the wind turbine blades, known as *loading noise*. Loading noise is primarily a result of unsteady aerodynamic loading of the blades during rotation, which is caused by mean shear variations in the atmospheric boundary layer due to the wind and temperature gradients explained in section 3.2.1 and 3.2.2 or by flow irregularities due to turbulence [28].

The levels of low frequency sound generated by wind turbines are generally low, however the sound is yet undesirable since it is proven to cause greater annoyance than broadband noise. Sound audibility is dependent on the relationship between frequency and pressure level, which follows the curve as shown in figure 3.1.

The sound pressure level within the low frequency range must thus be relatively high in order to exceed the limit of audibility, whereas mid-range frequencies are perceptible at much lower levels. However, once low frequency sound becomes perceptible to human ears, a small sound pressure increase will significantly amplify the loudness of the sound and may rapidly become painful to the auditor [25].

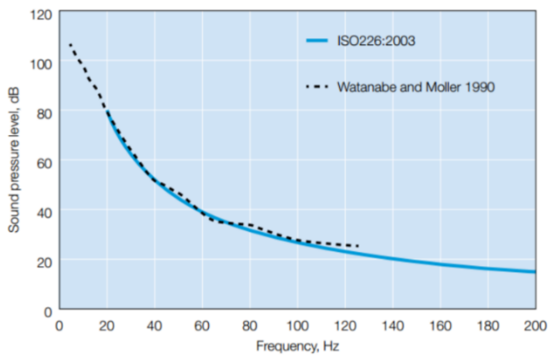

Figure 3.1. The hearing threshold based on international standard ISO226:2003 and research by Watanabe and Moller. Levels above the line are audible for most people [25].

Sound emitted by a point source will decrease with distance due to the spherical shape of the propagation. However, additional sound level reductions will also occur due to a variety of absorbing and reflecting elements in the ambient environment, including atmospheric absorption and ground effect explained in sections 3.3.1 and 3.3.2. Low frequency sound is less susceptible to such influencing factors, thus causing it to decrease at a lower rate than broadband sound. In consequence, the low frequency content of noise emitted by wind turbines is higher at some distance than at the sound source [25] [28].

As may be seen in figure 3.1 above, infrasound is perceptible to the human ear only at very high pressure levels. The sound is assessed by applying a G-filter, which emphasises the sound below 20 Hz, making infrasound audible at 85 dBG according to international standard. Research has however found wind turbine to emit infrasound within the range 50 to 70 dBG, which is significantly below the audibility threshold [25].

Impulsive sound is often described as a periodically occurring “thumping” noise. It is primarily caused by the interaction of rotating blades with turbulent air flow that is created around the tower of downwind turbines. However impulsive sound have also been known to occur in modern upwind machines for which the reasons are currently uncertain [65].

3.1.2 Directivity

The directivity of a sound source refers to the irregularities that may occur within the generated sound field, which is the result of an inhomogeneous radiation pattern. The sound pressure levels detected at a fixed distance from the source will consequently vary with angular position. Such sound pressure variations are often represented in a directivity pattern, the appearance of which is dependent on the type of source generating the sound [59].

As previously mentioned, wind turbines are often considered single point sources, generating an omnidirectional sound field that originates from the hub centre. Such sound sources are known as *monopole* and are characterized with a circular directivity pattern. In reality however, the directivity pattern of a wind turbine will correspond to that of a *dipole* sound source, thus resembling a horizontal eight as shown in figure 3.2 below [71].

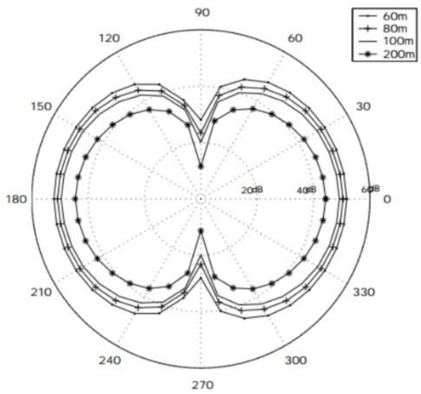

Figure 3.2. Directivity pattern of a wind turbine, the lines indicates various distance from the source [71].

The sound pressure levels identified along the rotor plane are considerably lower than those detected at the corresponding angular position of a monopole sound source. However in contrast, the levels identified in front and the back of the wind turbine are higher than compared to a monopole source.

For many sound sources, the error that occur due to deviations from the uniform sound field of a monopole source is corrected by adding a directivity index to the geometrical divergence. However, the sound power levels of wind turbines are generally measured downwind and predicted for downwind conditions and as a result wind turbine noise predictions do not require a directivity correction [37].

3.1.3 Noise regulations in Australia

Identifying sites appropriate for wind turbine installation is a vital part in the initial development stages of a wind farm. The main purpose of siting is to locate areas at which the net revenue can be maximized while undesirable aspects, such as noise emission and visual impact on the neighbouring community, is minimized. Sites suitable for wind energy extraction must meet a variety of objectives, including high average wind speeds with minimum turbulence, good road access, land availability as well as proximity to an electricity grid of adequate voltage. Such sites are however commonly positioned in areas of low ambient noise levels and the construction of a wind farm could thus have a negative impact on the tranquillity in such regions, possibly causing annoyance for surrounding residents [46].

Numerous standards have been developed to assess the noise generated by wind turbines at any relevant receiver points, in order to avoid irritation, sleep deprivation and various health issues related to the emitted sound. In Australia, the most commonly implemented guidelines are the Australian Standard AS 4959-2010 and the New Zealand Standard NZS 6808:2010. Both guidelines provide methodologies for measuring background and wind turbine noise as well as assessing the measured values with predicted noise levels. A unique characteristic of wind turbine noise is the increase in generated levels with escalating wind speeds, meaning the emitted sound is higher in strong winds than during calm ambient conditions. Though additionally, the background noise also increase in high winds. Generally the Relevant Regulatory Authority has established a minimum noise level, which should not be exceeded by a wind turbine or farm. However, due to the link between generated sound and wind speed, the specified limit may well be exceed by the background noise alone. The AS 4959-2010 recognizes the issue by proposing a noise limit which is equal to the minimum level during calm wind conditions, but equal to the background noise plus a specified amount at high wind speeds. The standard does however not specify the value to be supplemented [19].

The noise limit recommended in the NZS 6808:2010 resemble that previously proposed, however in contrast to the Australian standard it details the precise values to be adapted. Furthermore, the standard recognizes the increased noise sensitivity of high amenity areas by reducing the specified amount is such regions. The noise limits proposed by the New Zealand standard are summarized in table 3.1 below [50].

<table>
<tr><th>Background sound level
[dB]</th><th>Noise limit
$L_{I0\ (10\ min)}$ [dB]</th><th>High amenity noise limit
$L_{I0\ (10\ min)}$ [dB]</th></tr>
<tr><td>> 35</td><td>Background + 5</td><td rowspan="2">Background + 5</td></tr>
<tr><td>30 – 35</td><td rowspan="2">40</td></tr>
<tr><td>< 35</td><td>35</td></tr>
</table>

Table 3.1. New Zealand standard noise limits [50].

3.2 Speed of sound

The speed of sound is affected by several external factors that are dependent on the ambient environment of the emitted sound. Outdoors, the main influencing aspects are the wind speed and direction as well as the atmospheric temperature at the site. These factors will furthermore vary with height above ground as well as with time of day and year. For instance, wind speed increases with height above ground whereas temperature typically drop at higher altitudes. Temperatures are naturally lower during the winter season, however wind velocities are often higher during this period.

3.2.1 Wind speed

The influence of wind on sound propagation is significant, particularly for the noise emitted by wind turbines as these are generally positioned at sites with high mean wind speeds. Sound propagation in the presence of wind affects the speed of sound, which is supplemented with the wind speed vector in the direction of the propagation. The combination is known as the *effective speed of sound* and may be expressed according to equation (3.1) below [67] [32].

$$c_{eff}(\mathrm{z}) = \mathrm{c} + U(z)_{dir} \tag{3.1}$$

Where $c(z)_{eff}$ the effective speed of sound at height z [m/s]
$U(z)_{dir}$ the wind speed in the direction of propagation w. height [m/s]

The wind speed component in the direction of the sound propagation is dependent on the position of the sound source and receiver as well as the wind direction, according to figure (3.3). It may thus be calculated with equation (3.2).

$$U(z)_{dir} = U(z)\cos(\theta_R - \theta_W + \pi) \tag{3.2}$$

Where $U(z)$ the wind speed with height [m/s]
θ_W the direction of the wind [rad]
θ_R the direction of the sound receiver [rad]

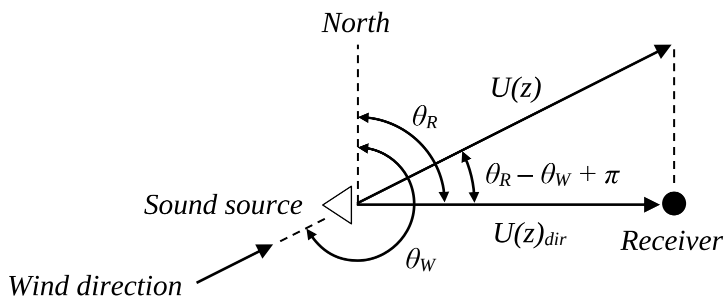

Figure 3.3. Illustration of the wind speed components in relation to sound source and receiver viewed from above, based on [66].

As previously mentioned, wind speed varies both with height above ground and with time. Changes may occur annually or over periods of seconds, however the wind conditions of a particular site are generally predicted by using monthly averaged values. An example is illustrated in diagram 3.1, presenting the averaged wind speeds at 10 m height in Melbourne.
Clear seasonal variations may be observed, high winds occurring in September and October while lower velocities appear in April and May. Furthermore, wind speeds differ considerably between 9am and 3 pm, the greatest difference occurring in February. The data presented in diagram 3.1 is based on measurements performed from 1955 to 2009 and may thus be considered reliable for forecasting wind speeds at the site.

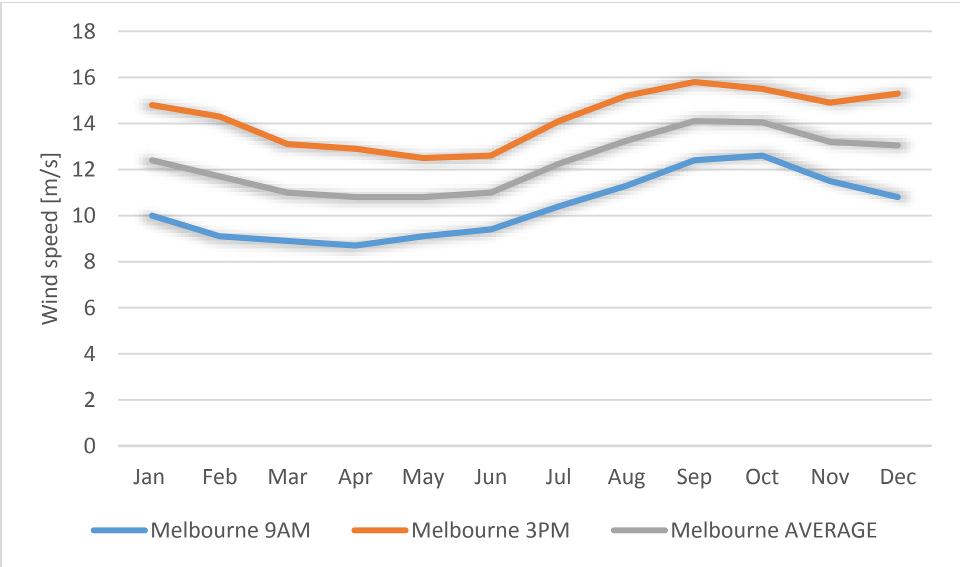

Diagram 3.1. Monthly wind conditions at the Melbourne regional office, Victoria (data 1955-2009) [14].

Wind speed deviations with increasing height is defined as the *wind gradient* and may be expressed as a logarithmic function. The wind speed at a particular height is commonly calculated by extrapolating the known value at a reference height, using the *log law* below [46].

$$U(z)/U(z_r) = \ln\left(\frac{z}{z_0}\right) \Big/ \ln\left(\frac{z_r}{z_0}\right) \tag{3.3}$$

Where $U(z_r)$ the wind speed at reference height z_r [m/s]
z the height above ground [m]
z_r the reference height above ground (typically 10) [m]
z_0 the surface roughness length [m]

The roughness length is a measurement of the ground surface unevenness for different types of terrain. Values vary immensely depending on the surrounding environment, from 0.00001 m for very smooth, ice or mud and up to 3.0 m for centres of cities with tall buildings. Characteristic values of the roughness length for various terrain conditions may be found in appendix B [55].

Diagram 3.2 below presents an example of the wind speed increase with height. Two separate roughness lengths have been chosen to empathize the impact of ground conditions on the wind speed, one representing lawn grass ground conditions as well as one for forests and woodlands. The reference wind speed at 10 m height have been selected so that the wind gradient of each roughness length will have a wind speed of 16 m/s at 100 m above ground. As a result, the influence of varying roughness length becomes evident.
A small roughness length indicates a terrain with relatively low friction, such as lawn grass. Winds in such environments will be relatively unaffected by the ground and consequently wind speeds will not increase much with height. Environments such as forests and cities are designated with high roughness lengths, meaning that the ground conditions are irregular. The differences in wind speed at increasing height will thus be large, since high surface friction causes low wind speeds close to ground. As may be observed in diagram 3.2, the wind speed increase with height is much greater in forested areas than on lawn grass. A wind speed of 16 m/s at 100 m elevation requires the reference speed to be 9 m/s in forests, whereas the same at grass terrain is 12 m/s [77].

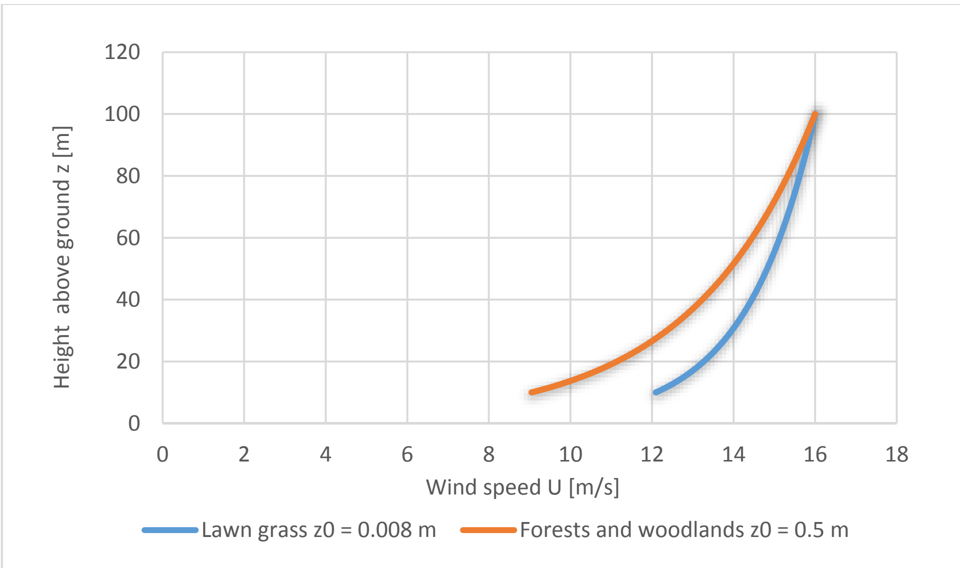

Diagram 3.2. Comparison of the wind gradient with varying surface roughness length (z_0). Wind speed U(z) = 16 m/s at height z = 100 m, reference height z_r = 10 m.

3.2.2 Atmospheric temperature

Most environments experience temperature variations with increasing height, a phenomenon known as the *temperature gradient*. Generally temperatures are lower at high altitudes than at ground level, which is primarily due to surface materials absorbing the sun radiated heat energy as well as the atmospheric pressure decrease at higher altitudes causing a drop air temperature. In such circumstances the temperature gradient is negative. At times, atmospheric temperatures differences will increase with height, i.e. a positive gradient. This is generally uncommon within the troposphere, which is closest layer of the atmosphere stretching to approximately 11 km above ground. However positive temperature gradients may occur at night as a result of heat losses being faster at the ground surface than in the ambient air.

The rate at which temperature changes occur is known as the *lapse rate*. In reality, the lapse rate varies with altitude due to atmospheric irregularities. However, standards have been established that provide averaged values of the temperature change rate for separate sections of the atmosphere. Within the troposphere the averaged lapse rate is typically – 6.5 K/km, a temperature drop that is much too small to have an impact on sound propagation at the hub height of wind turbines. Calculations have shown that a 200 m elevation will cause a mere 0.01 dB decrease with regards to geometrical divergence, assuming calm wind conditions [47] [12].

The sound propagation speed was defined in section 2.1.1 with equation (2.4). However, the speed of sound in air may be simplified as to merely be dependent on temperature variations with height.

$$c_0 = \sqrt{\gamma R T_K / M} = \sqrt{401.939 T_K} \tag{3.4}$$

Where c_0 the speed of sound in air [m/s]

The relationship between the speed of sound and increasing temperature is illustrated in Diagram 3.3 below.

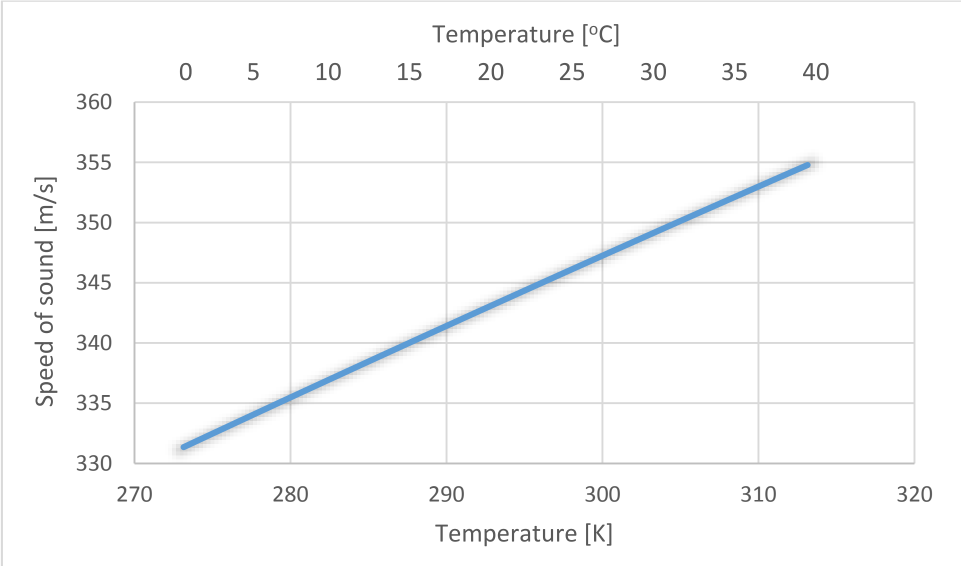

Diagram 3.3. The speed of sound in air with increasing temperature.

3.2.3 Refraction due to wind and temperature

The presence of wind and temperature in the surrounding environment of a sound source will have a refracting effect on the emitted sound waves. As was mentioned in section 2.1.6, transmission of sound between two separate medium will cause the waves to bend into regions of low sound speed. Variations in wind speed and temperature may thus be considered as different medium as it influences the speed of sound in air. For instance, a negative temperature gradient will cause the speed of sound to decrease with increasing height and as a result the sound waves will bend upwards, towards the lower sound speed region. This is called *upward refraction*. In contrast a positive temperature gradient, i.e. a temperature increase with height, will cause a *downward refraction*. The influence of temperature on sound refraction is illustrated in figure 3.4 (a) [67].

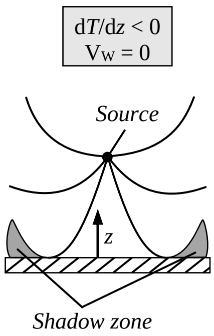

Propagation in calm wind conditions and a negative temperature gradient, i.e. temperature decreases with height, results in upward refraction around the source.

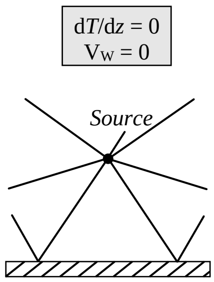

Free field conditions, meaning the wind and temperature gradients are absent, which allows for the sound waves to propagate in all directions and hence no refraction.

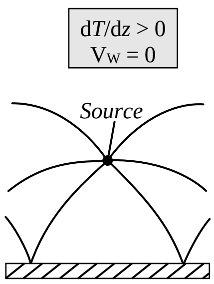

A positive temperature gradient during calm wind conditions causes a downward refraction of the sound waves around the source.

Figure 3.4. (a) The impact of the temperature gradient on sound propagation without influence of wind [67].

As mentioned previously, both the speed and direction of the wind will influence the behaviour of sound. The impact of wind and temperature gradients on sound refraction may be viewed in figure 3.4 (b) below [67].

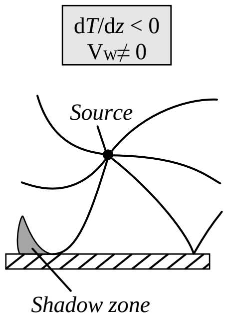

The sound propagation is affected by wind as well as a negative temperature gradient, causing the waves to bend in the direction of the wind on the downwind side of the source whereas upward refraction in created on the upwind side.

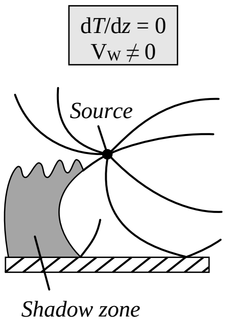

The emitted sound is merely influenced by wind, which causes the sound waves to propagate in the direction of the wind. As a result, a shadow zone is created in the upwind direction.

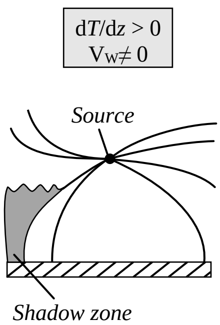

The sound propagation is affected by a wind as well as a positive temperature gradient, resulting in the sound waves being partly bent downwards and partly forced in the direction of the wind and hence creating a shadow zone on the upwind side of the source.

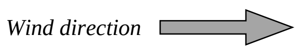

Figure 3.4. (b) The impact of the wind speed and temperature gradients on sound propagation [67].

Determining the effect that refraction due to wind and temperature has on sound attenuation is generally a complex process. Models have been developed that aim to predict the propagation of sound that is influenced by meteorological variations with height by using ray theory. The accuracy of these is however limited in outside environments due to the constantly changing meteorological conditions. Consequently, propagation of sound is often calculated assuming no refraction. Such simplified calculations are however based on the hypothesis that the time averaged meteorological conditions are spread relatively even, which is rarely the case. When not included, it is yet essential to acknowledge refraction during outside sound measurements as it may impact the credibility of the results [42].

3.3 Sound attenuation

Sound propagation is limited by the absorption and reflection or scattering it is exposed to by the surrounding environment. Reflection or scattering causes the sound to diverge from the direct path connecting the source and receiver, thus resulting in a sound pressure level decrease. During absorption, the energy contained within the emitted sound waves is partly converted into heat as the sound is transmitted between different medium. This process is repeated throughout the path of propagation until the sound has been entirely dissipated. The sound that reaches the receiver is thus dependent on the distance travelled as well as the absorbing or reflecting ability of ambient medium. The sound energy loss is known as *sound attenuation*.

Sound attenuation is typically divided into different categories, depending on the cause for absorption or reflection. *Excess attenuation* is defined as the total attenuation not including that due to spherical divergence and atmospheric absorption, according to the equation below [42].

$$A_E = A_{weather} + A_{ground} + A_{turbulence} + A_{barrier} + A_{vegetation} \tag{3.5}$$

Where A_E the excess attenuation [dB]

$A_{weather}$ the attenuation that occur due to varying meteorological conditions, mainly caused by the wind and temperature gradients [dB]

A_{ground} the ground attenuation [dB]

$A_{turbulence}$ the attenuation due to atmospheric turbulence [dB]

$A_{barrier}$ the attenuation caused by a barrier, such as a non-porous wall

or building [dB]

$A_{vegetation}$ the attenuation caused by vegetation [dB]

For open ground conditions, without surrounding obstacles such as trees and buildings, attenuation solely occur due to absorption by the atmosphere, ground and turbulence. However, attenuation in forested areas is also affected by the absorption of vegetation.

3.3.1 Atmospheric absorption

Sound that propagates through air will be partially attenuated due to the absorbing ability of the atmosphere. The pressure fluctuations that generate sound also causes the air molecules to vibrate, thus transferring a fraction of the energy contained within the sound waves into the atmosphere. The vibrational movement creates friction between the air molecules and as a result some of the transmitted energy is converted into heat. The remaining energy is stored temporarily within the air molecules to be released as sound at a later time. This is known as a *relaxational process*.
The attenuation due to atmospheric absorption may be calculated with equation (3.6).

$$A_{abs} = \alpha r/100 \tag{3.6}$$

Where A_{abs} the atmospheric absorption [dB]
α the absorption coefficient [dB/100m]

The absorption coefficient is dependent on the frequency, absolute humidity, atmospheric pressure as well as the air temperature according to the equation below [9].

$$\frac{\alpha}{p_s} = \frac{2000}{\ln(10)} \times \frac{f^2}{p_{s0}} \left\{ 1.84 \times 10^{-11} \left(\frac{T_K}{T_0}\right)^{1/2} + \left(\frac{T_K}{T_0}\right)^{-5/2} \left[0.01278 \frac{e^{-2239.1/T_K}}{F_{r,O} + f^2/F_{r,O}} + 0.1068 \frac{e^{-3352/T_K}}{F_{r,N} + f^2/F_{r,N}} \right] \right\}$$

Where $$F_{r,O} = 24 + 4.04 \times 10^4 h \frac{0.02 + h}{0.391 + h} \tag{3.7}$$

$$F_{r,N} = \left(\frac{T_K}{T_0}\right)^{-1/2} \left(9 + 280 h e^{\left\{-4.17\left[\left(\frac{T_K}{T_0}\right)^{-1/3} - 1\right]\right\}} \right) \tag{3.8}$$

$F_{r,O}$ the oxygen relaxation frequency [Hz]
$F_{r,N}$ the nitrogen relaxation frequency [Hz]
f the frequency [Hz]
h the absolute humidity (molar concentration of water vapour) [%]
p_s the atmospheric pressure [kPa]
p_{s0} = 101.325, the reference atmospheric pressure [kPa]
T_K the atmospheric absolute temperature [K]
T_0 = 293.15, the reference atmospheric temperature [K]

The absolute humidity may further be calculated with equation (3.9), which in turn requires determining the saturated vapour pressure with equation (3.10) below [9].

$$h = h_r \frac{p_{sat}/p_{s0}}{p_s/p_{s0}} \tag{3.9}$$

$$\log_{10}\left(\frac{p_{sat}}{p_{s0}}\right) = 10.79586\left[1-\left(\frac{T_{01}}{T_K}\right)\right] - 5.02808\log_{10}\left(\frac{T_K}{T_{01}}\right) + 1.50474 \times 10^{-4}\left(1 - 10^{-8.29692\left[\left(\frac{T_K}{T_{01}}\right)-1\right]}\right) - 4.2873 \times 10^{-4} \times \left(1 - 10^{-4.76955\left[\left(\frac{T_{01}}{T_K}\right)-1\right]}\right) - 2.2195983 \tag{3.10}$$

Where h_r the relative humidity [%]
p_{sat} the saturation vapour pressure [kPa]
T_{01} = 273.16, the triple-point isotherm temperature [K]

Diagram 3.4 illustrates the absorption coefficient as a function of frequency during standard ambient conditions (15°C, 101.325 kPa) and a relative humidity of 10 %, 50 % and 90 %, respectively.

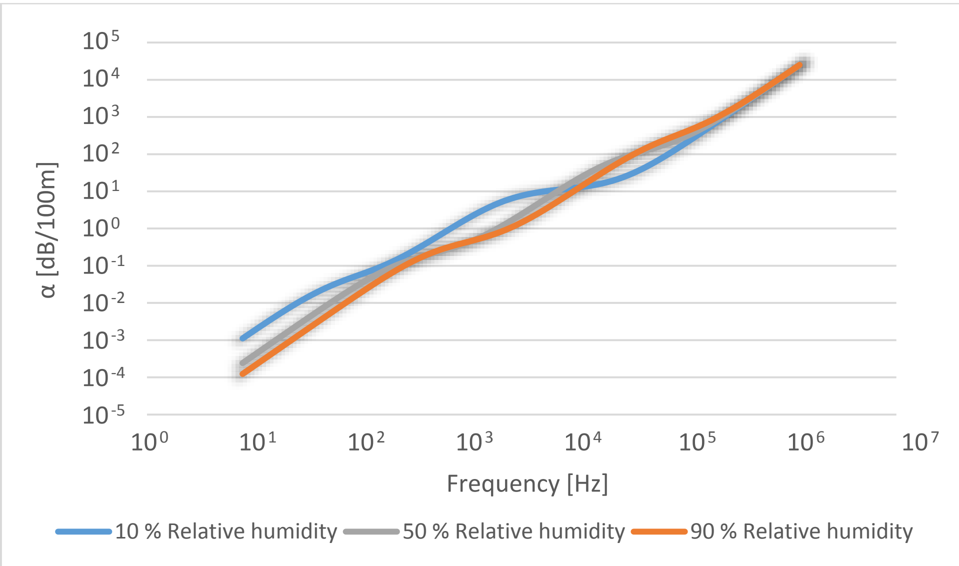

Diagram 3.4. The atmospheric absorption coefficient with frequency, for a relative humidity of 10 %, 50 % and 90 % (15°C, 101.325 kPa).

As may be observed in diagram 3.4 above, the absorption coefficient increases with frequency. At frequencies below 100 Hz, i.e. for low frequency and infrasound, the attenuation due to air absorption is close to negligible. The exception applies for very large source-receiver distances, however sound at such distances is likely to have dissipated due to other causes for attenuation. The relationship between atmospheric absorption and relative humidity also vary with frequency. Differences are generally greater at low frequencies than at very high, however large variations also occur around 5,000 Hz and 50,000 Hz. A comparison between the 1/3 octave A-filtered absorption coefficient and varying values of relative humidity indicates a maximum absorption at approximately 40 %, for standard ambient conditions. Furthermore, the A-weighted coefficient decreases for relative humidity above and below 40 % in accordance with a near semicircular arc plot.
Comparisons of the absorption coefficient with varying air temperatures generally shows an increase in the atmospheric absorption at lower temperatures. An exception is the atmospheric absorption at zero degrees Celsius, which is considerably lower than that at higher temperatures within the high frequency range. However, A-weighted values are maximized at approximately 20 degrees, for standard atmospheric pressure and 50 % relative humidity.

Values of the absorption coefficient for different atmospheric temperatures, relative humidity and frequencies may be found in appendix C. The atmospheric pressure has been set to a standard value of 1 atm (101.325 kPa).

3.3.2 Ground attenuation

Sound that is emitted by a source will be transmitted towards the receiver point through two separate ray paths. One path transfers the sound directly from the source to the receiver, while the other ray path will intersect with the ground before being reflected toward the receiver point. In consequence, the emitted sound energy will be partially exposed to ground absorption. As with air absorption, the energy absorbed by the ground will cause the contained air to vibrate, thus partly being converted to heat while the remaining part is transmitted through the ground before being re-radiated as sound once more [67] [42]. Ground absorption is commonly also referred to as the *ground effect*. The behaviour of sound in the presence of a ground medium is illustrated with figure 3.5 below.

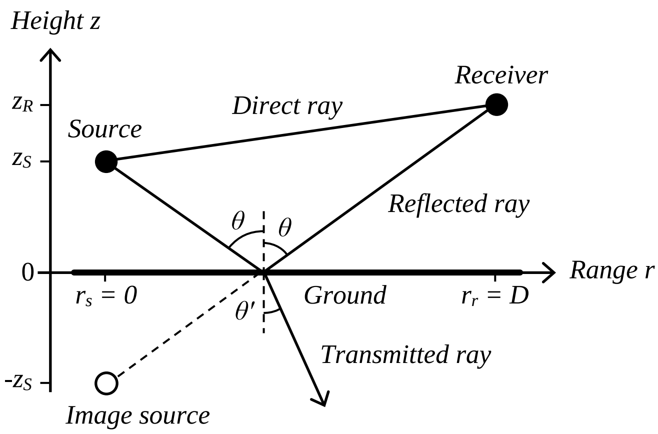

Figure 3.5. Demonstration of the divided sound transmission paths due to a ground interaction, based on [60].

In reality, the ray paths are affected by atmospheric refraction due to wind and temperature gradients and as a result they will be slightly curved. However for simplicity this has not been included in the following calculations, hence uniform ambient conditions are assumed [67].

The fraction absorbed sound energy is dependent on the *reflection coefficient* of the particular ground. The reflection coefficient is calculated differently for plane and spherical sound waves. A point source will generate spherical sound waves that decrease in sound intensity with increasing distance due to geometrical divergence, which was explained in section 2.2. Plane sound waves are transmitted in straight lines and will thus not be affected by the geometrical shape of propagation. Such waves do not occur naturally, however at large distances from the source spherical waves are approximately parallel and may thus be considered plane. The reflection coefficient for spherical sound waves is a function of that for plane waves and both are thus required.

Assuming locally reacting ground conditions, i.e. the reflected sound is independent of the angle of incidence and all absorbed sound energy will be dissipated (θ' = 0), the plane wave reflection coefficient is expressed according to the following equation [60].

$$R_p = \frac{Z\cos\theta - 1}{Z\cos\theta + 1} \quad \text{for } 0 \le R_p \le 1 \tag{3.11}$$

Where R_p the plane wave reflection coefficient [-]
Z the normalized ground impedance [-]
θ the reflection angle [rad]

The reflection angle depend on the length of the ray path that intersect with the ground, it may be seen as the line connecting an image source to the receiver as illustrated in figure 3.5 [60].

$$\theta = \cos^{-1}\left(\frac{z_R + z_S}{R_2}\right) \tag{3.12}$$

$$R_2 = \sqrt{D^2 + (z_R + z_S)^2} \tag{3.13}$$

Where R_2 the length of the reflected sound wave [m]
z_R the height of the receiver point [m]
z_S the height of the sound source [m]

The normalized ground impedance is defined as the ratio of the characteristic impedance for the particular ground conditions and the specific impedance of air, which is generally the media of sound transmission. The specific impedance of air is determined with equation (2.12) specified in section 2.1.4, however for standard ambient conditions (15°C and 101.325 kPa) a fixed value of 417.6 Pa · s/m is generally employed.

The characteristic impedance is a complex value, dependent on frequency as well as the structure of the particular ground. It is commonly determined with the Delany and Bazley model for porous media, which has been modified by Miki as to provide more accurate values at low frequencies [60] [48].

$$Z_c = \rho_0 c_0 \left\{1 + 0.070\left(\frac{f}{\sigma}\right)^{-0.632} + i0.107\left(\frac{f}{\sigma}\right)^{-0.632}\right\} \tag{3.14}$$

Where Z_c the characteristic ground impedance [-]
σ the flow resistivity [Pa · s/m^2]

ρ_0 the air density [kg/m^3]

The flow resistivity is the pressure difference that occur when air flows through a block of porous media, divided by the thickness of the block. It may be measured directly at the particular site or be determined through previously measured values, which is known as the *effective flow resistivity*. Values of the effective flow resistivity for various ground surfaces may be found in appendix D.
There are several more complex methods of determining the characteristic ground impedance, which generally provide more accurate results. However, these techniques generally require deep knowledge of the particular ground conditions and such data may be difficult to obtain [60].

The spherical wave reflection coefficient may furthermore be determined with equation (3.15).

$$Q = R_p + (1 - R_p)F(w) \quad \text{for } 0 \leq Q \leq 1 \tag{3.15}$$

Where Q the spherical wave reflection coefficient [-]
F(w) the boundary loss factor [-]

The boundary loss factor is a function of the standardized complementary error function as well as the numerical distance, according to the equations below [60].

$$F(w) = 1 + iw\sqrt{\pi}e^{-w^2}\operatorname{erfc}(-iw) \tag{3.16}$$

Where $$w = \sqrt{\frac{ikR_2}{2}\left(\frac{1}{Z} + \cos\theta\right)} \tag{3.17}$$

erfc(z) the complementary error function [-]
w the numerical distance [-]
k the wave number (see section 2.1.1) [rad/m]

The complementary error function is determined differently, depending on the value of the numerical distance. For small values of $|w^2| < 8$, the error function is calculated with equation (3.18) hence resulting in a boundary loss factor according to (3.19).

$$\operatorname{erfc}(z) = 1 - \frac{2}{\sqrt{\pi}}\sum_{n=0}^{\infty}\frac{(-1)^n z^{2n+1}}{n!\,(2n+1)} \tag{3.18}$$

$$F(w) = 1 + iw\sqrt{\pi}e^{-w^2}\left[1 + \frac{2iw}{\sqrt{\pi}}\sum_{n=0}^{\infty}\frac{(w^2)^n}{n!\,(2n+1)}\right] \quad \text{for } |w^2| < 8 \tag{3.19}$$

A good approximation is to end the series once the summand is lower than 10^{-6}.

For large values of $|w^2| > 8$, the complementary error function may be determined with equation (3.20). This expression is however valid solely for positive input values,
$z \to \infty$ and $|\arg z| < {}^3/_4\,\pi$. For negative values of $z \to -\infty$, the equation is converted as to comply with $\mathrm{erfc}(-z) = 2 - \mathrm{erfc}(z)$ and the boundary loss factor may hence be calculated with equation (3.21) [60].

$$\sqrt{\pi} z e^{-z^2} \mathrm{erfc}(z) = 1 + \sum_{m=1}^{\infty} (-1)^m \frac{1 \times 3 \times 5 \ldots (2m-1)}{(2z^2)^m} \tag{3.20}$$

$$F(w) = 2iw\sqrt{\pi} e^{-w^2} H(-Im\, w) - \sum_{m=1}^{\infty} \frac{1 \times 3 \times 5 \ldots (2m-1)}{(2w^2)^m} \quad \text{for } |w^2| > 8 \tag{3.21}$$

Where $\begin{cases} H(x) = 1 & \text{for } x \geq 0 \\ H(x) = 0 & \text{for } x < 0 \end{cases}$

$H(x)$ the Heaviside step function [-]

The sound attenuation that occur due to absorption by the ground is ultimately determined with equation (3.22) below. The complete derivation of the equation may be found in appendix E.

$$A_{ground} = -10 \log \left| 1 + Q \frac{R_1}{R_2} e^{(ikR_2 - ikR_1)} \right|^2 \tag{3.22}$$

Where $R_1 = \sqrt{D^2 + (z_R - z_S)^2}$ (3.23)

R_1 the length of the direct sound wave [m]

Diagram 3.5 demonstrates the ground absorption dependence on frequency for two ground types; the forest floor of pine or hemlock woods as well as grass lawn. In order to visualize the variations with frequency the sound source is located relatively low and the distance between source and receiver is short. At higher source elevations, as such expected from wind turbines, and at longer distances the ground attenuation varies more frequently. It may thus be more difficult to distinguish a difference in attenuation for different ground types. The flow resistivity of each ground category is based on data from appendix D.

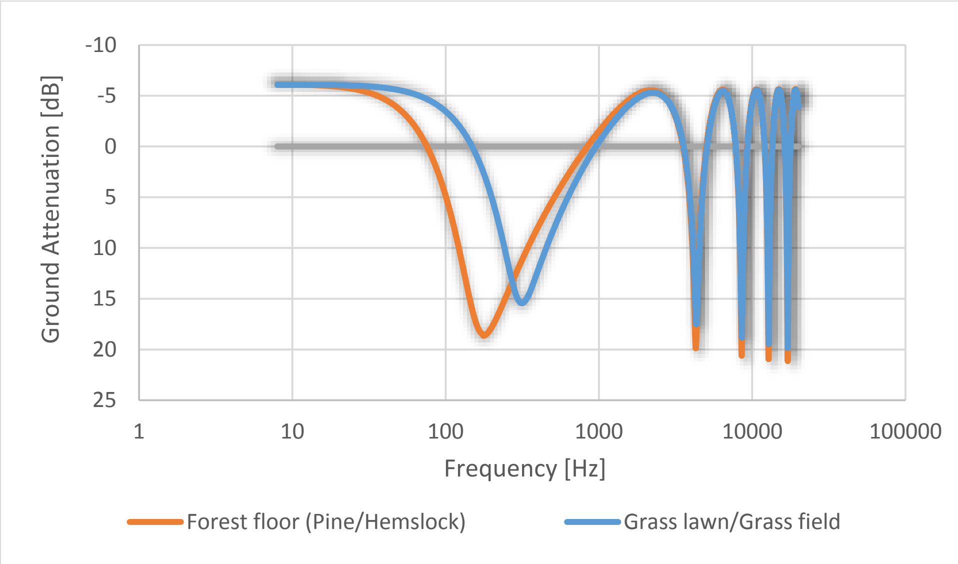

Diagram 3.5. The ground attenuation due to sound interaction with forest floor σ = 50 kPa · s/m^2 and grass lawn/grass field σ = 200 kPa · s/m^2, respectively. Source height, z_S = 2 m and receiver height, z_R = 2 m. Distance between sound source and receiver, D = 100 m. Standard ambient conditions apply (15°C, 101.325 kPa).

Due to the phase dependence of the ground attenuation, both positive and negative values occur. In the case of a negative ground attenuation factor, which occur at frequencies below 100 – 200 Hz for instance, the direct sound waves and the waves reflected by the ground surface will interfere *constructively*. Hence at the point of intersection the sound pressure amplitude of both waves will be of the same character, either positive or negative, which causes an amplification of the pressure amplitude and in consequence the emitted sound. Occasionally interference will occur at the maximum amplitude value, resulting in a positive peak in ground absorption. During such ray interferences the sound waves are in-phase, as may be observed at 2,000 Hz and 6,000 Hz in diagram 3.5 above.
A positive ground attenuation factor occurs once the direct and reflected sound waves interfere *destructively*, meaning the pressure amplitude of both waves will be of

opposing character at the point of intersection. Consequently the resulting sound pressure amplitude will be reduced, which causes an attenuation of the emitted sound. During a peak destructive interference the sound waves are out-of-phase, which occurs at 400 Hz and 4,000 Hz in diagram 3.5 [8] [60].

As may be observed from diagram 3.5 there is a slight difference in ground absorption for a forest floor and grass lawn. Positive values of the ground attenuation are intensified in forests, maximum differentiations occurring between 100 Hz and 200 Hz. This may be explained by the fact that the flow resistivity for forest floors is generally lower than that for grass fields. A low flow resistivity indicates a high air content in the ground and thus a large fraction of the incident sound energy will be absorbed and converted into heat. This relationship may also be demonstrated mathematically. According to equation (3.14), low values of the flow resistivity results in a low ground impedance and in consequence a plane wave reflection coefficient close to zero (3.11). Ground types for which $R_p \to 0$ are characterized as *acoustically soft*, meaning they are highly absorptive. In contrast, grounds with a plane wave reflection coefficient approaching one are highly reflective and thus characterized as *acoustically hard*. Completely reflective grounds for which $R_p = 1$, meaning no sound energy is absorbed by the ground, do not occur naturally since it would require $Z = \infty$ ($\sigma = \infty$). However, grounds such as concrete has sufficiently high flow resistivity as to be considered virtually completely reflective [60].

It should also be noted that ground attenuation differ depending on the time of year. For instance, the influence of ground absorption is generally less during winter months since a drop in temperature will cause the ground harden, thus decreasing its absorbing ability. Furthermore, periods of rain may also lessen the effects of ground absorption as it causes an increase in the ground moisture, thus decreasing the flow resistivity. These are factors that should be recognized when predicting the influence of ground on sound propagation [8].

The method of predicting ground effect that is presented in this chapter is somewhat limited as it applies for the ideal case of a perfectly flat surface. However, as was explained in section 3.2.1, in reality all ground types may be characterized by a surface roughness length, which is a measurement of the terrain unevenness. Sound that intersect with a rough surface will not be reflected directly towards the receiver, but will scatter in several directions. Methods, both empirically and theoretically based, have been developed to incorporate the effects of surface roughness when determining the ground attenuation, examples includes Twersky's semi-cylindrical boss model. However, due to the complexity of such models, these will not be treated in this work.

Furthermore, the methodology described above is restricted to source-receiver dimensions that constitute a *grazing incidence*, meaning a reflection angle that is close to perpendicular, $\theta \approx \pi/2$. Such conditions apply for large distances between the sound source and receiver in relation to the source height. There are alternative solutions available that have been proved valid for various other source-receiver geometries, however these will not be included in this report.

3.3.3 Atmospheric turbulence

The behaviour of wind and temperature within the atmosphere generally does not comply with the computed gradients at every point in time, but varies rapidly over intervals of minutes or seconds. Such fluctuations are characterized as *atmospheric turbulence* and are difficult to predict. The turbulent kinetic energy responsible for atmospheric instabilities is generated by a combination of shear forces and buoyant instabilities. Shear turbulence is commonly generated during high wind conditions and a low temperature gradient. Various surface obstacles, such as vegetation or residential buildings, will interfere with the natural flow of the air particles thus resulting in turbulence. Buoyancy or convective turbulence is caused by large variations in the ground and air temperatures, which commonly occur as a result of solar radiation heating up the ground surface. To balance the temperature discrepancy, air particles positioned higher up in the atmosphere are forced towards the ground surface, thus generating a vertical air flow that becomes irregular at low elevations due to interference with ground barriers [8] [1].

Unlike laminar atmospheric flow, in which the air particles are travelling at a constant velocity, atmospheric turbulence causes the particles to deviate from the mean flow speed. As a consequence, air particles moving at a higher velocity than other surrounding particles will be forced to deviate from the direct path of transmission, hence creating loops known as *eddies* in the air flow as shown in figure 3.6 below [60].

Figure 3.6. Illustration of laminar and turbulent air flow, respectively [60].

The atmospheric boundary layer, i.e. the layer of the atmosphere that is influenced by the ground surface, is dominated by turbulent air flow. Laminar flow is uncommon but may occur in confined spaces during low wind speeds, such as a pipe. Eddies generated by turbulent air flow varies in size depending on their position in the atmosphere. Large eddies commonly occur at high elevations, while smaller loops are generated close to the ground surface. The size of eddies are of importance since it correlates with the fluctuation rate. The rate of deviations in wind speed and temperature for small eddies are generally higher than that of larger loops.

Atmospheric turbulence affects sound propagation due to the relationship between wind speed, temperature and the effective speed of sound, shown in equation (3.1). Consequently, any fluctuations in wind speed will cause corresponding variations in the effective sound speed and thus affect the sound attenuation due to geometrical divergence. The effects of turbulence on sound propagation may be measured with the *refractive index*, which is determined with equation (3.24) below [60].

$$n = c_0 / c_{eff,t} \qquad (3.24)$$

Where n the refractive index [-]
$c_{eff,t}$ the effective speed of sound, including turbulence [m/s]

The refractive index is the amount of fluctuation that occur at a point in time from the mean value and may thus be expressed according to equation (3.25) below [60].

$$n = \bar{n} + \mu \qquad (3.25)$$

Where $\bar{n}$ the averaged refractive index [-]
μ $\ll \bar{n}$, the fluctuation [-]

The fluctuation factor squared is known as the *turbulence parameter* and is generally determined through estimated values based on experimental measurements. Table 3.2 below shows the turbulence parameter for various weather conditions [42].

Weather conditions	Turbulence parameter $< \mu^2 >$
Sunny, light wind (< 2 m/s)	5×10^{-6}
Sunny, moderate wind (2 – 4 m/s)	$9 \times 10^{-6} - 10 \times 10^{-6}$
Sunny, strong wind (> 4m/s)	$15 \times 10^{-6} - 25 \times 10^{-6}$
Overcast, light wind (< 2 m/s)	3×10^{-6}
Overcast, moderate wind (2 – 4 m/s)	$8 \times 10^{-6} - 9 \times 10^{-6}$
Overcast, strong wind (> 4 m/s)	$15 \times 10^{-6} - 25 \times 10^{-6}$

Table 3.2. The turbulence parameter for various weather conditions [42].

As may be seen from table 3.2, the turbulence parameter is generally higher during sunny weather conditions. This is a result of buoyant instabilities, a higher level of solar radiation will cause greater disparities between the ground and air temperatures thus resulting a turbulent air flow. However at high wind speeds, the generation of atmospheric turbulence is dominated by shear forces and not as reliant on ambient temperatures.

Atmospheric turbulence also causes fluctuations in the phase and amplitude of a propagating sound wave and will consequently influence the absorbing or amplifying effect of ground attenuation. As a result, turbulence may affect the coherence of the direct and reflected sound waves and thus decrease the accuracy of ground effect predictions. In general, atmospheric turbulence results in decreased attenuation due to ground interaction, which is a result of the changed behaviour of the reflected and direct waves causing a reduction of the sound pressure level amplitude peaks. Many studies that have been conducted to determine the influence of turbulence on sound propagation, indicate a greater variance between measured and calculated values of the ground attenuation with increasing turbulence parameter, i.e. with increasing fluctuations. Measurements have also shown that the effects of turbulence are maximized in two specific circumstances; sound propagation close to the ground surface at short distances and propagation over long distances with a strong negative speed of sound gradient, meaning with the speed of sound decreases rapidly with height [16]. In general, the impact of turbulence increases with increasing frequency and distance from the source. However for a distant sound source, the amplitude deviation have been found to not exceed a standard value of 6 dB [2] [1].

3.3.4 Effects of topography

Large ground surface irregularities between a sound source and receiver, such as hills and valleys, may have considerable effects on the propagation of sound. As was mentioned previously, the sound levels detected at a receiver point is significantly dependent on the reflective ability of the ground surface. During propagation over flat grounds, the reflected sound rays may be modelled by using the source-receiver dimensions. However in complex terrain situations, the reflected sound will behave differently due to the inclination of the ground surface. If a source is positioned at higher ground elevations than the receiver point, such as on top of a hill, more sound rays will be reflected towards the receiver point than would be expected during propagation over levelled grounds. As a result, higher levels of sound will be detected at the receiver compared to that over a flat surface. In contrast, if a source positioned at lower grounds than the receiver, such as in a valley, much of the sound will be reflected away from the receiver point by the inclining surface, thus resulting in a decrease in noise levels [8].

The behaviour of sound over complex terrain is generally less predictable than over a flat ground surface, which makes it difficult to model. There are currently several techniques for predicting sound propagation over irregular ground surfaces, which are based on approximate calculation methods. Many of these techniques utilize the similar characteristics of topographical features, such as hills and valleys, and atmospheric refraction. Sound propagating over a convex ground profile will act similar to that over a flat surface during upwards refraction.

The atmospheric refraction will affect the speed of sound profile and consequently the sound propagating path, as illustrated in figure 3.7. The shadow zone that is created behind the convex curvature is also generated in the upwards refracting atmosphere. Sound propagating over a convex ground surface may instead transformed into a flat surface during downwards refracting atmospheric conditions [60].

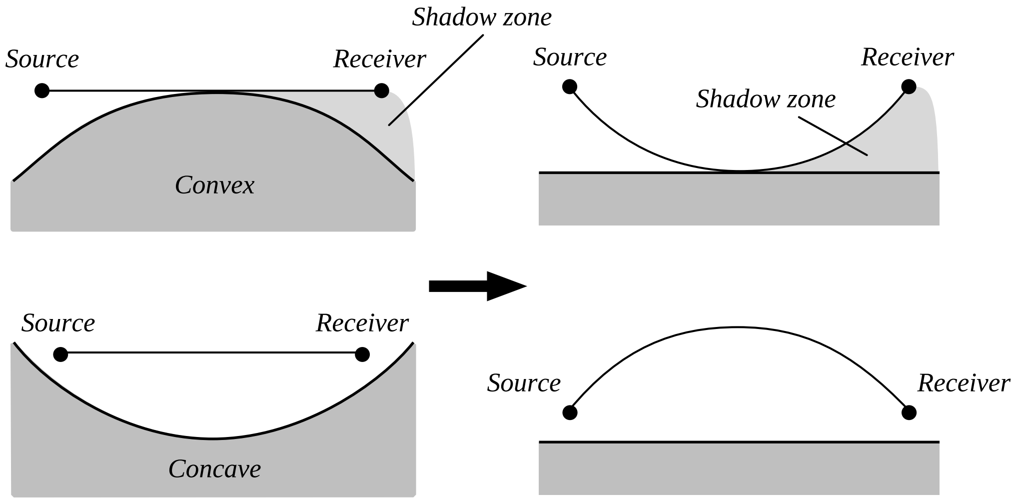

Figure 3.7. Illustration of the sound ray path behaviour over convex and concave ground profiles. Convex terrain correlates to a flat surface with an upwards refracting atmosphere, while concave terrain profile may be transformed to a flat ground surface during downward refraction.

3.4 Sound propagation in forest areas

Noise barriers consisting of trees and shrubs influence the propagation of sound. Sound propagating through forests will be subject to both refraction and scattering as well as absorption by various woodland components. A major absorbing element is the particular ground structure of forest floors, which often consist of several layers with varying flow resistivity.
The presence of forests within the source-receiver propagation path also alters the appearance of the wind and temperature gradient.

3.4.1 Australian forest configuration

Australia has approximately 125 million hectares of forest, which correspond to 16 % of the entire land area. The majority of Australian forest is native, 98 % of the total forest area consist of tree species indigenous to Australia, while the remaining part is occupied by industrial plantations or other forest types [4].
Forests are commonly classified according to the amount of crown cover they provide. Crown cover is defined as the ground area shielded by the tree canopies, disregarding any possible gaps in the canopy of individual trees. Australian forests may thus be divided into three categories; woodland, open and closed forests. Furthermore, each category is separated into three height classes; tall, medium and low [3]. Examples of three forest varieties may be viewed in figure 3.8 below.

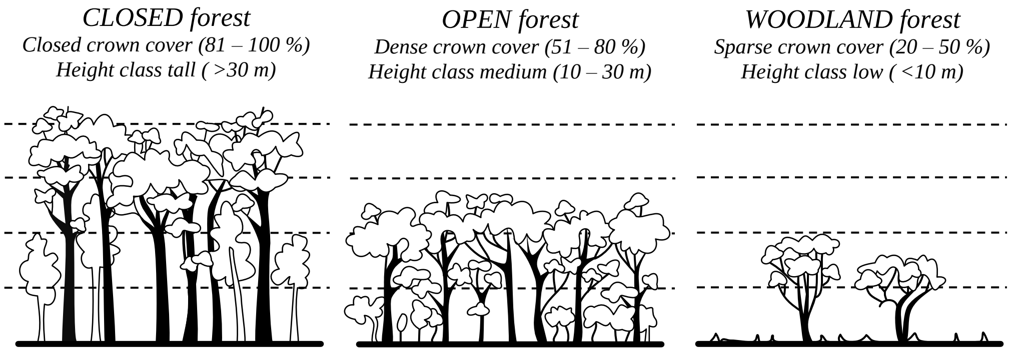

Figure 3.8. Examples of crown cover and height classes. Each dotted line represents 10 m above ground, based on [3].

The distribution of various forest types depend on the local climate, soil type and land usage. The most commonly found forest is the *eucalypt* forest, which accommodate 75 % of the native forest area in Australia. Tree species found in eucalypt forests are divided into three genera; *Eucalyptus*, *Corymbia* and *Angophora*. Eucalyptus trees originates from the rainforests of northern Australia, but has adapted to the conditions of drier regions with poor-nutrient soils and high fire risks, and is thus currently widespread. The foliage of eucalypt trees species consist of long narrow leafs that are rich of oil, hence making them highly flammable. The tree bark consist of a thin moist tissue, which dries annually thus also becoming a fire hazard. Eucalypt trees has however developed various strategies of recovering from fire, examples include encapsulating the seed during the fires and releasing them after the hazard has vanished. The majority of eucalypt species are evergreen, meaning they maintain their leaves during the entire year [4] [29].

3.4.2 Wind speed in forests

Due to the presence of vegetation and foliage, the wind gradient in forest areas vary from that at open ground conditions. Wind speeds are generally low inside the forest, owing to barriers such as tree trunks and bushes obstructing the wind flow, but increase rapidly at higher altitudes. The wind escalation typically commence above the *zero-plane displacement height d*, which is the height of minimum wind speed and is thus generally the location of maximum foliage density.

The wind gradient in forests may be divided into three segments; above and below the tree canopy as well as the transition layer. The transition layer is a part of the forest wind gradient that extends from the forest tree tops to a height z_*, as may be observed in figure 3.9. It describes the wind speed increase that is caused by the turbulence generated in this region.

The equations below assumes an idealized forest stand, i.e. a forest profile with fixed and horizontally homogenous conditions over a large area [66].

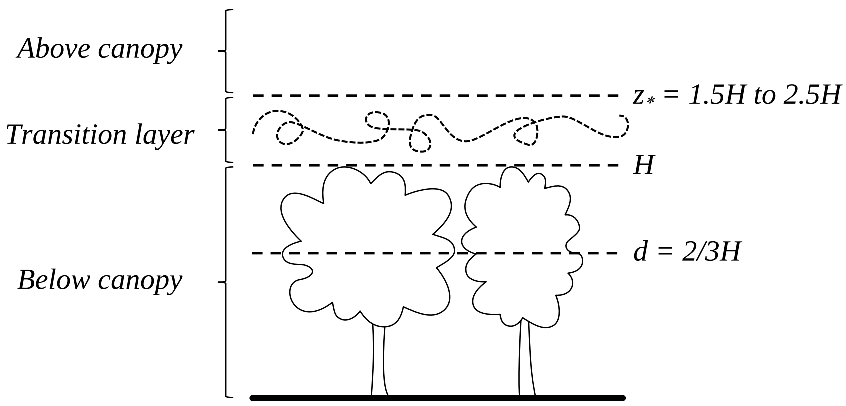

Figure 3.9. Layers of the wind gradient in forest areas.

Above canopy

Wind speeds above the transition layer may be calculated using a modified adaption of the standard power-law equation, shown below [66] [55].

$$U_{above}(z) = U_{z_2} = U_{z_1}\left(\frac{z_2 - d}{z_1 - d}\right)^P \text{ for } z > z_* \tag{3.26}$$

Where
- U_{z2} the wind speed at height z_2 [m/s]
- U_{z1} the wind speed at height z_1 [m/s]
- d the displacement height, often approximated to be two-third of the height of the canopy, H [m]
- P the power-law exponent, $0 < P < 1$ [-]

There are numerous methods of determining the power-law exponent. Equation (3.27) below is commonly applied within the wind power industry [46].

$$P = 0.096 \log z_0 + 0.016(\log z_0)^2 + 0.24 \tag{3.27}$$

At great distances above the tree canopy winds may be assumed to not be influenced by the forest. Wind speeds over forest areas are thus expected to be comparable to those obtained over lower roughness elements at high altitudes. As a result, measured reference values at open fields may be applied in equation (3.3) in order to determine the wind speed over an adjacent forest at corresponding height [66].

Transition layer

As previously mentioned, a significant wind speed increase generally occur at heights immediately above the forest tree tops due to the turbulence that is generated in this area. Winds within the transition layer are difficult to predict owing to the irregularity of turbulence. Many factors that influence wind turbulence vary rapidly over time. Equation (3.28) presents the averaged wind gradient within the transition layer region, based on the power-law equation that was shown previously [66].

$$U_{transition}(z) = U_{z_1}\left(\frac{z_2 - d}{z_1 - d}\right)^P + \left(\frac{u_*}{k_v}\right) \times \Psi^*{}_m \text{ for } \mathrm{H} \leq z < z_* \tag{3.28}$$

Where Ψ^*_m the diabatic influence function dependent on ϕ^*_m [-]
u^* the friction velocity [m/s]
k_v = 0.40, the von Kármán's constant [-]

The *friction velocity* describes the flow of momentum within the wind. Momentum is transported from a faster moving layer of the atmosphere to a slower and the momentum flow is thus directed downwards. As a result, the friction velocity is proportional to the wind speed deviation from a mean value and may hence me be used to scale wind turbulence [61].

$$u_* = \sqrt{\tau/\rho} = \sqrt{\overline{u'w'}} \propto \sigma \tag{3.29}$$

Where τ the effective shear stress [Pa]
u' the flow deviance from a mean value $\bar{u}$, in the u-direction [m/s]
w' the flow deviance from a mean value $\bar{w}$, in the w-direction [m/s]
σ the standard wind speed deviation [m/s]

The effective shear stress is approximately constant within the surface layer of the atmosphere, which expands to roughly 100 m above ground. The variation in air density within the surface layer is negligible and the friction velocity may thus be considered constant in this region [61].

The friction velocity is generally determined through measurements performed at the particular site of interest. A rough estimation may however be made as the ratio u^*/u typically vary between 0.05 and 0.1 in light and strong winds, respectively. The variable u indicates the wind speed at 10 m height [21].

The diabatic influence function is determined using the equation below, the symbol x denotes $(\phi^*_m)^{-1}$ [66].

$$\Psi^*_m = 2\ln\left(\frac{1+x}{2}\right) + \ln\left(\frac{1+x^2}{2}\right) - 2\tan^{-1}x + \frac{\pi}{2} \tag{3.30}$$

$$\phi^*_m = \exp\left[-0.7\left(1-\frac{z}{z_*}\right)\right] \text{ for } z < z_* \tag{3.31}$$

Where ϕ^*_m the mass transfer function, indicating atmospheric stability [-]

z_* the depth of the transition layer, often approximate to be between 1.5H and 2.5H depending on the forest tree density [m]

Below canopy

Within the forest, wind speeds decrease drastically. The lowest winds occur at the zero-plane displacement height due to this being the point of maximum tree foliage density. A slight wind speed increase later appear since tree trunks present less resistance to the natural wind flow, as may be observed in the figure 3.10 below. Such small wind deviations will have an insignificant impact on sound propagation [66].

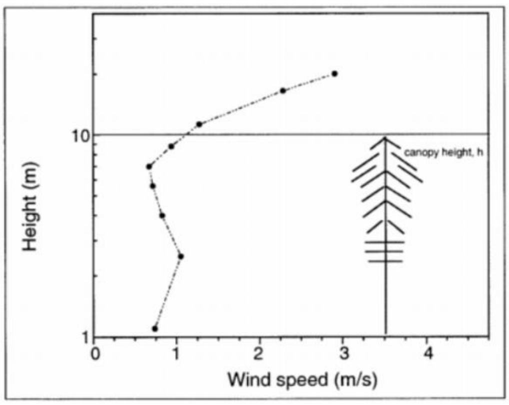

Figure 3.10. The wind speed gradient below the forest canopy [66].

Wind speeds below the forest canopy are calculated with the equation below.

$$U_{below}(z) = U_H \exp\left[-n\left(1-\frac{z}{H}\right)\right] \text{ for } z \leq H \tag{3.32}$$

Where U_H the mean wind speed at the height of the canopy H [m/s]
n the canopy flow index [-]

Calculating the canopy flow index is a complex process, as it is dependent of variables such as the leaf area density which may be difficult to determine accurately. Typical values of the canopy flow index for various forest configurations have therefore been provided in table 3.3 below [66].

Gum-Maple	4.42 ± 1.05
Maple-Fir	4.03 ± 0.69
Jungle	3.84 ± 1.52
Spruce	2.74 ± 1.29
Oak-Gum	2.68 ± 0.66

Table 3.3. Canopy flow indexes determined experimentally for various forests [66].

Diagram 3.6 illustrates the wind gradient in a gum-maple forest compared to that over an adjacent open field. In order to show the impact of turbulence, a large friction velocity of 3 m/s have been chosen. Such great turbulence are however rare in reality.

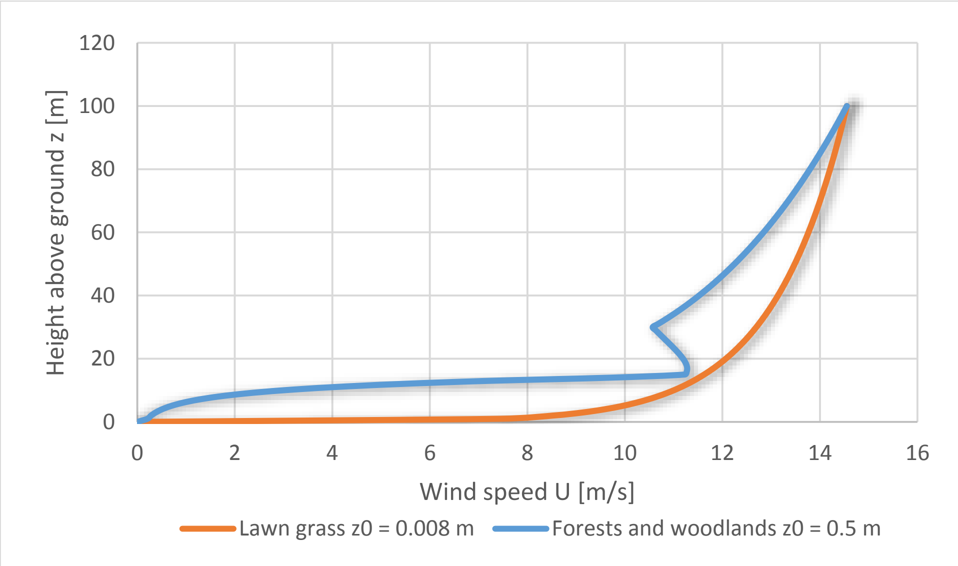

Diagram 3.6. Comparison of the wind gradient in a gum-maple forest area and over lawn grass. Reference values from Melbourne in March, $U(z_r)$ = 11.0 m/s at height z_r = 10m. Average tree height, H = 15 m. Displacement height, d = 2/3H and depth of transition layer, z_* = 2h. Friction velocity, u^* = 3 m/s.

Wind speeds are low close to the forest ground, but increase rapidly above the displacement height at 10 m. In contrast to reality, minimum wind speeds do not occur at the displacement height. However, winds are sufficiently low at this level for the error to not impact the accuracy of the sound speed.
The influence of turbulence is indicated by a clear drop in wind speed, which occur at the upper border of the transition layer. In reality, the transmission between the two upper atmospheric layers would presumably be smoother.
Calculations employing the various forest types presented in table 3.3, indicate an increase in wind speed below the forest canopy with decreasing canopy flow index, with maximum differences occurring around the displacement height. The canopy flow index is a measurement of the average air flow permeability of a particular tree species and is calculated using equation (3.33) below [7].

$$n = \frac{\ln(U(z)/U_H)}{z/H - 1} \tag{3.33}$$

In consequence, high values of the canopy flow index denote low wind speeds at a height z within the tree canopy compared to that at the canopy height H, thus indicating a high leaf density. However, calculations of the attenuation by geometrical divergence using the wind speed gradient of a gum-maple and oak-gum forest, respectively, have shown a negligible difference of less than 0.01 dB. The mentioned calculations were performed using the input values shown in diagram 3.6.

3.4.3 Atmospheric temperature in forests

As for wind, the temperature gradient in forest areas may be divided into separate parts. One part describes the behaviour of temperature above the forest canopy and one below the tree line.

The upper segment of the temperature gradient will behave in a similar manner to that observed in open field conditions. The canopy surface consist of leafs and branches which absorbs the radiating heat energy, i.e. resulting in a negative temperature gradient during the day and a positive gradient at night. However due to the existence of turbulence in the region immediately above the forest canopy, temperature variations with increasing height are generally small.

Below the canopy, tree foliage acts as a barrier which prevents the sun radiated heat from reaching the forest ground. The energy that is absorbed by the canopy will however be transmitted through the undergrowth, thus creating a positive temperature gradient during the day. Depending on the wind conditions at various heights below the forest canopy, temperature will vary slightly as may be observed in figure 3.11. At the displacement height wind speeds are minimal and as a result there will be a temperature increase at this point. Similarly the increased wind speed at heights corresponding to minimum tree foliage density will cause a drop in temperature. Temperature variations below the canopy are however generally small. As is illustrated in figure 3.11, the maximum temperature difference below the forest canopy is a mere 3 degrees for which the impact on sound propagation would be trivial. Depending on the ambient weather isothermal conditions, i.e. constant temperature with height, may also apply within the forest. Furthermore, near isothermal conditions or an unstable negative temperature gradient commonly apply at night [66].

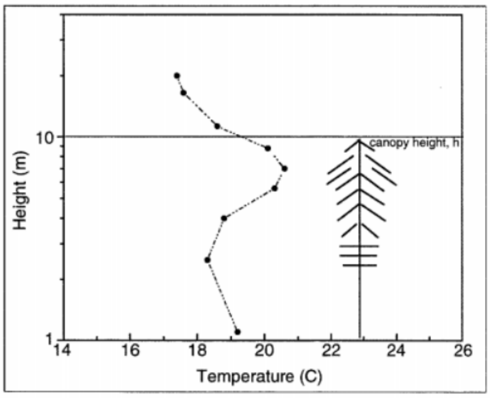

Figure 3.11. Temperature gradient above and below the canopy of a pine forest [66].

3.4.4 Ground attenuation in forests

Sound ray interaction with a ground surface causes either attenuation or amplification of the levels detected at the receiver point, as was explained in section 3.3.2. The behaviour of sound is largely dependent on the normalized impedance of the intersecting ground, which varies with frequency. The ground structure is often assumed semi-infinite and as a result the normalized impedance becomes a material constant, i.e. solely dependent on the flow resistivity of the particular ground type. In some cases such an assumption is sufficient to obtain accurate values of the ground attenuation, an example being grass lawns. However, in general the ground should be modelled as an accumulation of several layers of porous materials. For instance, the ground structure of a road surface covered by snow is built up by two separate layers with altering materialistic properties. Modelling the ground as a semi-finite medium will hence result in inaccurate values. The normalized impedance of such a ground structure is thus dependent on the layer thickness as well as the flow resistivity of the various layers [60] [1].

The ground structure of forest floors is built up by multiple layers. The upper ground layers mainly consist of litter such as decaying leaves, twigs and moss. This is followed by a layer of humus, i.e. organic material from decayed litter, and the substrate containing layers of sand and compacted soil. Examples of the ground structure for six separate ground surfaces are illustrated in figure 3.12 below.

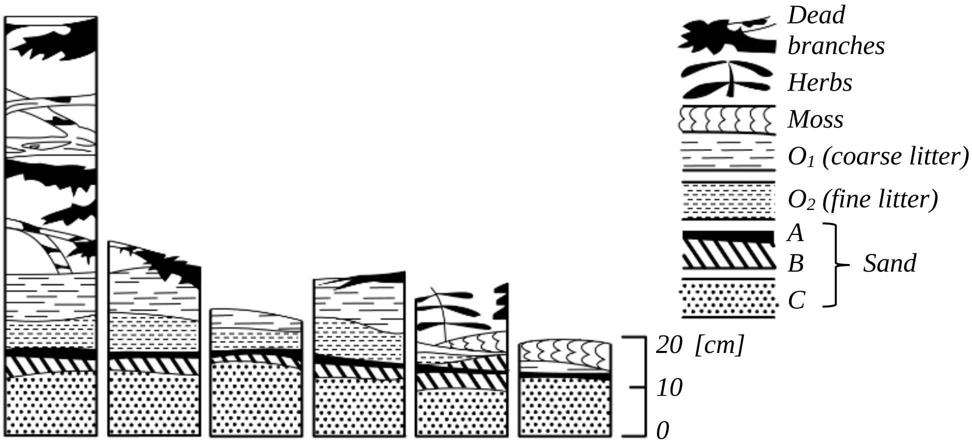

Figure 3.12. The schematics of six separate forest grounds, based on [34].

The ground structures presented in figure 3.12 are based on samples taken inside an Austrian pine forest. A maximum of six separate layers were identified in a single sample, each layer with a distinct flow resistivity. Furthermore, the amount and thickness of the layers found within each ground sample varied vastly throughout the woodland and consequently, as did the combined forest ground surface impedance [34].

Since the effective flow porosity is measured values, it incorporate all layers of forest floors. However, as may be observed from appendix D, the effective flow porosity is not a fixed value but ranges from 20 to 80 kPa · s/m^2. This is partly due to the varying arrangement of the ground layers within a single forest and partly because the overall floor structure generally differ depending on the type of forest considered. Although the range is not large, the choice of effective flow resistivity will impact the level of sound attenuation or amplification caused by the ground effect. For the dimensions demonstrated in figure 3.5, section 3.3.2, a maximum difference between the two peak values is approximately 17.0 dB, which occur at 100 Hz. The prominent variance demonstrates the importance of selecting a flow resistivity that correspond to the intended site.

The structure of a ground consisting of two separate layers is illustrated in figure 3.13 below. A sound wave normal to the ground surface intersects with the upper layer, which has the normalized impedance Z_I. As for a semi-infinite ground, a part of the incident sound wave will be reflected by the ground surface. The remaining sound energy will be either converted to heat or transmitted through the upper ground layer and intersect with the bottom layer at x = t. At this point the transmitted sound wave will be divided further, one part being reflected by the layer interface while the remaining sound energy is transmitted through the bottom ground layer, which has the normalized impedance Z_{II}. This process will be repeated at the interface of any succeeding ground layers until the sound energy has been entirely dispersed [60].

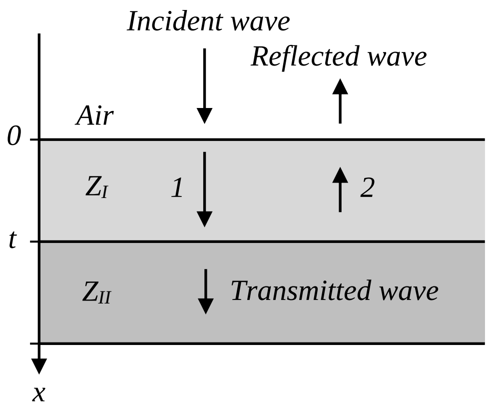

Figure 3.13. Normal intersection of a plane sound wave with a layered ground, based on [60].

Layered ground structures are modelled correctly by combining the normalized impedance of both layers in accordance with the equation below [60].

$$Z_{layer}(x = 0) = Z_I \frac{Z_{II}\cosh(-ik_1 t) + Z_I \sinh(-ik_1 t)}{Z_{II}\sinh(-ik_1 t) + Z_I \cosh(-ik_1 t)} \tag{3.34}$$

Where Z_{layer} the normalized impedance of the layered ground [-]
Z_I the normalized impedance of the upper ground layer [-]
Z_{II} the normalized impedance of the lower ground layer [-]
k_1 the complex wave number for the upper layer [-]
t the ground layer thickness [m]

The complex wave number is calculated by employing the Delany and Bazley model for porous media, which was mentioned in section 2.3.3. The model was later modified by Miki as to obtain more accurate results at low frequencies [48].

$$k_1 = \frac{\omega}{c_0}\left\{0.160\left(\frac{f}{\sigma}\right)^{-0.618} + i\left[1 + 0.109\left(\frac{f}{\sigma}\right)^{-0.618}\right]\right\} \tag{3.35}$$

Where ω the angular frequency (see section 2.1.1) [rad/s]

The normalized impedance of a layered ground may be used in equation (3.11) to obtain the plane wave reflection coefficient. Ground attenuation is later determined by employing the method described in section 3.3.2. The effective flow resistivity of various ground surfaces that can be included as layers of forest floors, may be found in appendix F [1].

The method proposed above has been developed for double-layered ground structures and is thus not suitable for grounds consisting of more than two layers, which is often the case in forests. However, studies have shown that modelling forest floors as two separate layers, consisting of a porous upper layer and a porous semi-infinite substrate, is sufficiently accurate with models including all ground layers [54]. It should also be mentioned that once the layer thickness exceeds 0.1 m, the process can be concluded since $Z_{layer} \cong Z$ [60].

The presence of snow on a ground surface will influence the attenuation or amplification of sound during ground interaction. As was mentioned previously, a road surface covered by snow should be modelled as a double-layered medium in order to obtain accurate results. Calculations have shown that a 5 mm layer of snow on a new asphalt road will increase the amount of sound energy absorbed by an average of 11.0 dB at each out-of-phase peak value, i.e. at approximately 4,500 Hz, 9,000 Hz and 13,000 Hz etc. The flow resistivity of snow is much lower than that of asphalt, thus indicating high air content. As the reflected sound ray intersects with the

snow layer, a large part of the sound energy will be absorbed and converted to heat whereas the remaining sound is either reflected or transmitted through the medium. However, at the asphalt interface the transmitted sound will be primarily reflected by the substrate, due to the high flow resistivity of the material. A comparison of the 1/3 octave A-weighted ground attenuation of the two grounds previously mentioned, indicates a 2.4 dBA higher absorption by the snow-covered surface. Calculations also show that increasing the snow layer thickness will result in an increased ground effect, however the snow depth dependence declines at great layer thicknesses, i.e. the ground attenuation curve of a surface consisting of a 50 mm layer of snow is comparable to that covered by 100 mm of snow.
The ground attenuation curves of two asphalt roads, of which one is covered by 5 mm of snow, is shown in diagram 3.7 below.

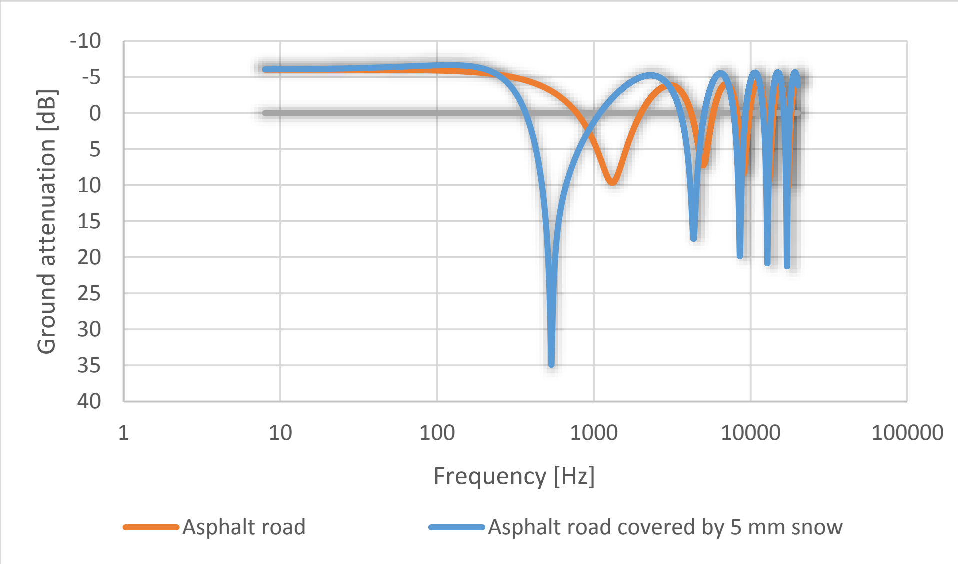

Diagram 3.7. Ground attenuation of a single asphalt road σ = 10,000 kPa · s/m^2 and an asphalt road covered by 5 mm snow σ = 29 kPa · s/m^2. Source height, z_S = 2 m and receiver height, z_R = 2 m. Distance between sound source and receiver, D = 100 m. Standard ambient conditions apply.

The calculations above demonstrate the effects a porous ground layer above a solid substrate have on the ground effect. The same structure is frequently viewed in forest floors, in which the upper layers generally comprise low flow resistivity materials, such as litter and moss, whereas the lower substrates consist of ground types that are more compact.

Sound emitted in an outdoor environment rarely propagates over a homogenous ground type, but will experience changes in the ground impedance over distance. Propagation situations involving impedance discontinuities are often referred to as *mixed ground* and should be treated differently than uniform impedance situations. In many cases the ground type between the sound source and receiver will change more than once. An example is highways with an intermediate strip of grass. The sound emitted by passing cars on one side of the highway will be affected by the acoustically hard asphalt ground as well at the acoustically soft grass lawn and the asphalt ground in the counter traffic lane, before reaching the receiver point.

Multiple impedance grounds commonly occur in situations where the sound source and receiver are positioned far apart, as is often the case of wind turbines and any surrounding residential buildings. The behaviour of sound over mixed impedance ground is illustrated with figure 3.14 below.

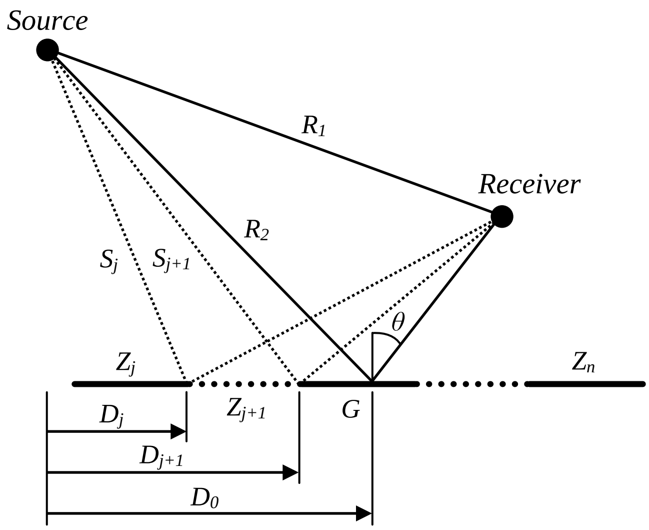

Figure 3.14. Illustration of ground attenuation in the presence of mixed ground conditions, based on [41].

The ground attenuation over mixed ground is determined similarly to that over a homogenous ground type (see appendix E), however the relationship between the complex pressure amplitude of the sound receiver and source differ and is calculated according to (3.37) [41].

$$A_{ground} = -10 \log \left| \frac{p_{receiver}}{p_{source}} \right|^2 \tag{3.36}$$

Where $$\frac{p_{receiver}}{p_{source}} = 1 + \frac{R_1}{R_2} Q_G \, e^{ik(R_2 - R_1)} + \sum_{j=1}^{n-1} \left(Q_{j+1} - Q_1\right) \frac{e^{-i\frac{\pi}{4}}}{\sqrt{\pi}} \frac{R_1}{S_j} \times \left[\mu_j F_2\left(\sqrt{k\left(S_j - R_1\right)}\right) + \gamma_j F_2\left(\sqrt{k\left(S_j - R_2\right)}\right) e^{ik(R_2 - R_1)} \right] \tag{3.37}$$

$F_2(x)$ the Fresnel function [-]
S_j the length of the source-discontinuity-receiver path for Z_j [m]
G the specular reflection point [-]
β =1/Z, the specific normalized admittance [-]

The Fresnel function as well as the constants γ_j and μ_j are determined in accordance with the relationships (3.38) to (3.40) shown below.

$$F_2(x) = \int_x^{\infty} e^{(iw^2)} \, dw \tag{3.38}$$

$$\gamma_j = \begin{cases} 1 & \text{for } D_o < D_j \\ -1 & \text{for } D_o > D_j \end{cases} \tag{3.39}$$

$$\mu_j = \begin{cases} 1 & \text{for } \beta_{j+1} < \beta_j \\ -1 & \text{for } \beta_{j+1} > \beta_j \end{cases} \tag{3.40}$$

The spherical reflection coefficient calculated at the specular reflection point Q_G is dependent on the position of G. For instance, if the specular reflection point is located on ground impedance Z_j, the spherical reflection coefficient $Q_G = Q_j$.

To simplify calculations, the Fresnel function may be expressed in terms of the complementary error function erfc (z), which was explained in section 3.3.2. The derivation is performed in appendix G and the resulting expression may be found below.

$$F_2(x) = \frac{(1+i)}{2}\frac{\sqrt{\pi}}{\sqrt{2}}\,\mathrm{erfc}\left[(1-i)\frac{\sqrt{2}}{2}x\right] \tag{3.41}$$

Contrary to the methodology mentioned in section 3.3.2, the technique above generally provides good accuracy for source-receiver dimensions other than grazing incidence. As result, the method described in this chapter is applicable for both elevated sound sources and receivers, thus making it appropriate for wind turbine noise predictions. However, in practice the method should be primarily employed while $kR_2 \gg 1$ and $|\beta| \ll 1$, meaning at large distances and preferably not over surfaces that are highly absorptive, such as snow [73].

3.4.5 Attenuation caused by vegetation

The presence of trees and plants generally has an attenuating effect on the propagation of sound. Attenuation from vegetation is partly caused by the reflection or scattering of sound by forest components such as foliage and tree trunks and partly by the absorption of sound energy from these elements. A third factor that significantly influences the attenuation of sound in forests is the particular ground structure that is modified by litter and plants, thus increasing the ground absorption as was explained in sections 3.3.2 and 3.4.4 [57].

The effects of vegetation on sound propagation may be divided into two parts, attenuation by foliage and that by tree trunks and branches. Sound attenuation by foliage is primarily caused by reflections or scattering, though sound absorption also occur due to viscous friction. Sound propagating through the tree canopy of a forest will be scattered many times before completely dissipated. As a result, the attenuation rate is often lower in forests with a small degree of foliage than that of thick greenery. Due to the complexity of sound scattering from foliage, the resulting sound attenuation is difficult to determine accurately. However, a rough estimation may be made with data of the specific tree species, according to figure 3.15 below [1] [6].

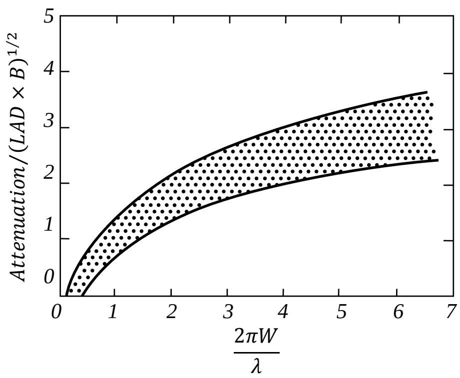

Figure 3.15. The attenuation of sound due to foliage, indicated by the shaded region. LAD is the leaf area density [m^2m^{-3}], B is the breadth of the canopy [m] and W is the leaf width [m], based on [6].

The method proposed by Aylor presents some problems when modelled since it requires deep knowledge in the characteristic of the forest species and will merely provide an approximation of the attenuation rate. However it indicates an increase in attenuation with increasing leaf width, but decreasing leaf area density and canopy breadth. The leaf area density is defined as the total one-sided leaf area divided by the tree canopy density. Consequently, maximum sound attenuation by foliage is obtained in forests with small wide leafs that are densely positioned. Furthermore, figure 3.15 suggests a high the attenuation rate for sound with small wavelengths, i.e. for high frequency sound.

As for foliage, the attenuation caused by tree trunks and branches depend on the wavelength of the emitted sound. Sound with wavelengths that are large in comparison with the tree diameter, i.e. sound within the low frequency range, will be largely unaffected by any interference and transmit through tree trunks. In contrast, high frequency sound will have wavelengths that are small compared to the trunk diameter and thus primarily scatter at the surface [6]. The transmission path for high frequency sound is thus longer than that of low frequency and sound within the high frequency range is consequently more susceptible to absorption by intersecting elements such as tree trunks. The absorption ability of tree trunks is however relatively small. In a study conducted by Reethof G et al (1977) the normal incident absorption was measured with the use of a impedance tube for six tree species; northern red oak, mockernut hickory, eastern white pine, American beech, eastern hemlock and cork oak. The results revealed an absorption coefficient of less than 10 % for all samples except for the mockernut hickory, which had a maximum absorption of 23 %. This may be due to the structure of the thick mockernut hickory bark, which consist of several layers with intermittent spaces of air. Furthermore, the study demonstrated minimum sound absorption by the American beech, which also had the least bark thickness [56].

Several models have been developed to predict the behaviour of sound when coinciding with tree trunks and canopies. Attempts have for instance been made to use Twersky's multiple-scattering theory, which models the propagation of sound through an array of identical parallel cylinders, with a surface impedance Z. The complex wave number of sound that travels through such an environment is calculated with the equation below [1].

$$k_b{}^2 = k^2 - 4iNg + (g'^2 - g^2)(2N/k)^2 \tag{3.42}$$

Where
- k_b the complex wave number of sound propagating through an array of parallel cylinders [-]
- N the average number of cylinders per unit area [m^{-2}]
- k the wave number (see section 2.1.1) [rad/m]
- g the forward scattering amplitude [-]
- g' the backward scattering amplitude [-]

The forward and backward scattering amplitude, respectively, are calculated according to the equations below.

$$g = \sum_{n=-\infty}^{\infty} A_n \qquad \text{and} \qquad g' = \sum_{n=-\infty}^{\infty} (-1)^n A_n \tag{3.43}$$

Where $$A_n = {[iJ_n(ka) + ZJ'(ka)]}\Big/{[iH_n(ka) + ZH'(ka)]} \tag{3.44}$$

A_n the scattering coefficient [-]
Z the normalized surface impedance (see section 3.3.2) [-]
a the cylinder radius [m]
J_n the Bessel function of the first kind [-]
J' the derivative of J_n [-]
H_n the Hankel function of the first kind [-]
H' the derivative of H_n [-]

A good approximation is to end the summand series once n = 1.25 ka + 7.25, beyond which extra terms have a negligible influence on the result.
Ultimately the attenuation by tree trunks and branches may be determined with (3.45) [54]. The equation merely includes the imaginary part of the complex wave number, as the real part is constant within 0.02 % and will thus have a negligible influence on the sound attenuation [69].

$$Attenuation = 20\ \mathrm{Im}(k_b) \times D_{forest}/\ln(10) \tag{3.45}$$

Where D_{forest} the distance into the forest [m]

Use of Twersky's multiple-scattering theory has resulted in varying levels of accuracy when compared with measured values. Errors are primarily caused by the fact that incoherent scattering between cylinders has not been included in the model, thus resulting in an over prediction of the attenuation rate that is mainly detectable in the high frequency range [1].
It should however be noted that Twersky's method indicates a strong frequency dependence, with the sound attenuation increasing with increasing frequency. Furthermore, the theory recognizes the relationship between the forest attenuation and configuration, by including the amount of cylinders per unit area and cylinder radius.

As previously mentioned, reflection or scattering causes sound to diverge from the direct path connecting the source and receiver. Although this commonly results in a sound pressure level decrease with distance, it has been found that the ensuing effect may be a sound amplification. Sound energy that intersect with the lower parts of a tree canopy may be reflected down towards the receiver point. The result is a negative attenuation due to vegetation, .i.e. a sound pressure level increase. This phenomenon is known as *downward scattering* and primarily occurs when both the sound source and receiver are positioned close to the ground. The degree of sound that is scattered downwards varies depending on the forest composition. A study conducted by Renterghem T.V et al (2012) for which the effectiveness of a sound barrier of vegetation towards road traffic noise was investigated, estimated the negative attenuation due to downward scattering to be between -0.8 and -0.4 dB for a light vehicle travelling at 70 km/h. The approximation was based on a 15 m deep vegetation belt, consisting of trees arranged in various periodical schemes [57].

In many situations the sound source will be positioned outside a forest, propagating to a receiver within or beyond the woodland area. During such circumstance the sound will be partially reflected at the edge of the forest, a phenomenon known as the *forest edge effect* [1]. In a study conducted by Herrington L.P (1977) sound pressure levels were measured at five positions from a point source; two outside the forest, one at the forest edge and two inside the forest. At each point, sound levels were measured at five separate heights, ranging from 5 to 45 feet. The results showed a general increase in the sound pressure level at the forest edge, which was explained by a reflection of acoustical energy. The sound level increase occurred at all heights with the exception of the 5 foot mark, for which the sound decreased. The reason for this may have been the lack of foliage at that height [33].

In conclusion from the previous text, one may deduce that the attenuating effect of foliage and tree trunks primarily occur within the high frequency range. Sound level reductions occur partly due to scattering by these elements and partly by viscous friction in the tree foliage. Studies have identified foliage as the dominant contributor for such decreases. Sound attenuation by forests for low frequency sound is however not affected by the vegetation but solely dependent on the ground effect.

Measurements performed by Price M.A et al (1988), in which the sound attenuation rate was determined for three different types of forest, suggested a linear relationship between sound level decrease by vegetation for logarithmic frequencies above 1 kHz and distance. The measurements were conducted for mixed conifers, mixed oak and spruce as well as spruce monoculture. The results are illustrated in diagram 3.8 below [1].

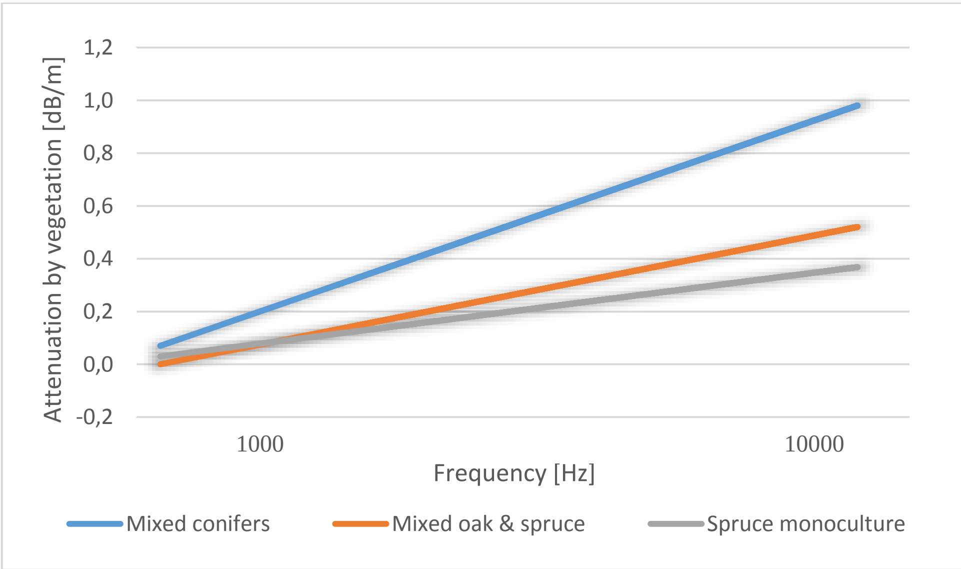

Diagram 3.8. The sound attenuation rate through three separate forest types, based on [1].

The attenuation rate through mixed conifers is considerably higher than that of the mixed oak and spruce as well as the spruce monoculture forest. At frequencies above 1,000 Hz the attenuation per meter distance from the source in the mixed conifers forest is over two times higher than the rate within both other forest types. A possible reason may be the forest density at these sites. Due to there being no independent data on planting density or tree diameter, optical visibility at head height was employed as a surrogate during the measurements. The visibility of a person clothed in white within the mixed conifers forest was less than 24 meters, however the visibility within the two other forest types was more than this, which indicates a greater tree density in the mixed conifers [72]. Research has shown an increase in noise shielding by vegetation with increasing tree density and trunk diameter. These parameters may thus have influenced the measured attenuation rates illustrated in diagram 3.8 above [13].

Similar sound measurement have also been performed by Huisman W (1990) through a pine forest. The resulting attenuation rate is linear for logarithmic frequencies within 2 kHz and 6 kHz with distance, however the sound level decrease is low in comparison with that of mixed conifers.

4 Sound measurements

The attenuation rate caused by sound propagating through an Australian forest was studied by performing several noise measurements. Since no wind turbines had been installed at the chosen site, a loudspeaker was employed to generate noise. The noise was subsequently measured at three equal distances from the source. A description of these measurements, the method employed for processing the data as well as the final results are explained in this chapter.

4.1 Site description

The *Wombat State Forest* is situated in the north western part of Victoria, Australia, extending from Daylesford to Woodend. The forest comprises approximately 45,000 hectares of land area and includes a wide variety of native fauna and flora species [40] [70]. Due to its large extent, crown cover commonly varies in different forest regions. Hence, in some parts of the forest the crown cover may be classified as open, whereas other regions are categorized as closed. The height classes also differ throughout the forest, mainly varying between tall and medium.

The Wombat State forest contains a diverse range of tall and medium sized native trees, some of which have been recorded as endangered. Common tree species include *Acacia Melanoxylon*, *Eucalyptus Obliqua*, *Eucalyptus Radiata* and *Eucalyptus Rubida*, all of which commonly grow to heights exceeding 30 m. However, the forest also comprise lower growing species, such as *Acacia Dealbata* and *Pomaderris Aspera*, which generally reaches heights of 4 – 12 m. Many of these trees are evergreen and the amount of forest foliage will thus remain virtually constant during the entire year. As was mentioned in section 3.4.1, eucalypt leafs are commonly glossy green and a long narrow shape. The same appearance applies to all tree species previously mentioned, though Acacia Dealbata leafs have a feathery form. The bark of eucalypt tree species is generally thin and peels from the trunk as it dries annually. In consequence, the tree trunk often consist of a variety of coarse scaly bark as well as smooth exposed areas where dead bark had shed off. The bark of Acacia trees is commonly smooth but deeply fissured, whereas Pomaderris Aspera generally has a bark that is more slender although some irregularities occur [49] [53].

The sound measurements were performed in an area adjacent to Campaspe Road, outside the community of Ashbourne in the northern part of the Wombat State forest. The site consists of an approximately 75 hectare plantation, managed by Hancock Victorian Plantations (HPV). The area had been recently harvested and was thus considered suitable for the open ground measurements to be performed. The neighbouring forest was deemed to have an open crown cover, due to relatively limited but not non-existent visibility through the tree canopy. The average tree height in the chosen area is approximately 20 – 25 m, hence implying a height class tall. Furthermore, the forest was considered very dense. The adjacent road and open area was not visible by a person standing 20 m from the forest boundary. The forest floor was heavily littered, covered by moss and in some areas by knee-high bushes. The entire area may be seen in figure 4.1 (a) below.

The particular site was chosen partly due to the remote location, as to assure low levels of background noise, and partly owing to good road access. Furthermore, the site offered a suitable combination of forest land and open terrain as well as virtually flat ground conditions. Since the effect of topography was not the topic under investigation, an essential aspect was to obtain a site at which ground irregularities would not be prominent enough as to affect the results. Another auspicious attribute of the chosen site was the distinct forest-open ground boundary, as it simplified the execution of the measurements. The forest edge effect and mixed ground conditions could be investigated without interference of lone trees. Lastly, the boom lift could be situated safely on Campaspe Rd during the elevated measurements owing to proximity to the forest boundary.

Measurements were performed in accordance with the points illustrated in figure 4.1 (b). The first point of each measurement sequence corresponds to the position of the loudspeaker, followed by three DUO sound pressure level meters. Points 1.1 to 1.4 are positioned within the open area. Since the plantation had been recently harvested, the ground conditions were rough but reasonably levelled, though a slight peak occurred between points 1.2 and 1.3. The aim of the open ground measurements was to obtain values of the attenuation rate within the chosen region, without influence of vegetation. As a result, measurements within the forest could be compared to those in the open field, thus providing some notion of the forest effect on sound propagation. Furthermore, the open ground measurements could offer an approximate value of the ground flow porosity, which would later be used while processing the results of the mixed ground measurements.

Measurements within the forest were conducted according to points 2.1 to 2.4. The loudspeaker was positioned on the brink of the forest. Ground conditions within the forest varied, however as previously mentioned, it was predominantly covered by litter and moss as well as large to medium-sized shrubs. Lastly, points 3.1 to 3.4 are located partly within the open area as well as at the edge of and inside the forest. The purpose of these measurements was to study sound propagation over mixed ground conditions using the methodology described in section 3.4.4 as well as to investigate the forest edge effect. The loudspeaker and DUO meters could be positioned in exact accordance with the measuring points by noting the coordinates of each point using Google Maps before commencing the measurements.

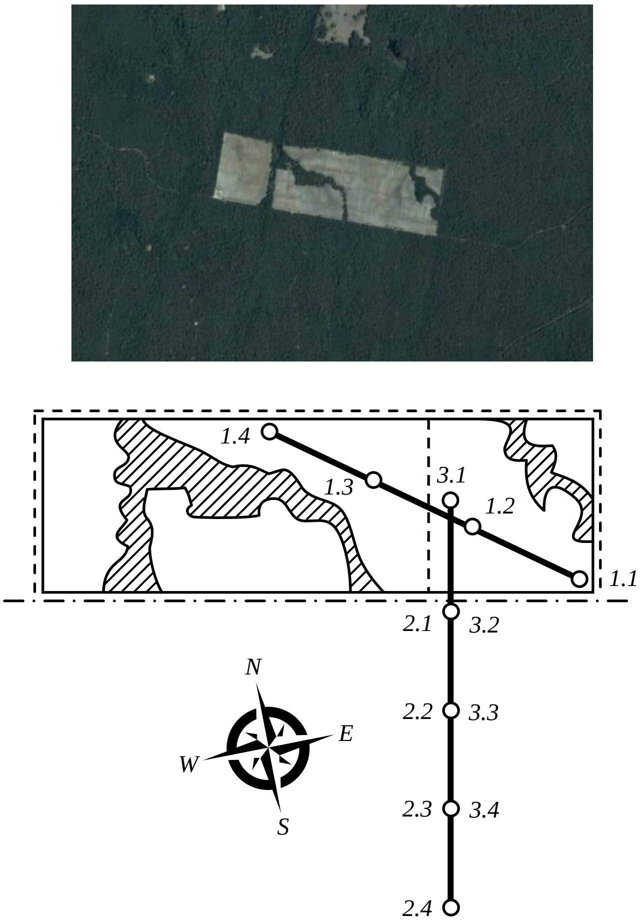

Figure 4.1. (a) Site map overview, (b) Site sketch including all measuring points.

4.2 Hypothesis

The forest area chosen for the noise measurements was considered dense, with a great variety of large and medium-small sized trees as well as some shrubs. The high density of trees suggested there would be a great level of scattering by tree trunks, hence resulting in a high attenuation rate. As was mentioned in section 3.4.5, scattering caused by noise interfering with trunks primarily affects high frequency sound. In consequence, during measurements performed close to the ground surface, the emitted noise was expected to decrease more rapidly within the high frequency range than at lower frequencies. A dominant part of the forest tree species possess thin bark of a rough fissured character, which suggests low levels of noise absorption by that element. Though in contrast, eucalypt bark partly consist of scaly layered tissue, thus indicating a high absorption coefficient similar to that of mockernut hickory, which also possess layered bark. However, it was assumed that absorption by tree trunks would not affect the results much.

A majority of the forest tree species have leafs of a long narrow shaped appearance, which indicates a low degree of attenuation due to foliage since the attenuation rate commonly increases with increasing leaf width, as was explained in section 3.4.5. Furthermore, the forest crown cover in the chosen area was deemed open, i.e. fairly dense foliage though not completely closed, which also suggests relatively low attenuation by that element. The forest foliage was hence assumed to have low influence on the propagation of the emitted sound.

As for tree trunks, sound absorption and scattering due to foliage predominantly affects high frequency sound, while noise within the low frequency range is largely unchanged. In consequence, sound attenuation of low frequency sound will primarily occur due to interaction with the ground surface. The forest floor at the chosen site was heavily littered, covered by moss and in some areas by medium-small sized shrubs. The absorbing ability of these elements was considered high and the uneven appearance of the ground surface suggested that much of the noise not absorbed by the forest floor would be scattered or reflected from the direct path of propagation, thus resulting in high levels of attenuation.

In comparison with the study conducted by Price M.A et al (1988), the forest measurements performed close to the ground surface were assumed to result in an attenuation rate comparable with or exceeding that of mixed conifers. The tree density of the mixed conifers forest, though not specified with an exact value but with optical visibility, was deemed similar to that of the Wombat State forest. Furthermore, the foliage of mixed conifers forests are dominated by needles instead of leafs, thus suggesting a very low attenuation rate by that element as was also predicted inside chosen forest area.

The behaviour of sound propagating from a point above the tree canopy is difficult to predict. Although, the forest foliage was deemed to have a small influence on the sound propagation, the glossy or semi-glossy character of a dominant part of the forest leafs may cause some degree of reflection at the tree canopy. Furthermore, the noise will be more affected by wind at high elevations than close to the ground surface. Presence of turbulence at great heights may also decrease the effects of ground attenuation as well as impacting the effective speed of sound.

However in comparison with noise emitted from a point close to the ground surface, it is believed that the attenuation caused by vegetation will be lower if the source is elevated above the forest canopy. Noise emitted by a sound source positioned close to the ground will be subject to a higher degree of low growing flora, such as shrubs and small trees, than noise generated by an elevated sound source, which may cause further attenuation of the sound.

4.3 Measurements

Noise measurements were performed at three separate occasions between May and October 2014. Although transpiring over a long period of time, the site did not change much in appearance. Since most tree species the Wombat State forest are evergreen, the amount of forest foliage and overall look remained very similar at each site visit. The sole difference between visits was a change in the ground dampness, which could have affected the absorptive ability of the forest floor and thus the ground effect. In the following section, the first period of measurements will be described as *initial*, while the following two occasions are termed *continued* and *final*, respectively.

4.3.1 Methodology

An initial methodology was formulated with the assistance of the GE team and Delphine Bard, at the Division of Engineering Acoustics, Lund University. The procedure was later refined several times in order to improve the results of the succeeding measurements period.

Initial measurements

The initial noise measurements were performed over a period of two days between 31st of May and 2nd of June 2014. Prior to commencing the measurements, the maximum level of white noise generated by the loudspeaker was recorded by the use of a sound level meter. The loudspeaker settings employed to generate such noise levels was also noted, as the same adjustments would be used during the continuation of the sound measurements.

The loudspeaker and three sound level meters were initially positioned inside the forest in accordance to measuring points 2.1 to 2.4 presented in figure 4.1 above, the distance between each point being 300 m. In addition, both the loud speaker and sound level meters were elevated to 2 m above ground. The A-weighted equivalent sound pressure level L_{eq} for 1/3 octaves was subsequently measured in one second intervals for the white noise emitted by the loudspeaker as well as for the background noise. The measurements were performed in intervals of 10 minutes and repeated three times. A weather station was also attached to the DUO sound level meter positioned closest to the loud speaker. The station had been programmed to record the ambient wind speed and direction as well as the atmospheric temperature, pressure and humidity.

The methodology was repeated for measuring points 1.1 to 1.4 and 3.1 to 3.4, during the second day. All sound pressure level meters were calibrated at the start and end of each day. The equipment arrangement inside the forest may be viewed below.

Figure 4.2. Arrangement of DUO meters during forest sound measurements. (a) 300 m. (b) 600 m.

The general characteristics of the forest were also measured, as these may influence the propagation of sound. The measurements included tree density and average trunk diameter as well as the ground conditions. The tree density was estimated by measuring the amount of trees located with a 2 m radius of each sound level meter, while the average trunk diameter was assessed by randomly measuring the circumference of 10 trees within the same area. Although this methodology did not provide a precise value, it served as an adequate estimation.

As previously mentioned, the ground structure may vary significantly within a single forest. The ground conditions within the forest considered for these measurements were thus estimated by making a 100 mm deep incision into the ground surface. The thickness of each layer constituting the forest floor were measured and categorized. The incisions were made approximately midway between the sound source and each sound level meter and thus three ground measurement were performed. The average tree height of that area was attainted from the local forest land and fire officer, at the department of environmental and primal industries.

Continued measurements

Sound measurements were resumed for two days between the 18th and 19th of October 2014. The loudspeaker settings were adjusted as to emit the same levels of white noise as in the initial measurements. The loudspeaker along with three DUO sound level meters were subsequently positioned according to points 3.1 to 3.4 in figure 4.1, all equipment was elevated to 2 m above ground. Due to relatively windy weather conditions, the distance between each measuring point was altered to 200 m. The unsteady climate was causing high levels of background noise, which could have exceeded the emitted noise levels at 900 m thus making the results unusable. Accordingly, the maximum distance was changed to 600 m.

After processing the data obtained from the initial measurements, it was found that the background noise increased slightly after each 10 minute interval. Large parts of the background noise consisted of bird song and other animal activities and it was thus considered possible that the unexpected increase was caused by the loudspeaker frightening the surrounding fauna. As a result, the continued measurements were conducted in two intervals, the background noise was measured at first for one hour followed by one hour of loudspeaker noise emissions. In both cases, the A-weighted 1/3 octave band equivalent sound pressure level was measured in one second intervals. The weather station was attached to the sound pressure level meter closest to the loudspeaker and was programmed with the setting employed in the initial measurements.
The same methodology was employed at measuring points 2.1 to 2.4 on the second day. Open field measurements were not attempted, due to unsatisfactory results from the previous occasion. All sound pressure level meters were calibrated at the start and end of each day.

Final measurements

The final noise measurements were conducted on the 29th of October 2014. The loudspeaker was positioned at the edge of the forest, denoted by 2.1 in figure 4.1, and four DUO sound pressure level meters were placed at points 2.1 to 2.4. The equipment was to be employed for two sets of noise measurements, one with the loudspeaker positioned at 2 m above ground and one with the sound source elevated to 26 m, thus exceeding the average tree height. Although the weather conditions were calm and sunny, it was unclear how the noise would behave above the forest canopy. The distance between each DUO meter was thus changed to 100 m, in order to ensure valid results.

The background noise was initially measured for one hour, followed by one hour of loudspeaker noise emissions at a 2 m height. The loudspeaker was subsequently elevated to 26 m above ground with the use of a boom lift and noise emissions were

recorded for an additional hour. During the entire period, the A-weighted equivalent sound pressure level for 1/3 octave was measured in one second intervals. The loudspeaker was adjusted to emit the same levels of white noise as previously. Furthermore, the weather station had been attached to the DUO meter positioned at point 2.1, and was thus placed on the boom lift along with the sound source.
Due to the limited availability of the lift, measurements over mixed ground conditions were not attempted. All sound pressure level meters were calibrated at the start and end of each day. The elevated loudspeaker and the view from the top of the boom lift may be seen in figure 4.3 below.

Figure 4.3. (a) The loudspeaker elevated to 26 m above ground. (b) View from the boom lift.

4.3.2 Treatment of data

The data obtained from the sound measurements was analysed with *dBTrait*, a software developed for treatment of environmental noise. DBTrait provided useful techniques of processing the measured values, including spectral time history, frequency spectrum analysis as well as coding.

As was mentioned previously, the emitted noise was measured in one second intervals, however assessment of the results under such short time periods proved difficult and the data was thus converted into the equivalent values obtained over one minute intervals. Furthermore, in order to exclude unrelated sources of noise, which could affect the accuracy of the results such as bird song or other animal activities, the data was filtered as to merely include 10% of the measured noise levels. Sound pressure levels exceeding a value L90 for 90% of each minute for the entire measurements period were thus excluded from the data. The value of L90 is commonly known as the background level and although the procedure may seem drastic it provides more accurate results, as even the lower noise levels have a high sound energy content [8]. The mentioned alterations simplified the analysis and interpretation of the results considerably, an example is shown below.

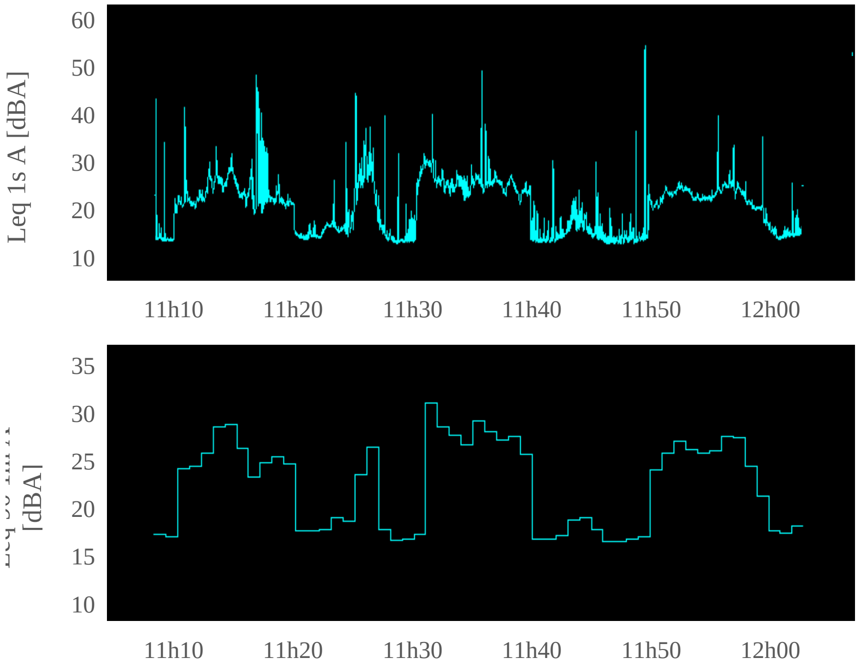

Figure 4.4. Time history for the DUO meter positioned 600 m from the loud speaker during mixed ground measurements (point 3.3). (a) Unfiltered data, one second intervals, (b) Filtered data, including 10% of measured noise levels in one minute intervals. Data was collected during the initial measurements.

Any unanticipated peaks that remained in the filtered data, such as may be seen in figure 4.5 below, were assumed to be other sources of unrelated noise, including motorbikes and bypassing cars. Such peaks were consequently eliminated from the time history.

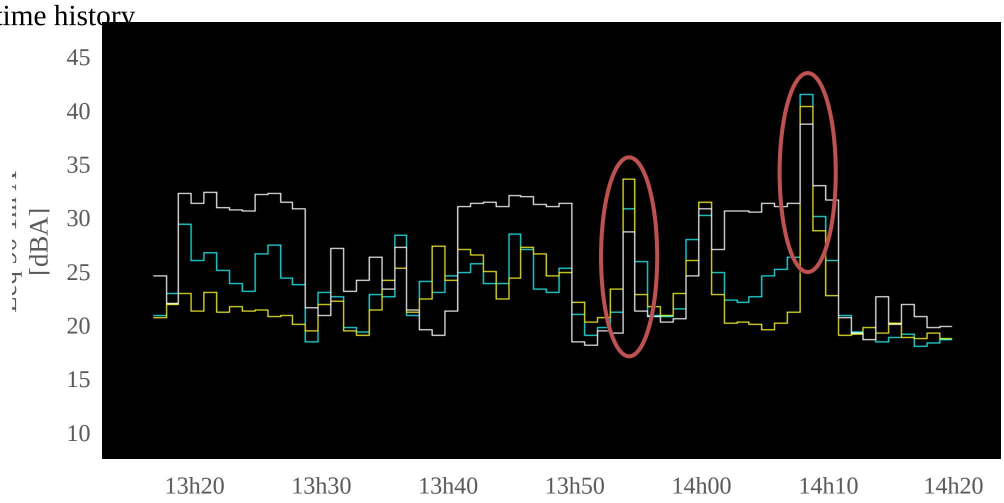

Figure 4.5. Time history for measurements performed inside the forest (points 2.2 to 2.4). The A-weighted equivalent sound pressure level for 1 minute intervals, Leq 90 1m A, versus the time period T. The white line represents the DUO meter positioned 300 m from the loud speaker, the blue line denotes the DUO positioned 600 m from the source and the yellow at 900 m distance. Data was collected during the initial measurements.

The average sound pressure level for each noise interval was calculated using functions provided in dBTrait. The procedure was performed for each 1/3 octave frequency as well as the A-weighted values, for each interval of noise emission and background noise measurements as well as for each measurement point shown in figure 4.1 (b). Since the initial measurements included a total of six 10 minute intervals, the combined average sound levels for the emitted and background noise was determined by employing equation (4.1) below [36]. This procedure was however not required for continued and final measurements data, as these were performed in single intervals.

$$L_{s+n} = 10 \log \left[\frac{1}{N} \sum_{j=1}^{N} 10^{\left(\frac{L_{i,j}}{10}\right)} \right] \tag{4.1}$$

Where L_{s+n} the average equivalent continuous sound pressure level of the emitted sound and background noise [dBA]

N the number of measurements [-]

$L_{i,j}$ the sound pressure level of 1/3 octave band *i* and measurements period *j* [dBA]

The results may be viewed as graphs in appendix H.

Once the data had been simplified and the averaged values had been obtained, miscellaneous factors causing a sound pressure level decrease could be removed from the resulting values using the techniques described in chapter 3. Factors which were deemed to have influenced the measurements include geometrical divergence, atmospheric absorption and ground attenuation. The effects of turbulence and topography were not included, due to the complexity of such calculations and the relatively even ground conditions in the area, respectively.

Although a weather station had been attached to one of the sound level meters used during the measurements, the ambient meteorological conditions were not recorded. A possible reason for this error may be a faulty installation or malfunctioning of the equipment. However, fortunately weather reports of a neighbouring area could be attained from the Australian Bureau of Meteorology.
The reliability of these reports varied depending on the weather conditions exhibited at the site each day. During the initial and final measurement, the weather reports were judged comparable to the meteorological conditions detected at the measuring site due to there being nearly no wind during these periods, which if present could have influenced the results. However, higher winds were observed during the continued measurements, thus making the meteorological reports less dependable. The presence of wind was detectable in the results as several identifiable peaks in the sound pressure level time history, which were particularly prominent in the data obtained inside the forest. In spite of this error, the weather reports obtained from the Australian Bureau of Meteorology were yet employed during treatment of data obtained during the continued measurements. Some distinct sound level peaks assumed to be caused by wind or animal activities were eliminated from the data, however due to the lack of precise weather information at the site the assumption could not be confirmed. The decreased reliability of the data obtained from the continued measurements was recognized during the analysis of the results. The weather data for each day may be found in appendix I.

The attenuation caused by sound propagation through forest including the background noise was ultimately determined using equation (4.2) shown below. As may be seen in section 4.3.3, the ambient noise levels were approximately constant inside the forest and the attenuation by vegetation factor per meter distance could thus be extracted by studying the sound pressure level decline at each point into the forest.

(4.2)

$$BG\ Noise + L_W - A_{vegetation} = L_{p,measured} - GD + A_{abs} + A_{ground}$$

The attenuation by vegetation factor obtained during each segment of sound measurements was later evaluated and combined. Using this data, a best-fit frequency dependent attenuation curve could be constructed for sound propagation through as well as above the forest.

As previously mentioned, three ground incisions were made during the initial measurements in order to study variations in the forest ground structure. Each sample was made approximately 100 mm deep and the layers constituting the ground structure was subsequently measured and classified. Using the technique described in section 3.4.4, the normalized impedance of all ground layers was subsequently calculated. To simplify these calculations, the ground incisions were assumed to consist of a maximum of two layers. The effective flow resistivity of each layer was obtained with the values specified in appendix F. Photos of the ground samples as well as simplified representations made be viewed below.

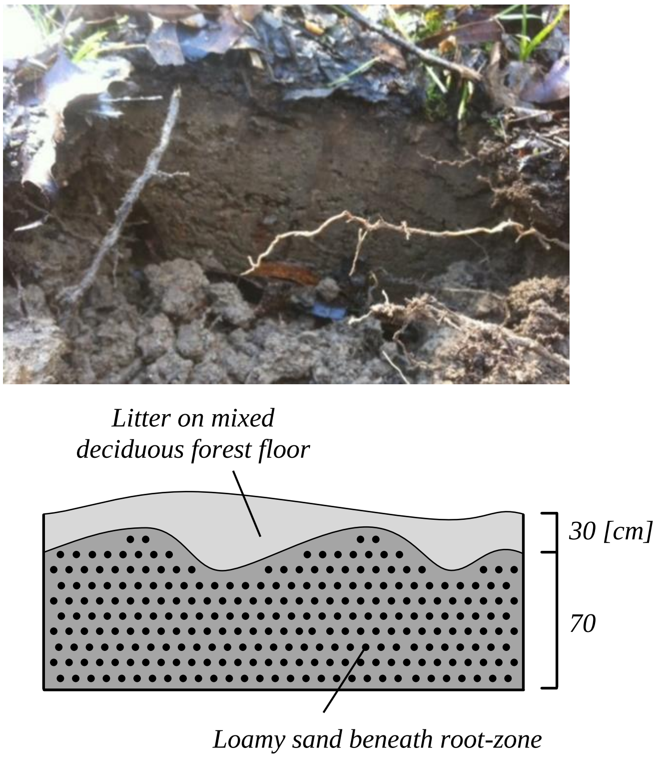

Figure 4.6. (a) Ground incisions performed at 150 m from the source.

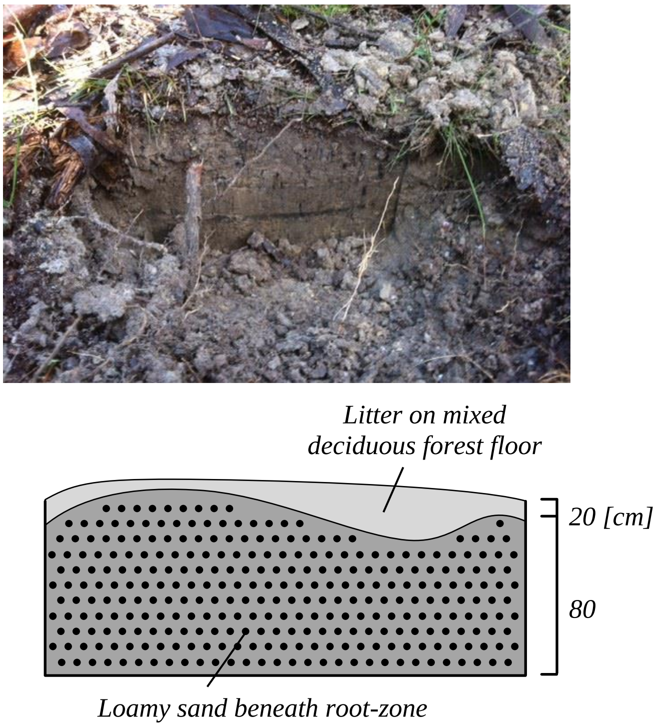

Figure 4.6. (b) Ground incisions performed during at 300 m from the source.

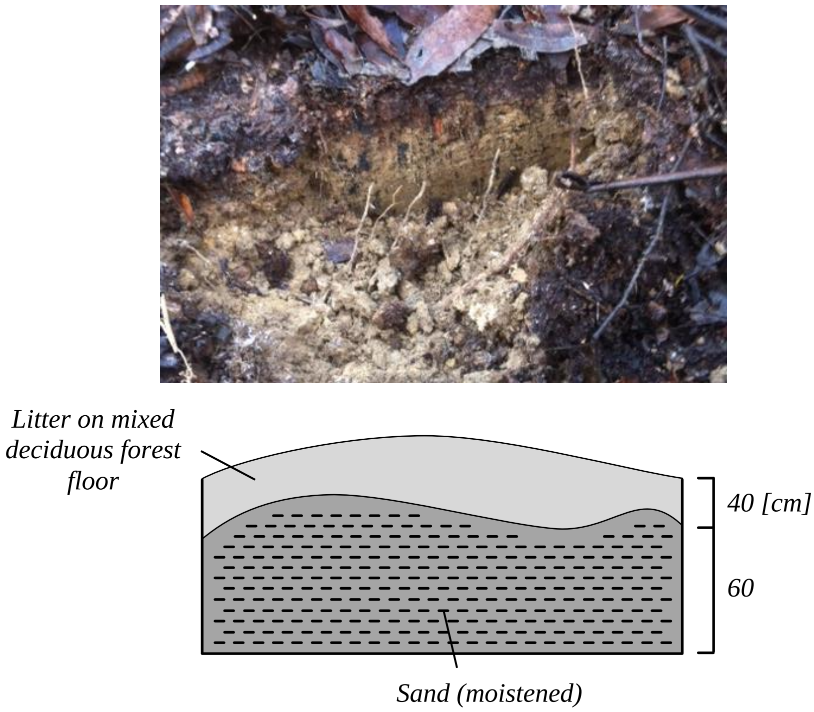

Figure 4.6. (c) Ground incisions performed at 450 m from the source.

Each layer was categorized according to the ground types found in appendix F to best ability. Small variations were found in each ground incision. The two former samples were similar in appearance, though the ground at 150 m was deemed to have a thicker layer of litter than the incision at 300 m. A great portion of these grounds consisted of a dense loamy sand, which was classified as loamy sand beneath root-zone. The sample obtained at 450 m into the forest consisted of a thick layer of ground that resembled sand, though not as dense as in the previous grounds. The layer was thus categorized as moistened sand, which has a lower flow resistivity.
During the initial measurements the grounds were very damp from preceding periods of rainfall, which increased the grounds reflective ability. However throughout the continued and final measurements the ground conditions were considerably drier, thus resulting in an overall decrease of the effective flow resistivity. The dry conditions were recognized by changing the thicker ground layers of the incisions made at 150 m and 300 m as well as 450 m to dry sand with a lower flow resistivity of 376 kPa · s/m^2 and 134 kPa · s/m^2, respectively.

Since a study of the entire ground structure of the forest floor up to 900 m could not be performed, the sample taken at 150 m was assumed to correspond to the ground structure of distances up that point, while the second sample was presumed to correspond to the forest floor between 150 m and 300 m. The ground structure at distances beyond 300 m was assumed to be consistent with the sample obtained at 450 m.

4.3.3 Results

The results from the measurements were analysed in two aspects. Firstly, the complied data was compared with the background noise but without taking into account the influence of sound level reduction factors, such as geometrical divergence and air absorption. The reason for this initial examination of the results was to verify that the sound behaved realistically, with a constant decrease with distance as well as to assure that the emitted sound was audible at all distances and not surpassed by the background noise. The measured data was also analysed with regards to various causes for attenuation but discounting the background noise. The sound pressure level reduction with distance could thus be studied and the attenuation caused by the forest extracted from the data.

Forest configuration

During the initial measurements some general forest characteristics were determined, including the tree density and average trunk diameter. The forest tree density was estimated by counting the amount of trees located within a 2 m radius of each DUO meter, i.e. within a 12.6 m^2 circle area. The average trunk diameter was determined by measuring the circumference of 10 random trees within the indicated area. The results from these measurements are presented in table 4.1 below.

Forest characteristics		Distance into the forest [m]			Average
		300	600	900	
Number of trees [-]		15	25	11	17
Tree trunk circumference [m]	1	0.30	0.20	0.15	0.58
	2	1.15	0.20	0.65	
	3	0.50	0.15	0.60	
	4	1.20	0.50	0.10	
	5	0.20	1.40	0.20	
	6	0.75	0.10	0.15	
	7	1.10	0.13	1.50	
	8	0.40	0.10	0.50	
	9	0.80	0.30	0.20	
	10	1.10	0.50	0.90	

Table 4.1. The result from forest characteristics measurements.

The obtained data indicates a relatively high forest tree density of 17 per 4 m in diameter circle, which roughly corresponds to 1.35 trees/m^2. The average tree trunk circumference inside the forest equals to approximately 0.58 m, thus resulting in a trunk diameter of 0.18 m. The results agree with observations made during the initial measurements. The forest was considered dense with a wide variety of thick and narrow tree trunks, spread evenly throughout the area. The relatively small average diameter suggests much of the inflowing sound waves will be unaffected by interaction with the forest tree trunks. In accordance with the information found in section 3.4.5, much of the sound of a wavelength exceeding 0.18 m, i.e. frequencies roughly below 2,000 Hz, will be transmitted through the tree trunks and not reflected or scattered by them.

Initial measurements

After the initial processing and simplification of measurements data as well as calculation of the combined average values, mentioned in section 4.3.2, the emitted white noise was compared with the results from the background noise measurements. The resulting A-weighted values may be viewed in diagram 4.1 below. WN denotes the white noise, while BN represents the background noise.

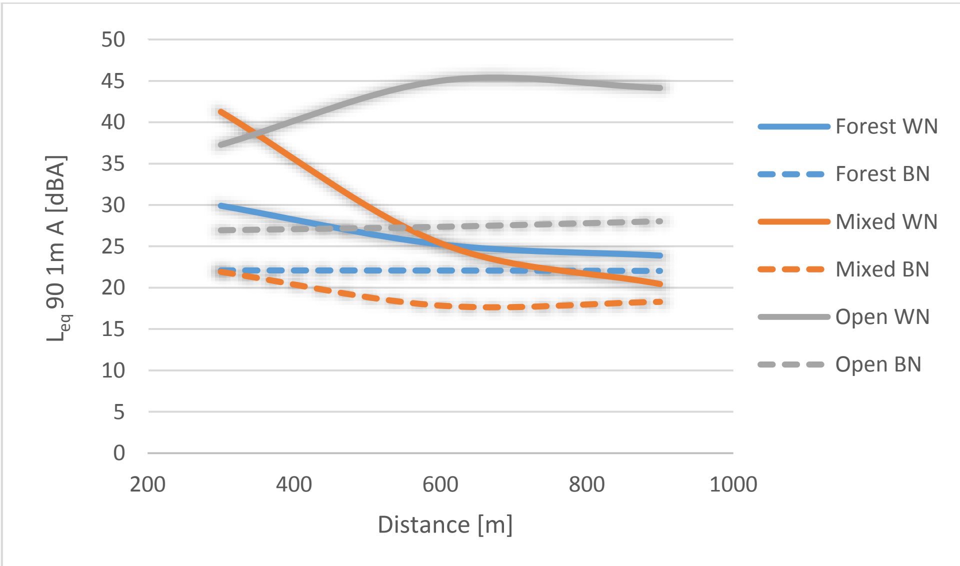

Diagram 4.1. Equivalent A-weighted results from the initial measurements.

The results from the forest and mixed ground measurements were in approximate agreement with projections performed before the measurements. The sound pressure level reduction rate with distance inside the forest is close to linear during white noise emissions, with a slight decrease after 600 m from the source. The linear appearance of the sound level regression curve may be due to the relatively uniform forest characteristics, with a close to constant tree density and evenly distributed variety of trunk dimensions. Furthermore, the ground conditions in the chosen area were relatively flat and the terrain was thus not expected to influence the sound propagation much. The sound level decrease that occur between points 2.2 and 2.3 is approximately 4.7 dBA, thus equal to 0.016 dBA/m. However, as was mentioned the rate decreases slightly after 600 m and the sound level variance is a mere 1.3 dBA between points 2.3 and 2.4, which corresponds to 0.004 dBA/m. Over the entire distance the average reduction rate is approximately 0.010 dBA/m.

The results from the mixed ground measurements indicate a rapid drop in the sound levels between 300 m and 600 m, thus verifying that some sound energy will be reflected at the edge of the forest. Based on a linear attenuation rate inside the wooded area, the forest edge effect causes a nearly 11.0 dBA reduction. It may be assumed that reduction caused by the forest edge will increase with tree density and trunk diameter, as this reduces the ability of the sound to penetrate the forest. However, since all measurements were conducted in one single area, this hypothesis could not be confirmed. The sound level reduction between measuring points 3.3 and 3.4, i.e. at 600 m into the forest, is roughly 4.9 dBA, which corresponds to 0.016 dBA/m.

The data obtained from the open field measurements provided unanticipated results, with the sound pressure levels increasing between 300 m and 600 m after which the emitted sound decreases. The reasons for the unexpected sound amplification are unclear. The hill located between measuring points 1.2 and 1.3 would theoretically cause an additional reduction of the sound levels detected at 600 m, since it places the DUO meter in a shadow zone. However, a possible explanation may be reverberation from the surrounding trees or simply an erroneous installation of the sound pressure level meter. Since the open field measurements provided unsatisfactory results they were not included in the continuation of the treatment of data.

As may be seen from diagram 4.1, the white noise emissions exceed the background noise in all three situations. Furthermore, the variance between the emitted noise and background noise decreases with distance in all cases, with the exception of the free field measurements.

The background noise remains reasonably constant at all distances, though a slight decrease occur between 300 m and 600 m during the mixed ground measurements. The background noise was generally lower inside the forest, which may be due to the calm wind conditions. High winds often cause high levels of background noise within a forest, as it instigates movement of trees and foliage. However, in contrast the forest may work as a barrier to surrounding noise during low winds. The time of day may also have influenced the noise measurements and in particular the background noise.

The open field measurements were performed early in the morning, during which bird song was audibly louder than later in the day.

Various factors that were deemed to have influenced the propagation of sound during the measurements were later predicted for each 1/3 octave band and frequencies between 6.3 Hz and 20,000 Hz. The total sound level reduction included calculation of geometrical divergence, atmospheric absorption and ground effect using a layered surface structure composed of damp ground types. These calculations were performed by employing the ambient conditions obtained from the Australian Bureau of Meteorology during the approximate time of measurements. Due to a faulty installation of the sound pressure level positioned at 300 m from the source, data of frequencies above 1,250 Hz obtained from that DUO meter was not included. The results from the mentioned calculations are summarized in appendix J. By employing equation (4.2) and the technique described in section 4.3.2 the attenuation by vegetation factor could be determined for each set of noise measurement. The results may be viewed in diagram 4.2 below.

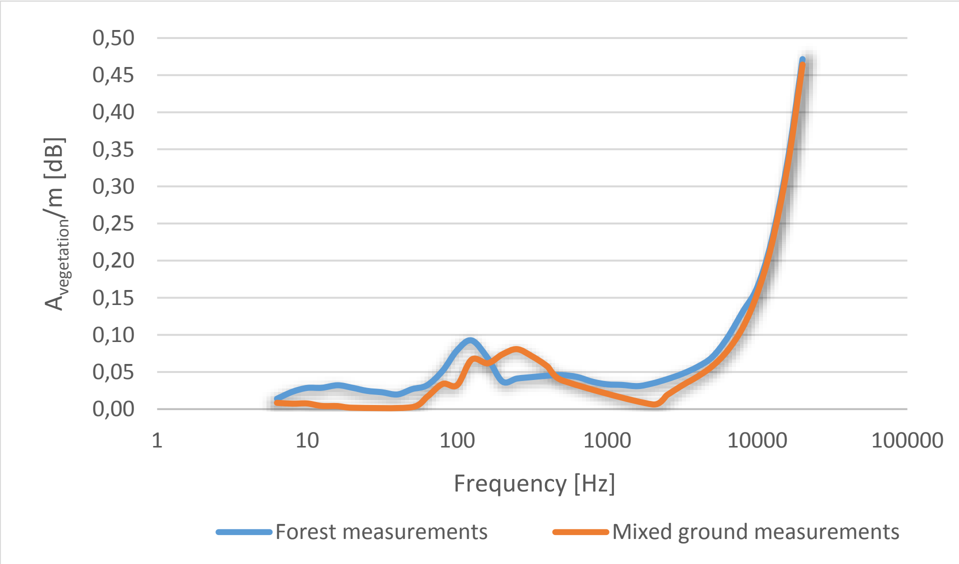

Diagram 4.2. The sound attenuation by vegetation factor per meter distance, obtained from the initial measurements.

The attenuation by vegetation factor strongly resembles an exponential curve, with merely a small deviation between 100 Hz and 500 Hz. As expected, the attenuation caused by vegetation is low for low frequency sound, while noise within the high frequency range is more affected by interaction with forest components such as foliage and tree trunks. In general, the difference in the attenuation curves obtained from the forest and mixed ground measurements is slight, with a maximum deviance

of
0.047 dB/m at 100 Hz. Furthermore, the variance between the two attenuation curves is generally greater at low frequencies, which may indicate that noise within that range is more susceptible to attenuation caused by factors such as refraction, turbulence and small changes in the ground topography, which were not included in the treatment of data. However the difference was not considered sufficiently large as to exclude any of results obtained from the initial measurements.
In conclusion it may yet be assumed that the accuracy of the attenuation by vegetation factor is greater at high frequencies than within the lower range.

During the initial measurements, the emitted white noise was also recorded at 1 m distance from the source and the loudspeaker settings were documented as to allow for the same noise to be emitted during each set of measurements. The resulting A-weighted sound level was 101.4 dBA.

Continued measurements

As previously, the data obtained from the continued noise measurements was compared with the background noise. Since the open field measurements had proved unsuccessful during the initial measurements, these were not repeated in the continued and final sets. The equivalent A-weighted results from the forest and mixed ground measurements are shown in diagram 4.3 below.

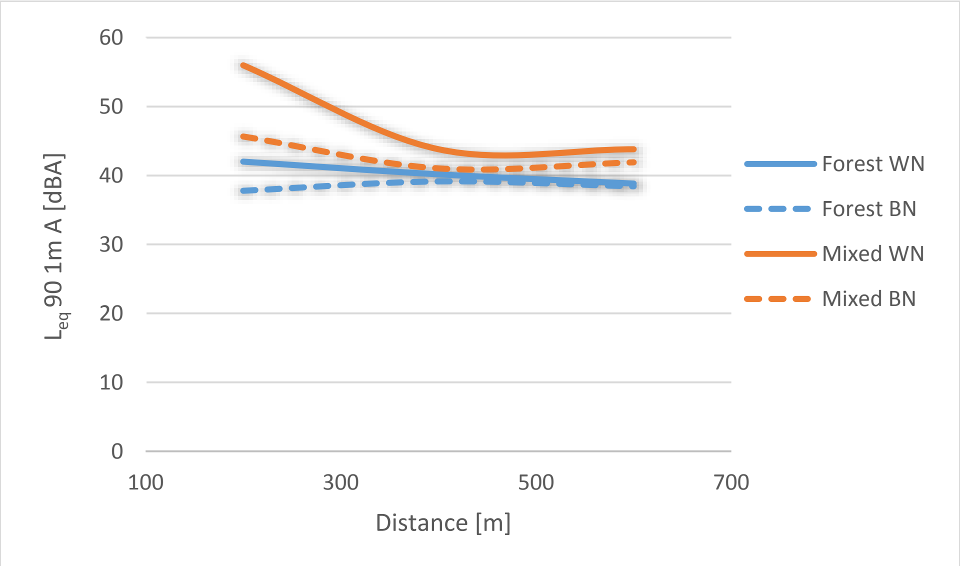

Diagram 4.3. Equivalent A-weighted results from the continued measurements.

The windy weather conditions present during the continued measurements are reflected in the results shown in diagram 4.3 above. Both the white noise and background noise measurements resulted in A-weighted values considerably higher than those obtained in the initial set. For instance, during the forest measurements the level of white noise detected at 400 m from the source was 40.2 dBA, while the A-weighted value found at a corresponding distance was a mere 28.3 dBA during the initial measurements. The latter value is based on a linear attenuation rate of 0.016 dBA/m between points 2.2 and 2.3. Similarly, the A-weighted noise level measured at 600 m into the forest is 38.8 dBA, however equivalent measurements resulted in 25.2 dBA during the initial set. The same effects are manifested in results from the mixed ground measurements.

As mentioned, the presence of wind instigates movement of trees and foliage, which increases the background noise. In diagram 4.3 above, the average A-weighted background noise inside the forest is approximately 38.5 dBA, which is 16.4 dBA higher than that found during the initial measurements, thus verifying the former statement. The increased levels of background noise can in turn cause an amplification of the recorded white noise. During periods of strong wind gusts, the background noise may exceed the emitted white noise, thus causing an erroneous increase in the averaged A-weighted value for the entire time interval. The decreased variance between the emitted white noise and background noise also attests that theory. As may be seen in diagram 4.3, the loudspeaker sound levels exceed the background noise in both situations, however the difference is considerably smaller than during the initial measurements. Furthermore, the variance decreases with increasing distances from the source. An example includes point 2.4, at which the variance is a mere 0.4 dBA. Although some distinct sound pressure level peaks, identified as wind or extraneous sound sources, had been eliminated during the treatment of data, it is expected that the white noise levels recorded at great distances may have been distorted by the high levels of background noise.

The presence of wind also influences the sound attenuation with distance. The sound pressure level reduction rate inside the forest is approximately linear, with a 0.009 dBA/m decrease between points 2.2 and 2.3 as well as 0.007 dBA/m between measuring points 2.3 and 2.4. Over the entire 600 m distance the attenuation rate is 0.008 dBA/m, hence slightly lower than during the initial measurements. During the mixed ground measurements, the A-weighted sound pressure level drops 12.2 dBA between 200 m and 400 m as a result of the forest edge effect. However, beyond 400 m the sound attenuation ceases and the measured sound levels remains constant for 200 m. It is possible that the background noise exceeded the emitted white noise for a part of the measuring time at 600 m from the source, thus causing an amplification of the noise at that point.

As during treatment of the initial data, various factors causing a reduction of the measured sound levels were calculated and employed in equation (4.2) in order to extract the attenuation by vegetation factor. Ambient conditions were obtained from the Australian Bureau of Meteorology and data from the entire frequency range was analysed. The results are shown in diagram 4.4.

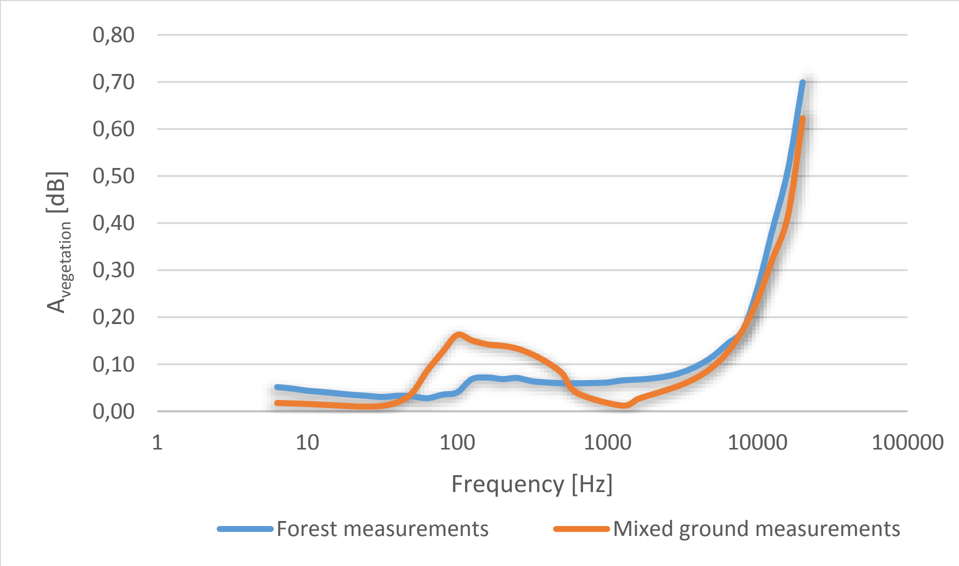

Diagram 4.4. The sound attenuation by vegetation factor per meter distance, obtained from the continued measurements.

The appearance of the attenuation curve resembles that acquired during the initial measurements. The unexpected increase in attenuation by vegetation between 100 Hz and 500 Hz found in the initial set is also exhibited in the measurements performed over mixed ground conditions, though not in the forest measurements. The reason for the increased attenuation is unclear, however a possible explanation may be a constructive or destructive interference between the direct and reflected sound waves at that particular distance and frequency range, which do not occur at the other measuring points thus causing a sound level variance.

As during the initial measurements, the difference between the attenuation curves obtained from forest and mixed ground measurements is greater within the low frequency range, with a maximum variance of 0.122 dB/m at 100 Hz, which is significantly higher than during the previous set of measurements. Furthermore, in comparison with the results attained during the initial measurements, the attenuation is considerably higher at high frequencies. A likely reason is the windy weather conditions exhibited during the continued measurements, which caused an increase of the background noise levels that also varied slightly with distance.

Final measurements

During the final measurements, white noise recordings were performed inside the forest with the use of a ground based as well as an elevated sound source. As a result of the unsatisfactory results attained from the previous set of measurements, the distance between each DUO meter was altered to 100 m. Diagram 4.5 comprise the results from the final measurements as well as the background noise recorded at the site.

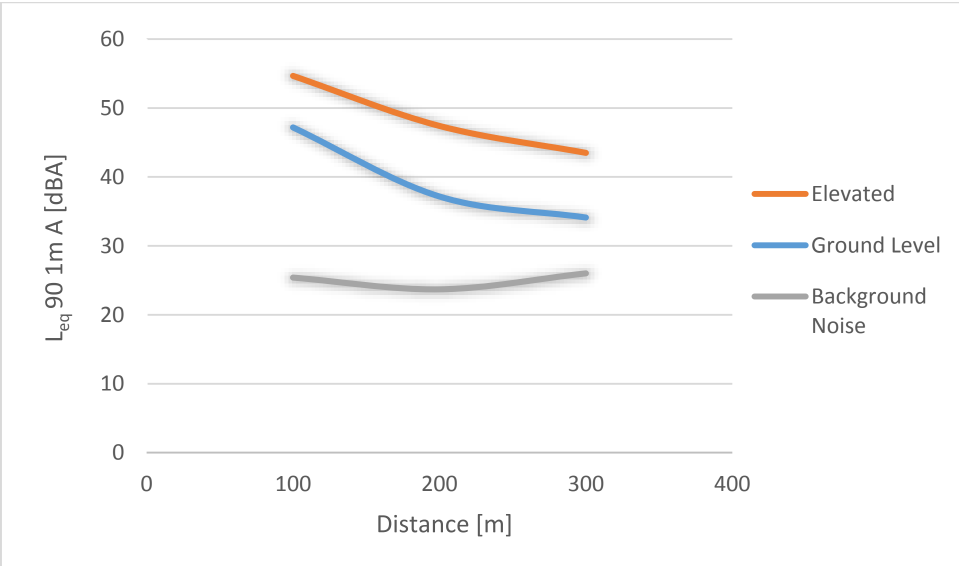

Diagram 4.5. Equivalent A-weighted results from the final measurements.

The attenuation curves of both the ground based and elevated measurements are consistent with the expected behaviour of the emitted white noise. The measurements performed using a sound source positioned at 2 m above ground, indicated with blue in diagram 4.5, result in a sound level reduction rate that is roughly linear. However, alike the noise regression curve obtained during the initial forest measurements, the attenuation rate decreases slightly after measuring point 2.3. The appearance of the curve is likely the result of geometrical divergence, which causes rapid sound level reductions close to the sound source but stabilizes at greater distances. Between points 2.2 and 2.3, the equivalent A-weighted sound level is reduced by 10.0 dBA, which is equivalent to 0.10 dBA/m. Though beyond 200 m, the attenuation rate decreases and the variance is a mere 3.0 dBA, i.e. 0.03 dBA/m. Over the entire 300 m distance, the sound reduction rate is approximately 0.065 dBA/m.

The results obtained from the elevated measurements suggest that the forest presents less of a noise barrier when the sound source is positioned above the tree canopy. The A-weighted noise levels recorded during the elevated measurements are on average

9.0 dBA higher than those obtained in the ground based set. The reason is likely that sound propagating from a point above the forest canopy will not experience reflection by the forest edge to the same extent as a source positioned at ground level. The appearance of the sound regression curve from the elevated measurements is largely consistent with that obtained during the ground based set. Between points 2.2 and 2.3, the attenuation rate is approximately 0.073 dBA/m, hence lower than that obtained in the ground based measurements. However, between 200 m and 300 m into the forest the A-weighted sound level drops by 3.9 dBA, which is equivalent to a reduction rate of 0.039 dBA/m, thus higher than the previous set. Over the entire 300 m distance the attenuation rate is 0.056 dBA/m, which is slightly lower than during the ground based measurements, though the difference is negligible.

As may be comprehended from diagram 4.5, the background noise is exceeded by the emitted white noise both during the ground based and elevated measurements. The background noise remains at a relatively constant level throughout the forest, with an average A-weighted value of 25.0 dBA, which is similar to that recorded during the initial measurements.

Alike the previous sets of measurements, the attenuation by vegetation curve was extracted from the data with the use of the methodology described in section 4.3.2. The entire frequency range was included in the calculations and the results may be found in diagram 4.6 below.

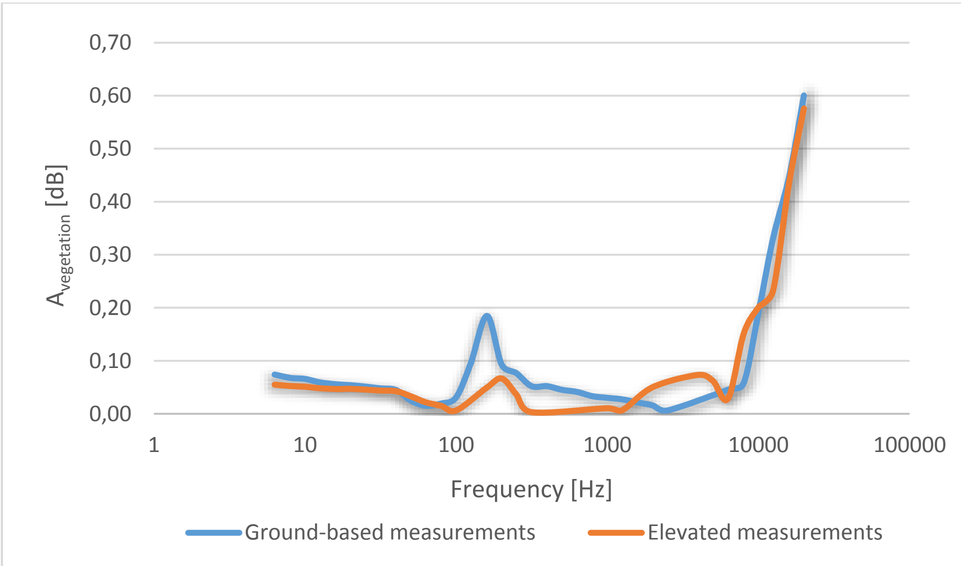

Diagram 4.6. The sound attenuation by vegetation factor per meter distance, obtained from the final measurements.

The attenuation by vegetation curve of the ground based measurements resembles that obtained during the preceding sets, although being slightly higher at very low frequencies. As previously, the attenuation also increases between 100 Hz and 500 Hz, which may be the result of ground effect. The attenuation at high frequencies is also higher than that observed in the initial measurements, for which the reasons are unclear.
Although complying with the exponential behaviour exhibited in the initial and continued sets, the attenuation curve obtained during the elevated measurements is irregular in appearance. A possible explanation may be that the emitted white sound was affected by turbulence, which often is more prominent at high elevations. However, the irregularity may also be result of some error made during the treatment of data in dBTrait. When compared with the ground based measurements, the attenuation curve obtained from the elevated set is in approximate agreement, though slightly lower in both the low and high frequency range.

4.3.4 Combined results

In conclusion of the data obtained from all measurements, one may deduce that the attenuation by vegetation with frequency curve behaves similarly in all three situations. The attenuation rate is low for sound within the low frequency range but increases exponentially at higher frequencies, which was also projected before commencing the measurements. However, the size of the attenuation factor varies slightly in all three cases. The factor obtained from the initial measurements is slightly lower than that found during the continued and final sets, primarily within the high frequency range. The reason for the deviance is unknown, but may be due to the weather conditions present during the time of these measurements, which varied from those exhibited later in the measurements campaign. In contrast, the attenuation factor extracted from the continued measurements is slightly elevated for high frequencies in comparison to that obtained in the initial and final sets. This is likely a result of the high winds exhibited during the time of the measurements, which is likely to have caused an amplification of the sound at some distances. Furthermore, the variance between the attenuation factor attained from the forest and mixed ground measurements is significantly higher than during the initial set. Although the difference is not immense, it was considered sufficient as to exclude the data obtained from the continued measurements from the combined attenuation factor.

Assessment of the attenuation caused by vegetation using a ground based source in relation to an elevated source provided unexpected results. Although the attenuation curve is lower when the source is elevated above the forest canopy for a majority of the frequency range, the difference is trivial. In general, the attenuation factor of both cases follows a similar curvature. However during comparison of the A-weighted measurements data that was obtained from that period, shown in diagram 4.5, the variance between noise propagating from a ground based and elevated sound source is on average 9.0 dBA, which is a substantial number. In conclusion from this information it was deduced that the difference is not caused by the absorbing ability of the wooded area, but by noise reflection at the forest edge. A higher amount of sound will thus be reflected by the edge of the forest if the sound source is positioned at a point that allows the sound to interfere with the edge of the forest instead of the canopy. It is however likely that some noise will also be reflected by the forest canopy. While comparing the results of the forest and mixed ground measurements obtained during the initial set, it was found that approximately 11.0 dBA of the emitted white noise had been reflected by the edge of the forest, which indicates a variance of roughly 2.0 dBA. However, that number was acquired by assuming a linear noise regression curve, which is unlikely in reality due to geometrical divergence. It is thus assumed that any reflection caused by the forest canopy may be disregarded.

Computation of a sound attenuation factor caused by vegetation was performed by calculating the mean value of all data acquired from the initial and final sets of measurements. A best-fit exponential attenuation curve was later calculated by employing the values for frequencies 6.3 Hz, 10,000 Hz and 20,000 Hz, resulting in equation (4.3) shown in table 4.2.

$y = m + kx^a$				
x	y	a	k	m
6.3	0.038	1.808	8.199×10^{-9}	0.038
10,000	0.178			
20,000	0.528			
$A_{vegetation} = 0.038 + 8.199 \times 10^{-9} f^{\,1.808}$ (4.3)				

Table 4.2. Calculation of best-fit attenuation by vegetation curve.

The attenuation by vegetation with frequency for all included measurements as well as the average values and the best-fit curve may be viewed in diagram 4.7 below.

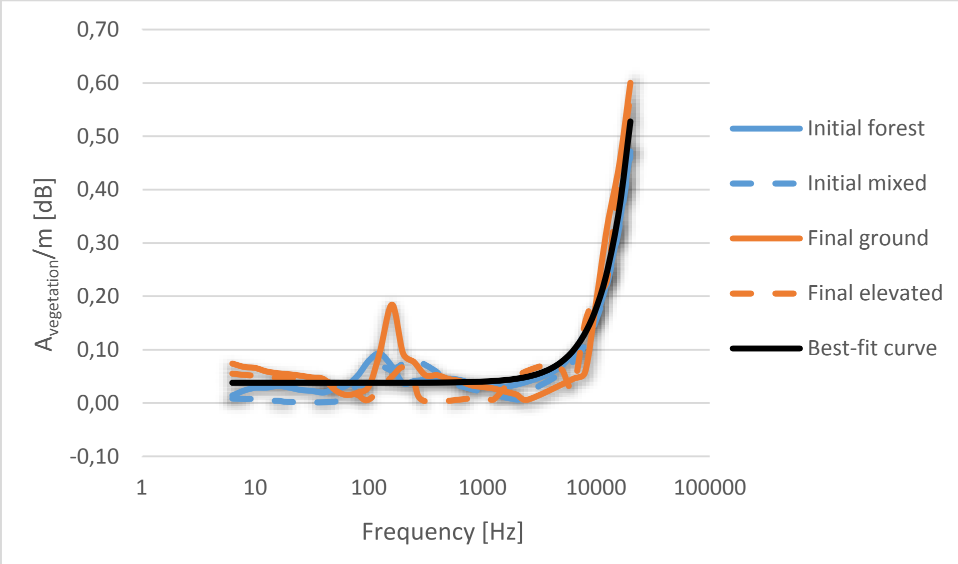

Diagram 4.7. The attenuation by vegetation factor per meter distance as a function of frequency.

5 Sound propagation model

The final calculation model will be outlined in this chapter. Decisions and generalisations made during the development of the model will be discussed, including choice of software, implementation and compilation of attenuation factors and input variables as well as design of the model interface.
Some propagation prediction methods that are commonly employed to calculate the sound attenuation from wind turbine noise sources will also be introduced and their limitations discussed. Furthermore, this chapter will examine methods of treating the various causes for attenuation used by these models.

5.1 Current prediction models

Several models have been developed to predict the propagation of sound in outdoor environments. Methods regularly treat the various causes for sound attenuation differently depending on the source type intended for the particular model. Three prediction models commonly used for wind turbine sound sources are the ISO 9613-2 international standard, CONCAWE and Nord2000 model.

5.1.1 ISO 9613-2 Model

The ISO 9613-2 international standard is an empirically based model, which was developed in 1996. The model predicts the equivalent continuous A-weighted sound pressure level detected at the receiver point for 1/1 octave band, assuming a known source sound power level. Calculations may be performed for source-receiver distances of up to 1,000 m. In case the sound power level for each octave band is unspecified, but merely the A-weighted sound power of the sound source is available, the standard recommends using attenuation values for 500 Hz.
The ISO 9613-2 was intended to form a link between existing prediction methods that are specified for a particular type of source, such as machinery or industrial plants. Consequently, the standard may be employed for a wide range of point sources, individually or as an assembly, that are ground-based. Examples include road or rail traffic, industrial sites and construction activities.

The model is however not applicable for aircraft sound sources, mining, military operations or similar activities [1] [38].

The equivalent continuous downwind sound pressure level for eight 1/1 midpoint octave bands ranging from 63 Hz to 8 kHz is determined with the following expression.

$$L_{fT}(DW) = L_W + D_C - A \tag{5.1}$$

Where $A = A_{div} + A_{atm} + A_{gr} + A_{bar} + A_{misc}$ (5.2)

$L_{fT}(DW)$	the equivalent continuous downwind octave-band pressure level [dB]
L_W	the octave-band power level [dB]
D_C	the directivity correction [dB]
A	the octave-band attenuation [dB]
A_{div}	the attenuation due to geometrical divergence [dB]
A_{atm}	the attenuation due to atmospheric absorption [dB]
A_{gr}	the attenuation due to ground effect [dB]
A_{bar}	the attenuation due to a barrier [dB]
A_{misc}	the attenuation due to miscellaneous other effects, including forests, industrial sites and housing [dB]

As previously mentioned, the sound field generated by a point source will propagate uniformly in all directions. However, in reality the sound field will be affected by many external factors which impact the directivity of the sound. The directivity correction is used to account for any deviations from the theoretical omnidirectionality of a point source. The ISO 9613-2 standard determines the directivity correction according to equation (5.3) below [38].

$$D_C = D_1 + D_\Omega \tag{5.3}$$

Where D_1 the directivity index [dB]
D_Ω an index that corrects the propagation of sound in solid angles that are less than 4π steradians [dB]

The correction index D_Ω is included to account for the sound power level increase that occur due to reflections by the ground surface near the source. It is calculated with the following expression.

$$D_\Omega = 10\log\left\{1 + \left[{d_p}^2 + (h_s - h_r)^2\right] / \left[{d_p}^2 + (h_s + h_r)^2\right]\right\} \tag{5.4}$$

Where h_s the height of the source above ground [m]
h_r the height of the receiver above ground [m]
d_p the source-receiver distance projected onto the ground plane [m]

The ISO 9613-2 standard distinguishes between short-term and long-term predictions, i.e. sound pressure levels for a given day and that averaged over a month or year respectively, by including a meteorological correction. Long-term predictions are calculated with equation (5.5) below [38].

$$L_{AT}(LT) = L_{AT}(DW) - C_{met} \tag{5.5}$$

Where $L_{AT}(LT)$ the long-term average A-weighted sound pressure level [dBA]

$L_{AT}(DW)$ the equivalent A-weighted downwind sound pressure level [dBA]

C_{met} the meteorological correction [dBA]

A particular site may be subject to weather conditions that are favourable or unfavourable to sound propagation. The meteorological correction allows for such factors to influence the average A-weighted sound pressure level. However the ISO 9613-2 meteorology predictions merely apply for downwind or inversion conditions, meaning situations where the wind direction corresponds that of the source-receiver path or the temperature gradient is positive, hence causing downward refraction. The standard will thus allow for worst case predictions to be made. The meteorological correction is calculated with the following equation [1] [38].

$$C_{met} = \begin{cases} 0 & \text{if } d_p \leq 10\ (h_s + h_r) \\ C_0\left[1 - 10(h_s + h_r)/d_p\right] & \text{if } d_p > 10\ (h_s + h_r) \end{cases} \tag{5.6}$$

Where C_0 a constant [dB]

The meteorological constant C_0 depends on the local meteorological statistics for wind speed and direction as well as temperature gradients. The constant range between 0 and +5 dB, however values exceeding +2 dB are rare.

Ground attenuation

The ISO 9613-2 standard predicts the sound attenuation due to ground interaction based on the assumption that the ground effect is primarily affected by floor surfaces close to the source and receiver. Consequently, three separate ground regions may be identified; the source, receiver and middle region. All three zones are shown in figure 5.1 below.

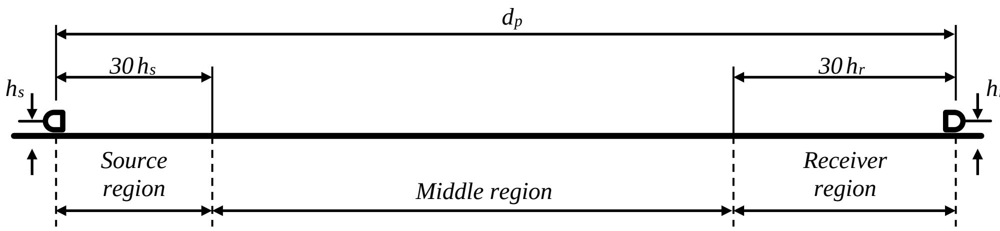

Figure 5.1. Dimensions employed for determining the ground attenuation, based on [38].

The ground attenuation is mainly affected by the ground properties of the source and receiver regions and less dependent on the attenuating or amplifying ability of the middle region. The acoustical properties of the ground surface is determined by the ground factor G, which has been divided into three categories; hard, porous and mixed ground. *Hard ground* indicates ground surfaces with a low flow porosity, including paving, water, ice and concrete. The ground factor for such surfaces is G = 0. Tampered ground, which is common within industrial areas, may also be considered hard. *Porous ground* includes grassland, trees, vegetation and farmland and has ground factor G = 1. *Mixed ground* denotes surfaces consisting of both hard and porous ground. For such surfaces the ground factor ranges from 0 to 1, depending on the fraction of each ground type within the region.

The ground attenuation is ultimately determined as an accumulation of the ground effect of each region, it is thus calculated with the following expression.

$$A_{gr} = A_s + A_r + A_m \tag{5.7}$$

Where A_s the ground attenuation for the source region, given by ground factor G_s [dB]

A_r the ground attenuation for the receiver region, given by ground factor G_r [dB]

A_m the ground attenuation for the middle region, given by ground factor G_m [dB]

The ground attenuation for each surface region is calculated according to formulas found in appendix K.

The ISO standard also provides an alternative method of determining the ground attenuation. The calculation method may only be employed under three specific conditions; the A-weighted sound pressure level is of interest, the sound propagation occur over porous ground or mixed ground predominantly consisting of porous surface and the sound is not a pure tone.

$$A_{gr} = 4.8 - \left(\frac{2h_m}{d}\right)\left[17 + \left(\frac{300}{d}\right)\right] \geq 0 \qquad (5.8)$$

Where h_m the mean height of the propagation path above ground [m]
d the radial distance from the source to receiver [m]

Attenuation by vegetation

Sound attenuation due to propagation through foliage is included in the ISO 9613-2 standard merely in situations of dense vegetation. As illustrated in figure 5.2 below, the propagation path simulates a circular arc and consequently attenuation by foliage will merely occur near the source, the receiver or both. Sound propagation distances close to and receiver, i.e. d_1 and d_2 respectively, may be determined by assuming the arc radius to be 5 km. Alternatively, these distances may be viewed as straight lines inclined by 15^o from the ground surface.

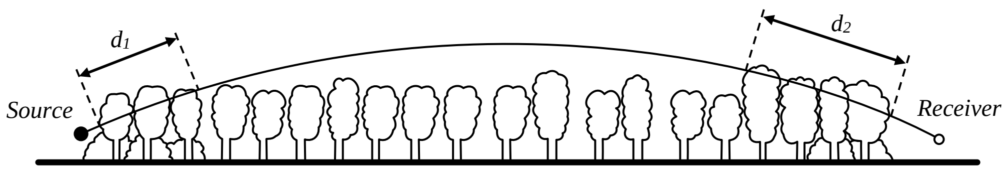

Figure 5.2. Attenuation by vegetation according to the ISO 9613-2 standard [38].

The attenuation factor for each 1/1 midpoint octave band is given in table 5.1 below. The propagation path distance trough foliage d_f is the combined length of d_1 and d_2.

Propagation distance d_f [m]	Nominal midband frequency [Hz]							
	63	125	250	500	1,000	2,000	4,000	8,000
$10 \leq d_f \leq 20$	Attenuation [dB]:							
	0	0	1	1	1	1	2	3
$20 \leq d_f \leq 200$	Attenuation [dB/m]:							
	0.02	0.03	0.04	0.05	0.06	0.08	0.09	0.12

Table 5.1. Attenuation of sound due to propagation a distance d_f through dense foliage for 1/1 octave band [38].

Limitations with the ISO 9613-2 model

Although the ISO 9613-2 prediction method represents an international standard, it has received much criticism. The model has for instance been criticized for being empirically based, due to it thus being primarily applicable for the particular sites at which the data was attained. Furthermore, much research on the topic of sound propagation has enabled prediction methods to be constructed based on theoretical formulas, hence allowing for good accuracy at great variety of sites. As previously mentioned, the ISO standard may be employed for a wide variety of ground-based point sources, including rail traffic and construction activities. However, the empirical data on which the prediction model was developed has merely been validated for certain industrial sites. The reliability of the model has consequently been questioned [1].

The ISO 9613-2 method of predicting the ground effect has also been subject to some critique. The model treats the attenuation or amplifying effect of ground interaction by dividing the source-receiver distance into three segments; close to the source, receiver as well as a middle section. The ground effect is later determined by combining the attenuation of each segment. This technique of calculating the ground effect does however present some problems. For instance, the attenuation for midrange frequencies above 2,000 Hz are assumed negligible for porous ground, i.e. for grassland and forest floors, and is furthermore independent of the source and receiver heights. However, as was demonstrated in section 3.3.2 the ground attenuation at these frequencies are clearly perceptible.

Furthermore, the standard employs a ground factor G to distinguish the absorbing or reflecting ability of the ground surface. In consequence, all ground types with low flow resistivities are assumed completely absorbing, whereas all high flow resistivity ground types are viewed as entirely reflective [1].

According to the ISO 9613-2 standard, foliage has a small attenuating impact on sound propagation and should merely be considered for dense vegetation. The definition of what classifies as dense is however poor and consequently subject to misinterpretation.
The ISO prediction method recognizes a low attenuation rate due to vegetation for low frequency sound, which corresponds to the information found in section 3.4.5. However, it does not consider the predominantly scattering effect of tree trunks and nor does it account for the average tree height or trunk diameter.

5.1.2 CONCAWE Model

CONCAWE (Conservation of Clean Air and Water in Europe) is an organisation that aims to investigate various issues associated with the oil industry. Areas of handling include fuel quality and emissions, air and water quality, soil contamination, waste as well as occupational health and safety etc. The group was established in 1963 and comprise most oil companies in Europe [20]. In 1981 CONCAWE published a noise prediction model for sound propagation from petroleum and petrochemical plants, which has since been the basis for many other noise models intended for various sound sources [51].

The CONCAWE model was constructed on theoretical formulas as well as field data, collected over a four year period. Sound measurements were performed at three separate petrochemical process plants of varying size in Europe. A variety of meteorological conditions were recorded during the measurements procedure, which was conducted at 1.2 meter height at distances of 800 m to 3,300 m from the source. Between 16 and 203 noise sources were identified within the plants [45].

The CONCAWE propagation model predicts noise levels for 1/1 octave bands from 63 Hz to 4,000 Hz at distances up to 1,100 m. The model is not to be used for source-receiver distances below 100 m. The sound pressure levels detected at the receiver point is calculated with the following expression [45].

$$L_p = L_W + D - \sum K \tag{5.9}$$

Where $$\sum K = K_1 + K_2 + K_3 + K_4 + K_5 + K_6 + K_7 \tag{5.10}$$

L_p	the sound pressure level [dB]
L_W	the sound power level [dB]
D	the directivity index [dB]
K_1	the attenuation due to geometrical spreading [dB]
K_2	the attenuation due to atmospheric absorption [dB]
K_3	the attenuation due to ground effect [dB]
K_4	the meteorological correction [dB]
K_5	the source and/or receiver height correction [dB]
K_6	the attenuation due to a barrier [dB]
K_7	the attenuation due to in-plant screening [dB]

Although the directivity index is included in equation (5.9), CONCAWE recommends employing a value of D = 0 as an initial approximation [45].

As for the ISO 9613-2 international standard, the CONCAWE model recognizes the attenuating or amplifying effect of refraction caused by the wind and temperature gradients. The meteorological correction is divided into six categories, dependent on the atmospheric temperature and average wind conditions at the particular site. The atmospheric temperature gradient is assessed using the Pasquill stability categories, shown in table 5.2. Classification is performed by entering approximate values of solar radiation or cloud cover, depending on the time of day, as well as the average wind speed. The cloud cover is measured in units of oktas, by which a minimum value of zero indicates a completely clear sky and maximum of eight denotes a sky entirely covered by clouds [45].

Wind speed * [m/s]	Day-Time Incoming Solar Radiation [mW/cm^2]				1 hour before sunset or after sunrise	Night-Time Cloud Cover [okta]		
	60	30 – 60	< 30	Overcast		0 – 3	4 – 7	8
≤ 1.5	A	A – B	B	C	D	F/G **	F	D
2.0 – 2.5	A – B	B	C	C	D	F	E	D
3.0 – 4.5	B	B – C	C	C	D	E	D	D
5.0 – 6.0	C	C – D	D	D	D	D	D	D
6.0	D	D	D	D	D	D	D	D

* Wind speed is measured to the nearest 0.5 m/s.

** Category G is restricted to night-time with less than 1 okta of cloud and a wind speed less than 0.5 m/s.

Table 5.2. Pasquill (meteorological) stability categories [45].

Although the Pasquill categorization requires the entry of average wind speed, it has been found that additional classification is required to obtain a reliable meteorological correction, a reason of which being that the wind direction is not specified in the Pasquill categories. Furthermore, category D is identified as equivalent to meteorologically neutral conditions, i.e. a logarithmic wind gradient and negligible temperature profile, despite of including a wide range of wind speeds as may be seen in table 5.2 [1].

The CONCAWE meteorological categories may be found in table 5.3 below. A positive wind speed indicates that the wind is blowing from the sound source towards the receiver, while negative values denote the reverse. Acoustically neutral conditions are applied in category 4.

Meteorological Category	Pasquill Stability Category		
	A, B	C, D, E	F, G
1	v < – 3.0	–	–
2	3.0 < v < – 0.5	v < – 3.0	–
3	0.5 < v < + 0.5	3.0 < v < – 0.5	v < – 3.0
4 *	+ 0.5 < v < + 3.0	0.5 < v < + 0.5	3.0 < v < – 0.5
5	v > + 3.0	+ 0.5 < v < + 3.0	0.5 < v < + 0.5
6	–	v > + 3.0	+ 0.5 < v < + 3.0

* Category with assumed zero meteorological influence.

Table 5.3. CONCAWE meteorological categories [45].

Once the meteorological class has been identified, the correction due to refraction is determined with various attenuation curves, which vary with frequency as well as distance from the source. The meteorological correction of category 1 for 1/1 octave bands is shown in diagram 5.1 below.

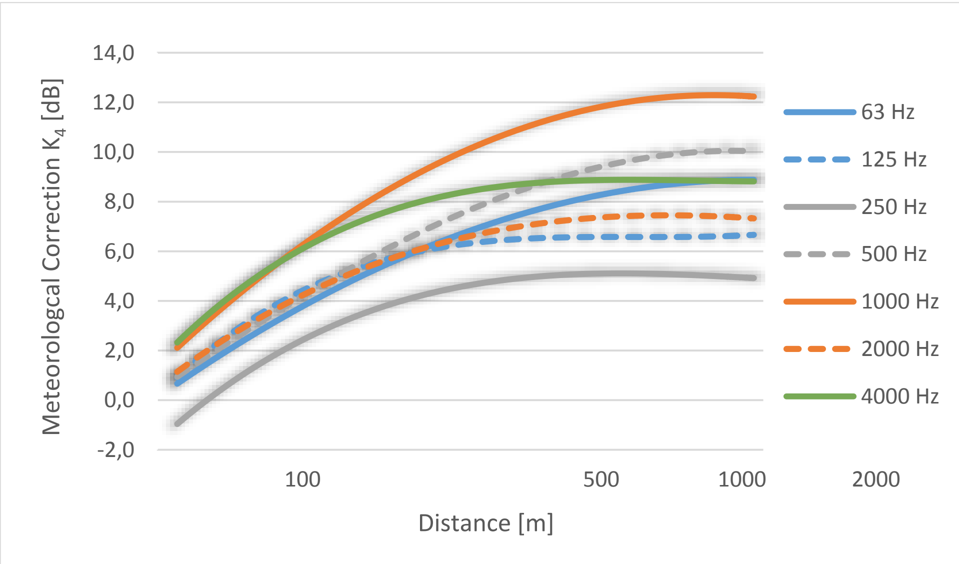

Diagram 5.1. The meteorological correction curves for CONCAWE category 1.

In order to predict the propagation of sound generated by elevated sources, as are common in large industrial and construction plants, the CONCAWE model incorporates a source and receiver height correction. As the ground effect is a function of the reflection angle, it will vary with source and receiver heights as well as with distance. According to CONCAWE, the ground effect decreases exponentially with increasing grazing angle for source heights greater than 2 m or receiver heights exceeding 1.2 m. The height correction proposed by CONCAWE has however merely been verified for grazing angles up to 2º.
The decrease in ground attenuation due to an elevated sound source or receiver point is calculated with equation (5.11) below [45].

$$K_5 = \begin{cases} (K_3 + K_4 + 3)(\gamma - 1) & \text{for } (K_3 + K_4) > -3 \\ 0 & \text{for } (K_3 + K_4) < -3 \end{cases} \tag{5.11}$$

$$\gamma = \begin{cases} 1 & \text{for } h_s \leq 2 \text{ m or } h_r \leq 1.2 \text{ m} \\ 1 - 0.478\,\psi + 0.068\,\psi^2 - 0.0029\,\psi^3 & \text{for } h_s > 2 \text{ m or } h_r > 1.2 \text{ m} \end{cases} \tag{5.12}$$

Where $$\psi = \tan^{-1}\left[\frac{h_s + h_r}{d}\right] \tag{5.13}$$

ψ	the grazing angle [rad]
h_s	the source height [m]
h_r	the receiver height [m]
d	the source-receiver distance [m]

In case the receiver point is positioned on a hillside or across a valley, CONCAWE recommends reducing the height correction by 3 dB as to incorporate the effect of multiple reflections.

Ground attenuation

The CONCAWE treatment of ground effect is based on empirical data, which was collected at three petrochemical plants of varying size. The attenuating or amplifying effect of sound interaction with a ground surface was isolated by separating the sound levels measured at a particular distance with the attenuation effect of geometrical divergence and atmospheric absorption. The measurements employed had been performed at periods of low meteorological influence, meaning the wind and temperature gradients were both negligible, which allowed the meteorological correction to be ignored. Furthermore, the data that was used had been collected from sites at which attenuation by in-plant screening and barriers could be disregarded [45].

In the CONCAWE prediction model, ground attenuation is treated differently depending on the acoustical properties of the ground surface. For acoustically hard surfaces, i.e. ground types of high flow resistivity such as concrete and water, the ground effect is – 3 dB for all frequencies and distances. However, for acoustically soft surfaces the ground effect is dependent on frequency as well as the source-receiver distance. The attenuation for such ground types is determined with various equations shown diagram 5.2 below.

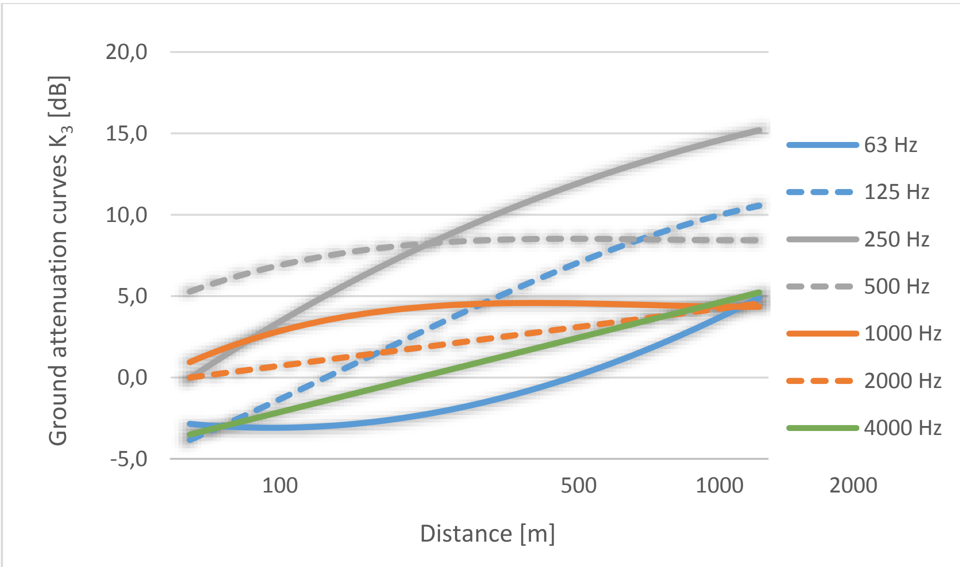

Diagram 5.2. Ground attenuation curves for 1/1 octave bands [45].

As previously mentioned, sound will rarely propagate over a homogenous ground type, but the propagation path will often include both acoustically hard and soft ground surfaces. In the CONCAWE model, mixed ground conditions are treated by merely employing the distance travelled over the acoustically soft surface, while hard ground types are ignored [45].

Limitations with the CONCAWE model

As for the ISO 9613-2 standard, the CONCAWE noise prediction model has received some criticism for being partially based on empirical data, collected from various petrochemical plants. Although the method is primarily applicable for petroleum and petrochemical plants, it has been the foundation of numerous prediction models intended for a variety of sound sources, including railway noise and gunfire. However, the accuracy of such models varies depending on the source type employed [51].

The CONCAWE model predicts ground attenuation differently for acoustically hard and soft surfaces, an approach which has received some critique as it does not consider other variations of ground conditions. Furthermore, it may be hard to categorize certain ground types as either highly reflective or absorptive and a misconception may result in an erroneous prediction. By allowing for several categories of ground conditions, the ground effect may be modelled more accurately.
Sound propagating from an elevated source will be less affected by ground effect than one positioned close to the ground surface. The CONCAWE model recognizes the decreasing influence of ground effect with increasing grazing angle by including a height correction. The correction factor has however merely been validated for grazing angles up to 2º, a value which may be applicable for petroleum and petrochemical plants but is less common for highly elevated sound sources, such as wind turbines and aircraft [1] [10].

CONCAWE provides a detailed methodology of predicting the refracting effects of various weather conditions, which has been proven to offer satisfactory accuracy with measured values based on studies conducted after the completion of the model. As was mentioned in section 3.3.3, the presence of atmospheric turbulence may have a great influence on various causes for sound attenuation, including geometrical divergence and ground effect. However, the effects of atmospheric turbulence have not been acknowledged in the model, although the meteorological factor is partly based on empirical data and would thus be influenced by turbulence. A possible reason for this may be that the extent of effects of turbulence was not completely understood at the time of the development of the model. By including a turbulence factor in the meteorological categories, more accurate predictions may be made [1].
Furthermore, although the CONCAWE prediction method includes a wide variety of sound attenuating factors, no consideration has been taken to the attenuating effect of sound propagation through vegetation.

5.1.3 Nord 2000 Model

The Nord2000 noise prediction model was developed in 2006 by the Danish Environmental Protection Agency. The model predicts the sound pressure level detected at a receiver point for 1/3 octave band, within the 25 Hz to 10 kHz range. It is primarily aimed for prediction of road and railway noise, however other source types may also be employed. Furthermore, the model has been validated for elevated sound sources, including wind turbines. The Nord2000 provides acceptable accuracy for source-receiver distances up to 3,000 m [23] [1].
The Nord2000 models the propagation of sound in outdoor environments assuming an atmosphere without significant refraction, i.e. close to acoustically neutral conditions. The model is based on geometrical ray theory and is applicable for any topography conditions, by approximating the terrain with several straight segments [24].

Nord2000 is applicable for both point and moving sources. The sound pressure level perceived at the receiver point is calculated with equation below.

$$L_R = L_W + \Delta L_d + \Delta L_a + \Delta L_t + \Delta L_s + \Delta L_r \tag{5.14}$$

Where L_W the sound power level [dB]
ΔL_d the propagation effect of spherical divergence [dB]
ΔL_a the propagation effect of air absorption [dB]
ΔL_t the propagation effect of the terrain (grounds and barriers) [dB]
ΔL_s the propagation effect of scattering zones, i.e. housing areas and forests [dB]
ΔL_r the propagation effect of obstacle dimensions and surface properties when calculating a contribution from sound reflected by an obstacle [dB]

The Nord2000 model may be applied for a wide variety of meteorological conditions.

Ground attenuation including topography

As was mentioned in section 3.3.4, irregular ground conditions often affect the propagation of sound. The changed behaviour of sound while interacting with such grounds, compared to a flat surface, is particularly apparent in the ground attenuation factor. Accordingly, the Nord2000 prediction model treats ground effect and topography as a combined cause for sound attenuation.

The model considers the effects off complex terrain as a two dimensional problem, in which the direct path connecting the sound source and receiver is divided into an array of straight line segments that outlines the topographical appearance of the ground surface. This procedure works to simplify the complex terrain into a practical geometry that is solvable through mathematical calculations. An example of three complex ground surfaces is shown below [24].

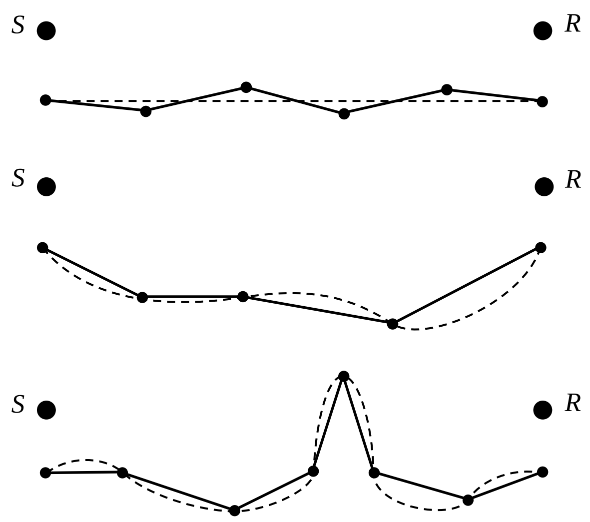

Figure 5.3. The segmentation of three complex terrains. (a) Virtually flat ground surface. (b) Valley-shaped ground surface. (c) Hill-shaped ground surface. The source point is symbolized by S and the receiver by R. Based on [24].

Each straight line segment is characterized by a normalized ground impedance Z as well as a roughness parameter σ_r. The ground impedance is calculated using the Delany and Bazley model for porous media previously described, however the Nord2000 model also allows for simplified predictions to be made by dividing certain surface types into impedance classes. The classification of such grounds may be viewed in the following table.

Impedance class	Representative flow resistivity σ [kNs/m^4]	Description
A	12.5	Very soft (snow or moss-like)
B	31.5	Soft forest floor (short, dense heather-like or thick moss)
C	80	Uncompacted, loose ground (turf, grass, loose soil)
D	200	Normal uncompacted ground (forest floors, pasture field)
E	500	Compacted field and gravel (compacted lawns, park area)
F	2,000	Compacted dense ground (gravel road, parking lot, ISO 10844)
G	20,000	Hard surfaces (most normal asphalt, concrete)
H	200,000	Very hard and dense surfaces (dense asphalt, concrete, water)

Table 5.4. Classification of ground impedance types [24].

Many of the ground attenuation prediction techniques currently employed are limited to some extent by not incorporating the unevenness of the surface terrain. Noise interacting with rough grounds will act differently than with a perfectly flat surface, the reflected sound may scatter in many directions instead of being completely transmitted towards the receiver point. The Nord2000 model acknowledges ground unevenness by including a surface roughness in the noise predictions. As for the ground impedance, the roughness length has been divided into four classes depending on the irregularity of the particular ground surface. These classes may be found in table 5.5 below.

Roughness class	Representative σ_r [m]	Range of heights [m]
N: Nil	0	± 0.25
S: Small	0.25	± 0.5
M: Medium	0.5	± 1
L: Large	1	± 2

Table 5.5. Classification of ground roughness types [24].

The Nord2000 model treats the effects of ground attenuation and topography differently for various terrain types. The model divides large ground irregularities into three categories; flat terrain, valleys and hills, and employs separate ground effect calculation methods for each category.
Calculations of the ground effect over *flat terrain* differs for homogenous and mixed ground surfaces. Sound propagating over a surface with uniform ground properties is determined using the technique described in section 3.3.2, i.e. by employing equation (5.15) below. The surface roughness of the terrain is treated as a separate incoherent effect.

$$\Delta L_{flat} = 20\log\left|\frac{p}{p_0}\right| = 20\log\left|1 + \frac{R_1}{R_2} Q e^{jk(R_2 - R_1)}\right| \tag{5.15}$$

Ground attenuation over mixed ground conditions, meaning terrain of varying impedance and roughness, is however calculated by employing a Fresnel zone model. Fresnel zones are commonly used to predict the behaviour of various radiation sources, such as electric currents and sound waves. Although comprising some uncertainties, the method is widely employed for calculating the effects of ground attenuation. The Fresnel zone is the ground surface area between the sound source and receiver that is assumed to influence the sound at the receiver point.
The Fresnel zone weight is equal to the size of a sub-surface divided by the size of the entire surface covered by the Fresnel zone. It is calculated with equation (5.16) below.

$$w_i = \frac{S_i}{S_{Fz}} \tag{5.16}$$

Where w_i the Fresnel zone weight of sub-surface S_i [-]
S_i the size of the sub-surface i [m]
S_{Fz} the size of the Fresnel zone surface [m]

The Nord2000 model employs a modified Fresnel zone method, in order to obtain more accurate results at high frequencies. In the adapted technique, the Fresnel zone is divided into a source and receiver region, as shown in figure 5.4 below. Each region may contain one or many combinations of the specific ground impedance and roughness, indicated by i and j respectively. The Fresnel zone weight is determined by calculating the size of the entire Fresnel zone surface as well as the size of the source and receiver regions for each combination these parameters. The resulting equation for calculating the ground effect over flat terrain with varying surface properties is specified in (5.17).

$$\Delta L_{flat} = \sum_i \sum_j w'_{i,j} \, \Delta L_{i,j} \tag{5.17}$$

Where $\Delta L_{i,j}$ the ground attenuation of sub-surface $S_{i,j}$, with impedance i and roughness j, calculated with equation (5.15) [dB]
$w'_{i,j}$ the Fresnel zone weight of subsurface $S_{i,j}$, for the high, low and intermittent frequency range [-]

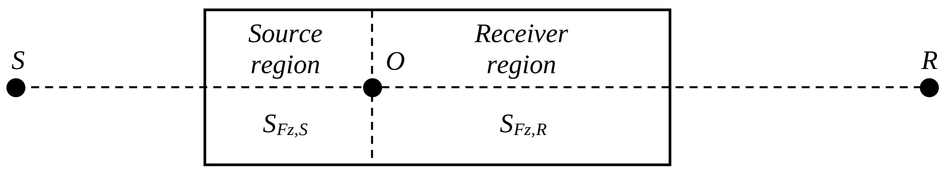

Figure 5.4. Fresnel zone for flat terrain with varying surface properties [24].

The behaviour of sound over *valley-shaped terrain* is more complex than that over flat grounds. The Nord2000 model simplifies the process by dividing the terrain structure into three categories; concave convex and transition segments. Depending on the type of segment considered, the Fresnel zone weight will be calculated differently. The complete attenuation caused by ground effect over a valley is later determined by combining the Fresnel zone weight of each segment in an equation.

Precise classification of each ground surface segment is a complex process, which involves computing the appearance of the Fresnel zone. However, general assumptions may be made merely from determining the source and receiver heights, h'_S and h'_R respectively, relative to an extended section of the segment in question. An example of each segment type is show in figure 5.5 below, the dashed line representing the extended segment.

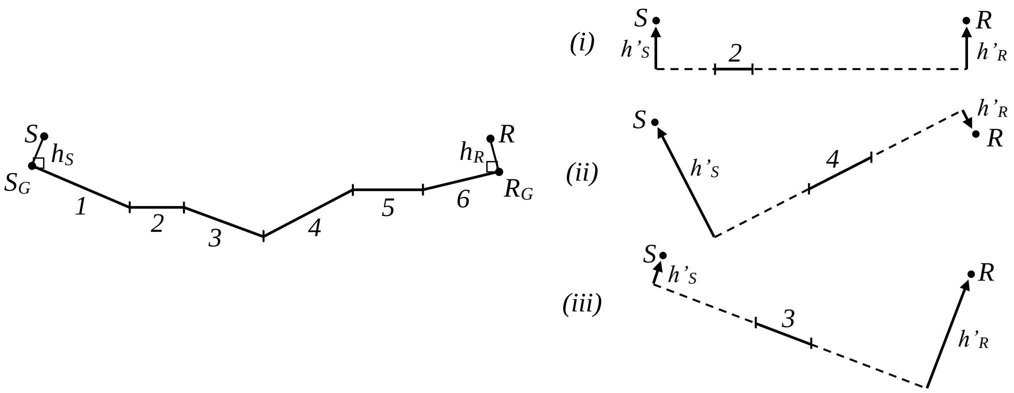

Figure 5.5. (a) Valley-shaped segmented terrain. (b) Determination of segment type, (i) Concave segment, (ii) Convex segment, (iii) Transition segment. Based on [24].

Topographical barriers are commonly viewed as screens, due the similar behaviour of sound while interacting with a ground surface peak and a manufactured obstacle. A similar approach is adopted by the Nord2000 model, in which ground attenuation over hill-shaped terrain is treated as one or a series of screens. However the model yet distinguishes barriers based on origin, which are thus described as either natural or artificial. A reason for the classification is that predictions of sound propagation over an artificial screen are less complicated than that of complex terrain, due to the finite length of such obstacles. Sound interaction with manufactured screens is thus not considered related to the ground effect, but may be treated as an independent cause for sound attenuation.

In order to transform sound predictions over natural screens into a two dimensional problem, the Nord2000 model assumes hills to be infinite merely in the dimension perpendicular to the direction of propagation. The barriers are later divided into three categories; one screen with one and two edges as well as two screens two one edge, while the surrounding and intermittent terrain is assumed flat. This procedure also simplifies the prediction process. The ground attenuation is calculated differently for each category. If more than two screens are present within the source-receiver space, the two most prominent hills are considered [24].

The entire propagation effect of the terrain is determined by combining the results of the flat, valley and hill shaped ground by the use of several equations, which will not be covered in this work.

Attenuation by vegetation

In the Nord2000 prediction model, the sound attenuation caused by propagation through vegetation is considered a scattering effect. In accordance forests are treated as *scattering zones*, along with housing areas. If the scattering zone is of a single type, meaning if the zone consist of solely forest, the attenuation factor is calculated with the following equations [24].

$$\Delta L_s = k_f T k_p A_e(R_{SC}) \tag{5.18}$$

Where $$A_e(R_{SC}) = \Delta L(h', \alpha, R') + 20\log(8R') \tag{5.19}$$

$$h' = nQh \tag{5.20}$$

$$R' = nQR_{SC} \tag{5.21}$$

$A_e(R_{SC})$	the level correction due to scattering [dB]
h’	the normalized scatter obstacle height [m]
R’	the normalized effective distance through a scattering zone [m]
h	the average scatter obstacle height [m]
R_{SC}	the total sound path length of the scattering zones [m]
α	the absorption coefficient of the forest, $0.1 \leq \alpha \leq 0.4$ [-]
k_f	the frequency weighting function [-]
k_p	= 1.25, a constant [-]
T	a variable [-]

The level correction due to scattering is calculated by employing cubic interpolation of the three-dimensional table found in appendix L. The normalized scatter obstacle height and effective distance through the scattering zone, denoted by h’ and R’ respectively, are both dependent on a variable nQ. In forests, the nQ-term is the product of the average tree density and the mean trunk diameter, according to equation (5.22) below.

$$nQ = n''d \tag{5.22}$$

Where n'' the density of trees [m^{-2}]
d the mean trunk diameter [m]

The sound pressure level decrease caused by propagation through forests is largely dependent on the distance travelled through that environment. The total sound path length of the scattering zone is the accumulated distance of each direct ray segment exposed to forest, assuming the straight line propagation path is not blocked by unrelated obstacles. If the direct path is obstructed by a barrier, such as an artificial screen or residential building, the total path length of the scattering zone is instead the summation of each segment of the source-barrier-receiver length that is subjected to forest. An example of unhindered propagation through a scattering zone is shown in figure 5.6.

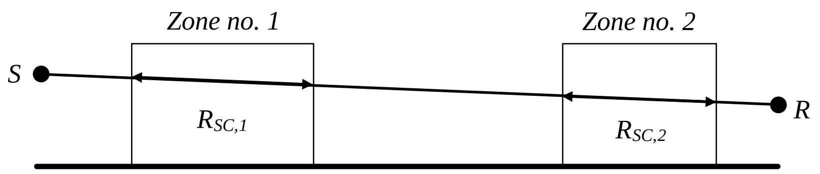

Figure 5.6. Direct ray path during unobstructed sound propagation through forest, the total sound path length is the sum of $R_{SC,1}$ and $R_{SC,2}$ [24].

The variable T is dependent on the mentioned nQ-term as well as the total sound path length of the scattering zone, in accordance with the following relationship.

$$T = \left(\frac{R_{sc} n Q}{1.75}\right)^2 \quad \text{for } T \leq 1 \tag{5.23}$$

The frequency weighting function k_f is determined by employing interpolation of table 5.6 below. The ka-term is the product of the wave number k and the mean tree trunk radius a measured in metres [24].

ka	k_f
0	0.00
0.7	0.00
1	0.05
1.5	0.20
3	0.70
5	0.82
10	0.95

20	1.00

Table 5.6. The frequency weighting function k_f as a function of the product ka [24].

Limitations with the Nord2000 model

The Nord2000 prediction model have been proven to provide reasonable accuracy with measured values, compared to noise predictions performed by other models. In a study conducted by Søndergaard B et al (2009), noise levels calculated with the Nord2000 and ISO 9613-2 models were compared to measured values. Various input parameters were investigated, including flat and complex terrain, the receiver positioned both upwind and downwind as well as several combinations of source-receiver distances and heights. Wind turbine noise was also measured and compared with predictions by the mentioned models. The results showed that the Nord2000 model provided greatest agreement with measurements for downwind situations over flat ground conditions. Nord2000 predictions of wind turbine noise also resulted in acceptable accuracy, with an average A-weighted variance of 1 dBA and standard deviation of 2.3 dBA. The wind turbine measurements were performed on flat grounds at distances 4 km, 3 km and 2.5 km from the source.

Although being proven accurate in some situations, the Nord2000 may yet be criticised on some aspects. In the model, ground attenuation over flat terrain is treated by employing the methodology described in section 3.3.2. However as was mentioned in that chapter, calculations using that approach provide accurate result primarily for source-receiver dimensions close to grazing incidence. During predictions of wind turbines noise, the sound source will be elevated to heights approaching 200 m, thus making the proposed method impractical since the receiver point must be positioned at vast distances from the source in order to obtain reliable results.
Furthermore, large parts of ground attenuation calculation method involves the use of Fresnel zones. However, implementation of the methodology has been proven to provide some uncertainty.

In the Nord2000 model, surface roughness is treated as a separate incoherent effect, meaning an element that may cause a decreased coherence between different sound waves. However, incoherent effects are merely presented in a theoretical version of the model and are not included in the edition presently available. Moreover, the methodology employed for implementing surface roughness in the theoretical model is currently highly unreliable, since there has not been sufficient outdoor noise measurement conducted to validate the results [24].

The suitability for employing the Nord2000 model during predictions of sound propagation in forests was investigated in a study by Tarrero A.I. et al (2008). In the study, experimental noise measurements were compared with values predicted by the model. The results show that predicted values of the ground effect in forests are reasonably accurate merely in 60 % of the cases. Furthermore, the study revealed that the Nord2000 model predicts the effect of trees with acceptable accuracy primarily within the low and mid frequency range, whereas high frequency sound is not predicted well.

5.2 Calculation model

A noise prediction model was developed based on the information and measurements data previously obtained. The software chosen for the model was Microsoft Excel, for which the reasons were many. Primarily, Excel was selected as it is a software that is well recognized within engineering and other business sectors and operating the model would thus not require the user to learn basic procedures, which facilitated easy handling and a satisfactory user experience. Microsoft Excel was also considered a suitable choice of software since it enabled the design of a user friendly interface, which would not be possible for other potential operating systems such as Matlab. Furthermore, Excel was a program that the developer was highly familiar with, which simplified the developing process. There were some negative aspects of employing Excel, including having to limit the number of equations comprised in the model in order to minimize the file size and calculation time. However, generally the benefits of employing Excel were considered more prominent than the disadvantages.

5.2.1 Calculations

Development of the noise prediction model required the implementation and synchronisation of several calculation techniques, mentioned in chapter 3, into one single file. The process demanded the use of some further calculations, such as insertion of source and receiver coordinates as well as a noise regulation exceedance control. The aim was to create a simple and user friendly model that provides accurate results, while minimizing the Excel file size.

Coordinates

The development of a wind farm commonly requires the exact coordinates of each turbine included in the scheme. Wind energy projects are generally managed with the assistance of mapping software such as Google Earth, in order to supervise the wind turbine layout, the site ground conditions, the proximity to any surrounding obstacles and residential buildings etc. Accordingly, coordinates of the sound source, i.e. the wind turbine, and the receiver was implemented in the model. The source-receiver distance could later be determined by entering the coordinates into the *haversine formula*, shown in equations (5.24) to (5.26) below.

$$a = [\sin(\Delta\varphi/2)]^2 + \cos\varphi_1 \times \cos\varphi_2 \times [\sin(\Delta\gamma/2)]^2 \tag{5.24}$$

$$b = 2 \times \text{atan2}\left(\sqrt{a}, \sqrt{(1-a)}\right) \tag{5.25}$$

$$D = R_{Earth} \times b \tag{5.26}$$

Where φ the latitude coordinates [rad]
γ the longitude coordinates [rad]

R_{Earth} = 6,371,000, the Earth's radius [m]

In the equations above the first coordinates denotes the position of the receiver, while the second signifies the coordinates of the wind turbine.

As was mentioned in section 3.2.1, the direction of the receiver point in relation to the direction of the wind may affect the propagation of sound. However, since the average wind direction at a particular site may not be known to the user, that element was not included in the model. In consequence a worst case scenario was adapted, in which it is assumed that the direction of the wind equals that of the receiver point at all times.

The technique for calculating the source-receiver distance and the angular direction of the receiver point requires the coordinates to be entered as a single value. However in many mapping software currently used, coordinates are expressed in units of degrees-minutes-seconds. In order for the model to be compatible with such programs it was designed as to allow for both units to be inserted. The conversion is performed according to equation (5.27).

$$Decimal\ degrees = Degrees + \frac{Minutes}{60} + \frac{Seconds}{3{,}600} \tag{5.27}$$

Figure 5.7 shows the model interface for entering the coordinates of the wind turbine. The latitude and longitude position is initially specified by inserting "N" or "S" for north or south, respectively, as well as "E" or "W", which denotes east or west, respectively. The coordinates are subsequently entered, either as decimal degrees or in units of degrees-minutes-seconds.

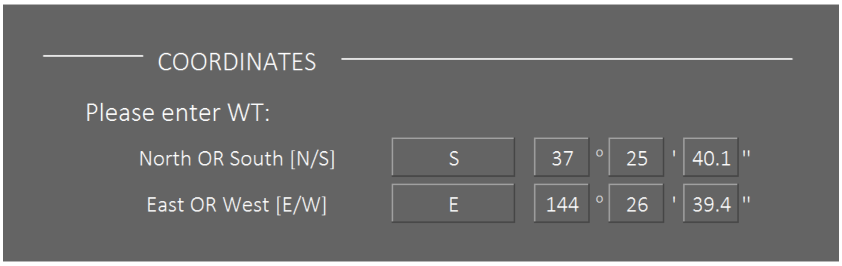

Figure 5.7. The model interface for wind turbine coordinates.

Weather conditions

The ambient conditions at a particular site constitute an essential part for forecasting the propagation of sound in that area. In the model, the general weather conditions required for noise predictions include the atmospheric temperature in degrees Celsius, the atmospheric pressure as well as the relative humidity. These parameters may be entered manually or selected out of three prearranged sets of weather conditions; standard, summer and winter. The two latter categories represent the average climate in the Melbourne area during the summer and winter season, respectively, however they may be adjusted as to correspond with a different area if desired. All three classes are outlined in table 5.7.

Weather input variables	Standard	Summer	Winter
Atmospheric temperature [^{o}C]	15.0	21.0	9.0
Atmospheric pressure [kPa]	101.325	101.250	101.667
Relative humidity [%]	50	60	75

Table 5.7. Meteorological classes used in the model.

To simplify entry of meteorological classes, each category has been designated by a number 1 to 3. A particular set of weather data is selected by inserting the corresponding number into the indicated frame.

Wind gradient

As described in chapter 3, the wind gradient behaves differently over an open ground surface and forest land. The behaviour of winds travelling over grounds comprised of both forests and open fields will thus differ from that over a single element. Since the model incorporates mixed ground conditions, the wind gradient was altered as to incorporate both types. This was achieved by calculating the height at each ground type transition, shown in figure 5.8 below, by employing equations (5.28) to (5.30).

$$\delta = \tan^{-1}\left(\frac{z_S - z_R}{D}\right) \tag{5.28}$$

Where $z_1 = z_S - D_1 \tan\delta$, the height at ground 1-2 transition [m] (5.29)

$z_2 = z_1 - D_2 \tan\delta$, the height at ground 2-3 transition [m] (5.30)

δ the inclination angle [rad]

The wind gradient between the height of the sound source and the first transition is equal to that found over ground type one, whereas the gradient between the height of the first and second transition corresponds to wind speeds projected over that particular ground etc.

Since the wind speed changes with height, the geometrical divergence will also differ with distance above ground. In order to incorporate the effects of wind, the geometrical divergence was initially calculated for wind speeds corresponding to the height of the sound source, i.e. the wind turbine hub height. Wind speeds generally decrease with declining height, resulting in an increase of the geometrical divergence. The change is accounted for by calculating the variance in geometrical divergence for each one vertical meter step by subtracting the geometrical divergence of the previous step. The methodology may be visualized in figure 5.8.

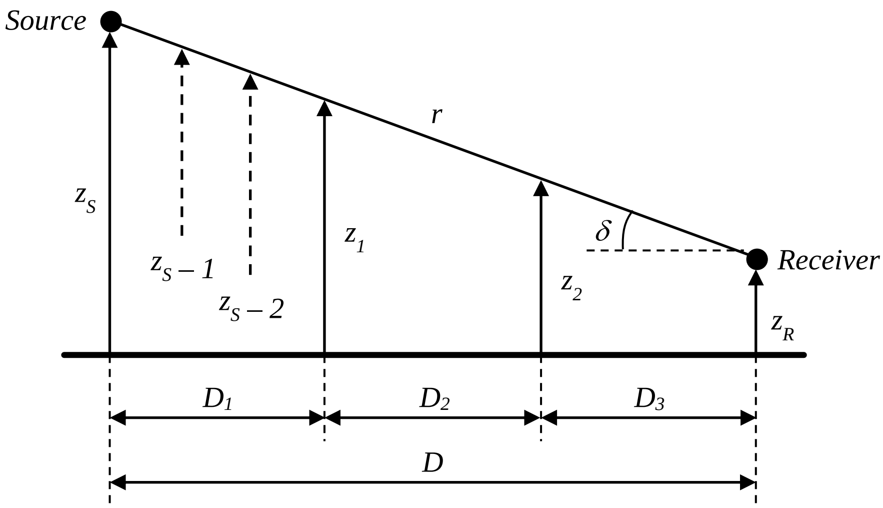

Figure 5.8. Illustration of the geometrical divergence calculated in steps of one vertical meter from the height of the sound source in order to incorporate the wind gradient.

The geometrical divergence of a point source is calculated with equation (2.16), however in order to incorporate the wind gradient the expression is altered according to that below.

$$L_p = L_W - 20\log r + \left[10\log\left(2\times 10^{-4}\times \rho_0 c_{eff,z_S}\right)\right] + \sum_{n=0}^{z_S - z_R} 10\log\left[\frac{c_{eff,\,z_S-(n+1)}}{c_{eff,\,z_S-n}}\right]$$

$$= L_W - 20\log r + \left[10\log\left(2\times 10^{-4}\times \rho_0\left(c_0 + U_{z_S}\right)\right)\right] + \sum_{n=0}^{z_S - z_R} 10\log\left[\frac{c_0 + U_{z_S-(n+1)}}{c_0 + U_{z_S-n}}\right]$$

Where $c_{eff,\, z_S}$ $= c_0 + U_{z_S}$, effective speed of sound at the height of the source [m/s]

U_{z_S} the wind speed at the height of the sound source [m/s]

A similar approach may be applied to the temperature gradient, which also vary with height and will thus cause the geometrical divergence to differ slightly from that of isothermal circumstances. The variance is however not sufficient to impact the complete attenuation of sound by more than a fraction and the temperature change was consequently not be included in the model.

Mixed ground

Sound propagating over large distances will be influenced by changes in the ground type impedance. Surface discontinuities were incorporated in the model by employing the ground effect calculation methodology described in section 3.4.4. As previously established, the model includes a maximum of three discontinuities, a number which was deemed appropriate considering the limitations of Excel. The surface type is selected for each ground discontinuity by entering a value 1 to 6 into the designated frame, the options include old and new asphalt, dirt road, sand, grass lawn as well as forest floor, respectively. A manual entry was not made available as it was considered unlikely that any potential user of the model would be familiar with the flow resistivity of various ground types.

The length of each ground type is entered in units of percentage, since exact dimension may not be known. In order to encourage understanding of the context of various grounds, the position of all discontinuities in relation to the wind turbine and receiver point is also demonstrated with an illustration, shown in figure 5.9. In general, unknown parameters are easier to grasp when visualized.

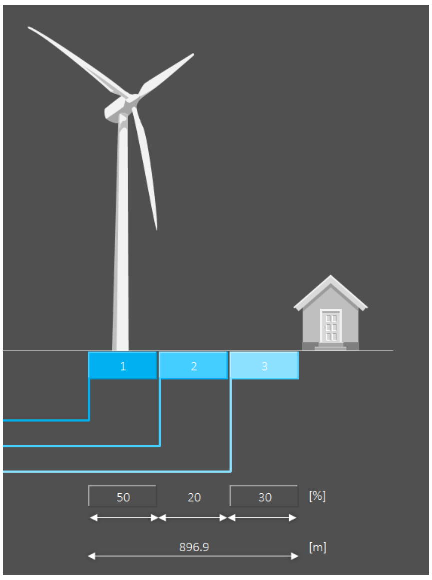

Figure 5.9. Illustration of the wind turbine and receiver point in relation to varying ground types.

Wind turbine model

As during selection of weather conditions, the particular wind turbine used may be selected from a range provided by GE Power & Water or entered manually on page "WTManual" of the Excel file. The GE wind turbines are chosen by entering a value 1 to 5 in to the designate frame. The manual entry requires the user to insert the turbine hub height as well as the sound power curve for 1/3 octaves and frequencies of 25 Hz to 20,000 Hz and wind speeds of 3 m/s to 10 m/s.

Vegetation

The effects of sound interaction with forest areas is treated in two steps; firstly the attenuation caused by propagation through the forest is calculated using equation (4.3) found in section 4.3.4. The resulting attenuation factor is multiplied with the distance travelled through the forest area, which is calculated differently depending on the position of the forest in relation to the source and receiver as well as whether the direct sound wave interferes with the forest edge or the canopy.
The second part is related to the reflection caused by the forest edge and is thus also dependent on where the direct wave will intersect with the forest. If the interference occur above the tree canopy no sound will be reflected, whereas if the noise intersects with the vertical forest edge an A-weighted sound reduction of 9.0 dBA will occur. To simplify calculations, the forest is viewed as a rectangle, with the height equal to the average tree height H and the length equivalent with the length of the particular ground type the forest is positioned on D_{1-3}. The dimensions required for the mentioned calculations may be viewed in figure 5.10 below. In this particular case, the forest is positioned on ground type 2.

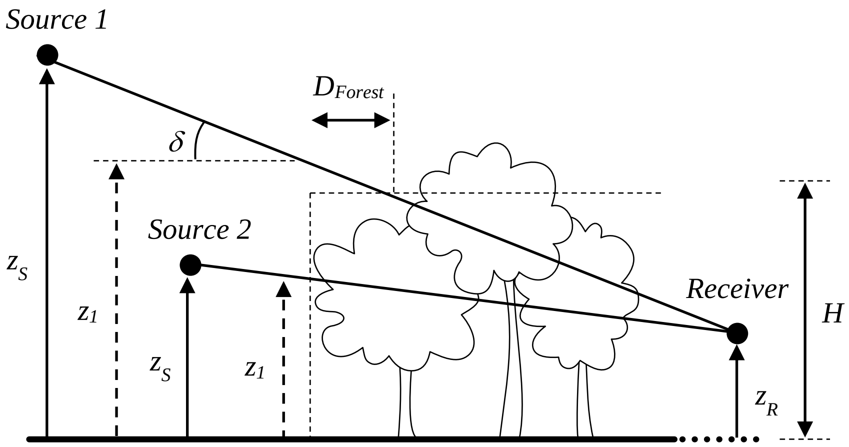

Figure 5.10. Dimensions required to determine the effects of forestry on sound propagation. The geometry corresponds with the particular case of a forest positioned on ground type 2.

Modelling of the effects of vegetation is performed in a similar manner to that adapted during calculation of the wind gradient over mixed grounds. In figure 5.10 two cases are displayed. In case one, the source-receiver dimensions are positioned so that the direct sound ray will intersect with the vertical edge of the forest. The distance travelled inside the forest is thus calculated with the use of equation (5.31).

$$R_{Forest} = \sqrt{(z_1 - z_2)^2 + D_2{}^2} \quad \text{for } z_1 \leq H \tag{5.31}$$

In case 2, the source and receiver points are situated so that the direct sound wave will interfere with the forest canopy before entering the forest. The sound will thus travel a shorter distance into the forest, calculated with equations (5.32) and (5.33) below.

$$D_{Forest} = \frac{z_s - H}{\tan\delta} - D_1 \tag{5.32}$$

$$R_{Forest} = \sqrt{(H - z_2)^2 + (D_2 - D_{Forest})^2} \quad \text{for } z_1 > H \tag{5.33}$$

Noise limitations

Wind turbine noise regulations is as an optional feature of the model as it does not affect the predicted noise levels, however it serves as a useful indicator of noise limit exceedance. The feature requires the user to insert background noise levels for the site in question for wind speeds of 3 m/s to 10 m/s into the indicated frames. The model offers a choice of either using the New Zealand standard guideline or a manual entry of noise limits between specified background noise level intervals.

Noise prediction results

The resulting values predicted at the receiver point are presented as the A-weighted sound pressure level for wind speeds ranging from 3 m/s to 10 m/s. The results also include the chosen noise limit as well as calculation of guideline compliance, a “Yes” signifying that that the restriction has been obeyed and a “No” that the noise limit has been exceed. The wind turbine noise level may also be viewed in relation with the background noise and guidelines as a graph.

Since wind farms commonly comprise a great number turbines, the noise detected at the receiver point may be the result of several uncorrelated sources. The total A-weighted sound pressure level of the entire wind farm or merely a few turbines in the proximity of the receiver, such as a residential building, is calculated by copying the A-weighted values obtained for one turbine into the indicated frames below. The procedure is subsequently repeated for a different wind turbine. The combined noise is calculated with equation (2.6).

5.2.2 Interaction design

In order to develop a prediction model that offers good usability as well as a satisfactory user experience, considerations have been taken into the interactional aspect of system design. Many areas comprised in the subject of interaction design have thus been incorporated in the model, including overview, orientation, navigation, visibility, feedback and error management. However, due to the limitations of the selected software Excel, some interactional elements could not be fully included in the development process. For instance affordance, i.e. the design of an object to encourage the user to perform a particular action, which is in part incorporated in the software itself.

Overview, orientation and navigation

The categories overview, orientation and navigation are central concepts within interaction design, informing the user of what is offered in the system, where the user is located within the system as well as how the user may navigate to a specific part of the system, respectively. The model offers a well-developed orientation by dividing the various input variables required for predicting noise levels detected at a receiver point into natural groups. In total the model encompasses five groups of input variables, including weather, wind turbine, position, site data and guidelines as well as a single group presenting the resulting noise levels. Each group is also provided with one or several subheadings, which further explains the data required within the group. For instance, the group “Position” includes two subheadings; “Coordinates” and “Altitude”, thus further dividing the group into natural subdivisions. The positioning of each group within the interface has also been designed as to allow for good overview. The entire input interface measures into the Excel software screen when completely maximized at 100 % zoom. In Excel, a vertical motion is often considered more natural than horizontal and the groups were consequently positioned as to allow for vertical movement within the interface.

In Excel the conditions for good orientation is integrated into the system by the use of pages. Assuming the user of the model is familiar with the chosen software, each page positioned at the bottom of the screen will inform the user of his or her current position within the system. All of the six main groups positioned on the main page of the Excel file are connected by a thread in order to simplify navigation through the model. At the bottom of the input section of the main page the thread guides the user to the right, thus directing him or her into towards the results.

Visibility

The concept of visibility involves developing a user interfaces which merely includes information that is important for operating the system. It is the balance of incorporating too much information onto the model interface, thus making it difficult to locate and interpret significant data, and not including enough information, which may cause confusion and mishandling of certain tasks. Visibility is facilitated by dividing the model information into natural groups, as described previously, as well as by employing a suitable colour scheme. In the model the amount of colours have been limited to a maximum of three, including a variety of greys as well as blue and orange. The grey colours covers most of the model interface, while blue and orange denotes significant features that the user should identify, such as error messages.

Feedback

Once the user of the model has completed a task, it is important to convey that it has been concluded successfully by providing feedback. In the model, feedback is incorporated by equipping each of the five main groups with a tick. Once all information has been filled in correctly within a group the tick will appear into a designated frame, thus notifying the user that the task has been completed.

Error management

Regardless of the amount of interactional features incorporated into a particular system interface, the user of the model may unconsciously make an error during handling of some task. Error handling involves providing the user with the means of correcting his or her error without external assistance. Generally error handling is implemented by incorporating warning messages, informing the user of the mistake. This approach has also been in applied into the model. An example include situations during which a value is to be entered within a certain range. If the user was to exceed the designated range, an error message appears below the particular task informing the user of the mistake. All error messages have been given an orange colour as capture the attention of the user.

The model has also been developed so that if an error is made, it will not affect the noise prediction results. For instance, the Excel file has been made into a read-only format for all frames that do not require and input value by the user. Furthermore, file has also been constructed so that in case there is an option, for instance in the entry of weather conditions, only one alternative will be processed even if both are filled out. For example, during entry of noise guidelines the user is given a choice between employing the New Zealand standard and manually inserting a limit for some background noise interval. If both options are entered, the model will use the New Zealand standard during sound level calculations, hence the manual entry will merely be applied if the standard option has been left empty. The same approach is adapted in other parts of the model, at which the user is given an option of manual entry or selection of set alternatives [68].

6 Discussion

Although best effort was made in order to create a master thesis project that will be beneficial to both GE Power & Water as well as for Lund University, some errors may be comprised in the final results. Such errors may have been made deliberately or unconsciously. This chapter will explain some of the major decisions made during the process of the thesis, intentional errors or simplifications as well as limitations included in the results.

Noise measurements

As previously mentioned, the amount of measurements performed during the course of the thesis project has significantly limited the reliability of the results. This primarily applies to the elevated measurements, of which only one set of measurements were performed. It is likely that these as well as other measurements will be affected by factors not considered during the analysis of the results, such as refraction due to wind and temperature. By performing more measurements, the result presented in this thesis report could have been made more accurate, covering a wide variety of meteorological conditions. Another limiting factor was that merely one site was employed during the noise measurements, thus making the results primarily suitable for that particular area. The main reason for that choice was that the area in question was ideal for the type of measurements performed, providing a good variety of forestry and open area, reasonably flat ground conditions and good road access. The site was also positioned in a remote location, which was desirable since the background noise levels would be low.

Another limiting factor was not taking attenuation by refraction into consideration during both the analysis of data as well as development of the prediction model. The reason for that error was that there is currently no mathematical method of determining the effects of refraction due to wind and temperature on sound propagation. As was mentioned in section 5.1, the prediction models that are currently used all employ empirical data when estimating that factor. An idea was to incorporate the technique employed in one of these models into the developed prediction model, however it was found not to be possible since ISO 9613-2 and CONCAWE both perform noise calculations in 1/1 octaves, which I did not want to use for the model as it would decrease the accuracy of it. The Nord2000 model does calculate noise in 1/3 octave, but does not disclose how to determine attenuation by refraction to the public.

Inexperience in acoustical field work has been a major limiting factor throughout this project. Although I had partaken in some noise measurements prior to commencing this thesis, it did in my opinion not provide me with sufficient knowledge in this particular area of acoustics. As a result, many of the measurements performed during the duration of this project has been limited by errors, an example include the faulty installation of the weather station during the measurements. Fortunately, weather data from a neighbouring area could be obtained from the Australian Bureau of Meteorology and I have thus been able to use the majority of the data obtained during these measurements, though not the extent or with the accuracy I would have wanted.

Model development

A predicament commonly encountered during the course of the project has been that this field within acoustics is constantly evolving and consequently there are often several ways of determining various parameter. If faced with contradicting calculation methods, I have generally chosen the most recent technique or that which does not require extensive knowledge of the surrounding environment. For example, when determining the behaviour of sound above a layered ground structure, a calculation method had been developed by Attenborough K et al in 2007. However, this method requires deep understanding of the materialistic properties of each layer, such as the ground density and the speed of sound. As such information may not be available for the user of this model, a different method was employed which had been developed by Salomons E.M in 2001.
When selecting a suitable method for the calculation model of this project, an important factor to consider has been to choose a procedure that is applicable in Excel. There are for instance also many methods available for predicting the behaviour of sound over mixed grounds, however many of these techniques could not be implemented in Excel, which was the chosen software. The technique proposed by Lam Y.W & Monazzam M.R (2006) was ultimately chosen for the model, since provides an accurate and relatively simple approach. Furthermore, this technique was deemed appropriate for calculations using wind turbine sound sources as it provides most accurate results for source-receiver dimensions not approaching grazing incidence, i.e. elevated sound sources or receiver points.

One of the objectives of this thesis was to develop noise prediction model that is accurate and user friendly, while not compromising the Excel file size. However, increasing the accuracy has generally resulted in more variables and in consequence made the model more complex. Throughout this work, I have had to make many decisions on whether to include a certain variable that impact the sound propagation or not. In general, my rule has been that if the variable influence the sound with more than ± 0.1 dB, it should be included. In many cases however, such decisions have been made from approximations, consulting with acoustical experts or by calculations and as a result I may have overlooked some variable that should have been included in the model. Examples of such approximations includes the influence of the temperature gradient. Furthermore, the effects of topography and turbulence was not included as the calculation method for such parameters are much too complex as to incorporate in Excel.

Ultimately, this thesis project has been an incredible learning experience for myself and I hope it will be beneficial for future wind energy projects commenced in Australia.

7 References

[1] Attenborough K, Li K.M & Horoshenkov K. 2007. “*Predicting Outdoor Sound*”. Taylor & Francis, London, United Kingdom & New York, USA.

[2] Attenborough K (1), Waters-Fuller T (2), Li K.M (3) & Lines J.A (4). 2000. “*Acoustical Properties of Farmland*”. (1) School of Engineering, University of Hull, England. (2) School of Built Environment, Napier University, Edinburgh, Scotland. (3) Department of Mechanical Engineering, Hong Kong Polytechnic University, Hong Kong. (4) Silsoe Research Institute, Silsoe, England.

[3] Australian Government – Bureau of Rural Sciences. 2008. “*Australian forest profiles – Australia's forests*”. Canberra, Australia.

[4] Australian Government – Department of Agriculture. 2013. “*Australia's State of the Forest Report 2013*”. Canberra, Australia.

[5] Australian Government – Department of Industry, Geoscience Australia, Bureau of Resources and Energy Economics. 2014. “*Australian Energy Resource Assessment*”. 2nd edition.

[6] Aylor E.D. 1977. “*Some Physical and Psychological Aspects of Noise Attenuation by Vegetation*”. Department of Ecology and Climatology, the Connecticut Agricultural Experiment Station, New Haven, USA.

[7] Baldocchi D.D, Verma S.B & Rosenberg N.J. 1982. “*Characteristics of air flow above and within soybean canopies*”. Institute of Agriculture and Natural resources, University of Nebraska, USA.

[8] Bard D. 2013. *“Acoustics VTAF05*”. Department of Engineering Acoustics, Lund University, Sweden.

[9] Bass H.E (1), Sutherland L.C (2), Zuckerwar A.J (3), Blackstock D.T & Hester D.M (4). 1994. “*Atmospheric absorption of sound: Further developments*”. (1) Physical Acoustics Research Group, University of Mississippi, USA. (2) Longhill Drive, Rancho Palos Verdes, California, USA. (3) NASA/Langley Research Group, Hampton, Virginia, USA. (4) Applied research Laboratories and Mechanical Engineering Department, University of Texas, USA.

[10] Bass J.H (1), Bullmore A.J (2) & Sloth E (3). 1998. "*Development of a wind farm noise propagation prediction model*". (1) Renewable Energy Systems Limited, Kings Langley, United Kingdom. (2) Hoare Lea & Partners Acoustics, London, United Kingdom. (3) Acoustica A/S, Copenhagen, Denmark.

[11] Bérengier M.C, Gauvreau B (1), Blanc-Benon Ph. & Juvé D (2). 2003. "*Outdoor Sound Propagation: A Short Review on Analytical and Numerical Approaches*". (1) Laboratoire Central des Ponts et Chaussées, Bouguenais Cedex, France. (2) Ecole de Lyon, Laboratoire de Mécanique des Fluides et d'Acoustique, Ecully Cedex, France.

[12] Beychok M. 2013. "*Atmospheric lapse rate*". The Encyclopedia of Earth. Accessed 18 February 2014. <http://www.eoearth.org/view/article/170859/>

[13] Botteldooren D & Renterghem T.V. 2012. "*Noise shielding by tree belts of finite length and depth along roads*". Ghent University, Department of Information technology, Acoustics group, Belgium.

[14] Bureau of Meteorology. 2014. "*Climate statistics for Australian locations – Melbourne regional office*". Australian Government, Australia. Accessed 16 February 2014. <http://www.bom.gov.au/climate/averages/tables/cw_086071_All.shtml>

[15] Cederlöf K (1), Troedsson U (2) & Jakélius S (3). 2001. "*Ljud från vindkraftverk – Rapport 6241*". (1) Naturvårdsverket, Stockholm, Sweden. (2) Boverket, Karlskrona, Sweden. (3) Energimyndigheten, Eskilstuna, Sweden.

[16] Chevret P, Blanc-Benon Ph & Juvé D. 1996. "*A numerical model for sound propagation through a turbulent atmosphere near the ground*". Laboratoire de Mécanique des Fluides et d'Acoustique de l'Ecole Centrale de Lyon, Ecully, France.

[17] Chief Medical Officer of Health (CMOH). 2010. "*The Potential Health Impact of Wind Turbines*". Ontario, Canada.

[18] Colby W.D, Dobie R, Leventhall G, Lipscomb D.M, McCuney R.J, Seilo M.T, Søndergaard B. 2009. "*Wind Turbine Sound and Health Effects – An Expert Panel Review*". Prepared for American Wind Energy Association and Canadian Wind Energy Association.

[19] Committee EV-016, Acoustic – Wind Turbine Generator Noise. 2010. "*AS 4959-2010: Acoustics – Measurement, prediction and assessment of noise from wind turbine generators*". Standards Australia, Sydney, Australia.

[20] CONCAWE – Environmental Science for the European Refining Industry. 2010. "*About us*". Accessed 17 July 2014. <https://www.concawe.eu/content/default.asp?PageID=545>

[21] CPS – Center of Chemical Process Safety. N.d. "*Friction velocity, u**". New York, USA. Accessed 12 March 2014. <http://www.aiche.org/ccps/glossary/process-safety-glossary/friction-velocity-u>

[22] Crocker M.J. 1998. "*Handbook of Acoustics*". Wiley, New York, USA.

[23] Danish Ministry of the Environment – Environmental Protection Agency. N.d. "*Nord2000: Nordic noise prediction method*". Copenhagen, Denmark.

[24] DELTA – Danish Electronics, Light & Acoustics. 2006. "*Nord 2000. Comprehensive Outdoor Sound Propagation Model. Part 1: Propagation in an Atmosphere without Significant Refraction*". Hørsholm, Denmark.

[25] Department of Health. 2013. "*Wind farms, sound and health: Technical Information*". The Victorian Government, Australia. Accessed 11 February 2014. <http://docs.health.vic.gov.au/docs/doc/5593AE74EB486F2CB57B5E0014E33C/$FILE/Wind%20farms,%20sound%20and%20%20health%20-%20Technical%20information%20WEB.pdf>

[26] Department of Health. 2013. "*Wind farms, sound and health: Community Information*". The Victorian Government, Australia. Accessed 20 August 2014. <http://docs.health.vic.gov.au/docs/doc/03C56FFC34F658CB57B5E00164599/$FILE/1212016_wind_turbine_community_WEB.pdf>

[27] Department of Nurse Anesthesia. 2012. "*Reflection, refraction, scattering and attenuation*". Virginia Commonwealth University, USA. Accessed 5 February 2014. <http://www.vaultrasound.com/educational-resources/ultrasound-physics/reflection-refraction/>

[28] Doolan C. 2013. "*A Review of Wind Turbine Noise Perception, Annoyance and Low Frequency Emission*". School of Mechanical Engineering, University of Adelaide, Australia.

[29] Gill A.M, Groves R.H & Noble I.R. 1981. "*Fire and the Australian biota*". Australian Academy of Science, Canberra, Australia.

[30] GWEC – Global Wind Energy Council. 2013. "*Global Wind Report – Annual Market Update 2013*". Brussels, Belgium.

[31] Hansen C.H. 2001. "*Fundamentals of acoustics*". Department of Mechanical Engineering, University of Adelaide, Australia.

[32] Heimann D. 2003. "*Meteorological aspects in modelling noise propagation outdoors*". DLR Institute of Atmospheric Physics, Germany.

[33] Herrington L.P & Brock C. 1977. "*Propagation of Noise over and through a Forest Stand*". College of Environmental Science and Forestry, State University of New York, USA.

[34] Huisman W. 1990. "*Sound propagation over vegetation-covered ground*". PhD Thesis, University of Nijmegen, the Netherlands.

[35] IEC 61400-11 International Standard. Edition 2.0. 2006. "*Wind Turbine generator systems – Part 11: Acoustic noise measurement techniques*". Geneva, Switzerland.

[36] IEC 61400-11 International Standard. Edition 3.0. 2012. "*Wind Turbines – Part 11: Acoustic noise measurement techniques*". Geneva, Switzerland.

[37] ION Acoustics. 2011. "*Noise Assessment – Harrington Parks Farm Land West of Harrington Parks Farm, Cumbria*". Bristol, United Kingdom.

[38] ISO 9613-2 International Standard. 1996. "*Acoustics – Attenuation of sound during propagation outdoors. Part 2: General method of calculation*". Edition 1.0. Geneva, Switzerland.

[39] Jacobsen F, Poulsen T, Rindel J.H, Gade A.C & Ohlrich M. 2011. "*Fundamentals of acoustics and noise control*". Department of Electrical Engineering, Technical University of Denmark, Lyngby, Denmark.

[40] Kelsall Y, Kirkwood J, Ruchel M, Clinton M & Ingamells P. 2010. "*Better Protection for Special Places – Victorian National Parks Association Small Parks Project*". Victorian National Parks Association, Melbourne, Australia.

[41] Lam Y.W & Monazzam M.R. 2006. "*On the modelling of sound propagation over multi-impedance discontinuities using a semiempirical diffraction formulation*". Acoustics Research Centre, School of Computing and Engineering, University of Salford, United Kingdom.

[42] Lamancusa J.S. 2009. "*10. Outdoor sound propagation*". Pennsylvania State University. USA.

[43] Laugier P & Haïat G. 2011. "*Chapter 2 Introduction to the Physics of Ultrasound*". Paris, France.

[44] Lund Institute of Technology. 2013. "*Kompletterande teorimaterial och uppgifter till kursen 'Ljud i Byggnad och Samhälle'*". Lund University, Sweden. Accessed 4 February 2014. <http://www.akustik.lth.se/fileadmin/tekniskakustik/education/LjudBS2013/K.pdf>

[45] Manning C.J (1), Biji L.A, Barchha R.R, Grashof M, Marsh K.J, Sarteur R & Sutton P (2). 1981. "*The propagation of noise from petroleum and petrochemical complexes to neighbouring communities*". (1) Acoustic Technology Limited, Southampton, United Kingdom. (2) CONCAWE Special Task Force on Noise Propagation, Den Haag, Netherlands.

[46] Manwell J.F, McGowan J.G & Rogers A.L. 2009. "*Wind Energy Explained*". 2nd edition. John Wiley & Sons Ltd, West Sussex, United Kingdom.

[47] Marshall J & Plumb R.A. 2008. "*Atmosphere, Ocean and Climate Dynamics*". Massachusetts Institute of Technology, Cambridge, Massachusetts, USA.

[48] Miki Y. 1990. "*Acoustical properties of porous materials – Modifications of Delany-Bazley models*". Faculty of Engineering, Takushoku University, Japan.

[49] Museum Victoria Australia. N.d. "*Plants*". Melbourne, Australia. Accessed 30 August 2014. <http://museumvictoria.com.au/forest/plants/index.html>

[50] P 6808 Committee. 2010. "*NZS 6808:2010: Acoustics – Wind farm noise*". Standards New Zealand, Wellington, New Zealand.

[51] Parry G. 2008. "*A review of the use of different noise prediction models for wind farms and the effects of meteorology*". ACCON UK Limited, Reading, United Kingdom.

[52] Pedersen E & Persson Waye K. 2003. "*Perception and annoyance due to wind turbine noise – a dose-response relationship*". Department of Environmental Medicine. Göteborg University, Sweden.

[53] PlantNET – The Plant Information Network System of the Royal Botanic Gardens. 1991 – 2012. "*NSW Flora Online*". National Herbarium of NSW, Royal Botanic Garden, Sydney, Australia. Accessed 30 August 2014. <http://plantnet.rbgsyd.nsw.gov.au/>

[54] Price M.A (1), Attenborough K & Heap N.W. 1988. "*Sound attenuation through trees: Measurements and models*". (1) Institute of Sound and Vibration Research, the University of Southampton, United Kingdom. (2) Faculty of Technology, the Open University, Milton Keynes, United Kingdom.

[55] Ray M.L, Rogers A.L & McGowan J.G. 2006. "*Analysis of wind shear models and trends in different terrains*". Department of Mechanical & Industrial Engineering Renewable Energy Research Laboratory, University of Massachusetts, USA.

[56] Reethof G, McDaniel O.H (1) & Heisler G.M. 1977. "*Sound Absorption Characteristics of Tree Bark and Forest Floor*". (1) Noise Control Laboratory, the Pennsylvania State University, USA. (2) USDA Forest Service, Northeastern Forest Experiment Station, Pennington, USA.

[57] Renterghem T.V (1) Botteldooren D & Verheyen K (2). 2012. "*Road traffic noise shielding by vegetation belts of limited depth*". (1) Department of Information Technology, Ghent University, Belgium. (2) Department of Forest and Water Management, Ghent University, Belgium.

[58] Rogers A.L, & Manwell J.F. 2002 "*Wind turbine noise issues*". University of Massachusetts, USA.

[59] Russel D.A, Titlow J.P & Bemmen Y.J. 1988. "*Acoustic monopoles, dipoles, and quadrupoles: An experiment revisited*". Science and Mathematics Department, Kettering University, Michigan, USA.

[60] Salomons E.M. 2001. "*Computational Atmospheric Acoustics*". Springer, Berlin, Germany.

[61] Schlichting H & Gersten K. 2000. "*Boundary-Layer Theory*". 8th Edition. Springer, Berlin, Germany.

[62] Søndergaard B, Plovsing B (1) & Sørensen T. 2009. "*Noise and energy optimization of wind farms – Validation of the Nord2000 propagation model for use on wind turbine noise*". (1) DELTA – Danish Electronics, Light & Acoustics, Hørsholm, Denmark. (2) EMD International A/S, Aalborg, Denmark.

[63] Tarrero A.I, Martin M.A (1), González J, Machimbarrena M (2) & Jacobsen F (3). 2008. "*Sound propagation in forests: A comparison of experimental results and values predicted by he Nord2000 model*". (1) EU Politécnica, Departamento de Física Aplicada, Valladolid, Spain. (2) ETS Arquitectura, Departamento de Física Aplicada, Valladolid, Spain. (3) Acoustic Technology, Technical University of Denmark, Lyngby, Denmark.

[64] Tickell C.E (1), Ellis J.T (2) & Bastasch M (3). 2004. "*Wind turbine generator noise prediction – Comparison of computer models*". (1) Connell Hatch, Sydney, Australia. (2) EMA Ltd, Newcastle, Australia. (3) CH2M HILL, Portland Oregon, USA.

[65] Tonin R. 2012. "*Sources of wind turbine noise and sound propagation*". Renzo Tonin & Associates, Sydney, Australia.

[66] Tunick A. 2002. "*Coupling Meteorology to Acoustics in Forests*". Army Research Laboratory, Adelphi, Maryland, USA.

[67] Wagner S, Bareiß R & Guidati G. 1996. "*Wind Turbine Noise*". 1st edn. Springer, Berlin, Germany.

[68] Wallergård M. 2013. "*Interaktionsdesign*". Department of Design Sciences, Lund University, Sweden.

[69] White M & Swearingen M. 2004. "*Sound Propagation Through a Forest: A predictive model*". Construction Engineering Research Laboratory, Champaign, USA.

[70] Wombat Forestcare Inc. 2010. "*Welcome to Wombat Forestcare*". Accessed 30 August 2014. <http://www.wombatforestcare.org.au/index.php?page=Home>

[71] Zhu W.J. 2004. "*Modelling Of Noise From Wind Turbines*". Mechanical Department, Technical University of Denmark, Denmark.

Personal communication

[72] Attenborough K. Department of Design, Development, Environment and Materials, the Open University, United Kingdom. 20 May 2014.

[73] Lam Y.W. Acoustics Research Centre, School of Computing and Engineering, University of Salford, United Kingdom. 25 June 2014.

[74] Lian D. GE Power & Water, Melbourne, Australia. 18 December 2013.

[75] Stålne K. Lund Institute of Technology, Sweden. Continuous communication from 4 February 2014.

[76] Sjöström A. Lund Institute of Technology, Sweden. Continuous communication from 11 February 2014.

[77] Svensson J. Lund Institute of technology, Sweden. 24 February 2014.

8 Abbreviations

Name	Symbol	Unit
Absolute humidity	h	%
Absorbed sound intensity	I_a	W/m^2
Absorption coefficient	α	dB/100m
Adiabatic bulk modulus	K_S	Pa
Adiabatic index (= 1.402 for air)	γ	[-]
Air density	ρ_0	kg/m^3
Angle between sound source and receiver	φ	rad
Angular frequency	ω	rad/s
Atmospheric absolute temperature	T_K	K
Atmospheric absorption	A_{abs}	dB
Atmospheric pressure	p_s	kPa
Atmospheric temperature	T	^{o} C
Attenuation caused by a barrier	$A_{barrier}$	dB
Attenuation caused by vegetation	$A_{vegetation}$	dB
Attenuation due to atmospheric turbulence	$A_{turbulence}$	dB
Attenuation due to varying meteorological conditions	$A_{weather}$	dB
Average equivalent continuous sound pressure level	L_{s+n}	dBA
Average tree height	H	m
Averaged refractive index	$\bar{n}$	-

Boundary loss factor	F(w)	-
Canopy flow index	n	-
Characteristic ground impedance	Z_c	-
Combined sound pressure level of several sources	$L_{p, tot}$	dB
Complementary error function	erfc(z)	-
Complex pressure amplitude	p_c	Pa
Complex velocity amplitude	v_c	m/s
Complex wave number of the upper ground layer	k_1	-
Depth of the transition layer	z_*	m
Diabatic influence function dependent on ϕ^*_m	Ψ^*_m	-
Direction of the sound receiver	θ_R	rad from N
Direction of the wind	θ_W	rad from N
Displacement height	d	m
Distance sound travels into the forest	R_{Forest}	m
Earth's radius (= 6,371,000)	R_{Earth}	m
Effective sound pressure	$\tilde{p}$	Pa
Effective speed of sound at height z	$c_{eff}(z)$	m/s
Effective speed of sound at the height of sound source	c_{eff, z_S}	m/s
Effective speed of sound, including turbulence	$c_{eff, t}$	m/s
Equilibrium density of a medium	ρ	kg/m^3
Equivalent sound pressure level	$L_{eq, T}$	dB
Excess attenuation	A_E	dB
Flow resistivity	σ	$Pa \cdot s/m^2$
Fluctuation	μ	-
Frequency	f	Hz
Fresnel function	$F_2(x)$	-

Friction velocity	u^*	
Ground attenuation	A_{ground}	dB
Ground layer thickness	t	m
Heaviside step function	H(x)	-
Height above ground	z	m
Height at ground 1-2 transition	z_1	m
Height at ground 2-3 transition	z_2	m
Height of equal wind speed, far above the tree canopy	$\hat{z}$	m
Height of the receiver point	z_R	m
Height of the sound source	z_S	m
Height of transition layer	z_*	m
Horizontal distance between sound source and receiver	D	m
Incident sound intensity	I_i	W/m^2
Inclination angle	δ	rad
Latitude coordinates	φ	rad
Length of the direct sound ray	R_1	m
Length of the reflected sound ray	R_2	m
Length of source- discontinuity-receiver path for Z_j	S_j	m
Longitude coordinates	γ	rad
Mass transfer function	ϕ^*_m	-
Molecular weight (= 0.029 for air)	M	kg/mole
Nitrogen relaxation frequency	$F_{r,N}$	Hz
Normalized ground impedance	Z	-
Normalized impedance of a layered ground	Z_{layer}	-
Normalized impedance of the upper ground layer	Z_I	-
Normalized impedance of the lower ground layer	Z_{II}	-

Number of measurements	N	-
Numerical distance	w	-
Oxygen relaxation frequency	$F_{r,O}$	Hz
Particle velocity, dependent on time and position	v	m/s
Plane wave reflection coefficient	R_p	-
Power-law exponent	P	-
Radial distance from sound source to receiver	r	m
Reference atmospheric pressure (= 101.325)	p_{s0}	kPa
Reference atmospheric temperature (= 293.15)	T_0	K
Reference height above ground	z_r	m
Reference intensity (= 10^{-12})	I_{ref}	W/m^2
Reference power (= 10^{-12})	W_{ref}	W
Reference sound pressure (= 2×10^{-5} for air)	p_{ref}	Pa
Reflection angle	θ	rad
Refractive index	n	-
Relative humidity	h_r	%
Roughness length, forest	$z_{0\ forest}$	m
Roughness length, open ground	$z_{0\ open}$	m
Saturation vapour pressure	p_{sat}	kPa
Sound intensity	I	W/m^2
Sound intensity level	L_I	dB
Sound power	W	W
Sound power level	L_W	dB
Sound pressure amplitude of a sound wave	$\hat{p}$	Pa
Sound pressure, dependent in time and position	p	Pa
Sound pressure level	L_p	dB

Sound pressure level of time interval i	L_i	dB
Specific impedance	Z_s	Pa ·m/s
Specific normalized admittance	β	-
Specular reflection point	G	-
Speed of sound	c	m/s
Speed of sound in air	c_0	m/s
Spherical wave reflection coefficient	Q	-
Static pressure	p_o	Pa
Surface roughness length	z_0	m
Triple-point isotherm temperature (= 273.16)	T_{01}	K
Universal gas constant (= 8.314)	R	J/K
Von Kármán’s constant (= 0.40)	k_v	-
Wave number	k	m^{-1}
Wavelength	λ	m
Weighted sound pressure level	$L_{Weighted}$	dB
Wind speed far above the tree canopy	$U(\hat{z})$	m/s
Wind speed above the canopy	U_{above}	m/s
Wind speed at the height of the sound source	U_{z_S}	m/s
Wind speed at the reference height	$U(z_r)$	m/s
Wind speed at the top of the canopy	U_H	m/s
Wind speed at the top of the transition layer	$U(z_*)$	m/s
Wind speed below the canopy	U_{below}	m/s
Wind speed in the direction of propagation with height	$U(z)_{dir}$	m/s
Wind speed with height	$U(z)$	m/s
Wind speed within the transition layer	$U_{transition}$	m/s

Appendix A: A- and C-filters

Values of standard A- and C- weighting filters in one-third octave bands [39].

Centre frequency (Hz)	A-weighting (dB)	C-weighting (dB)
8	-77.8	-20.0
10	-70.4	-14.3
12.5	-63.4	-11.2
16	-56.7	-8.5
20	-50.5	-6.2
25	-44.7	-4.4
31.5	-39.4	-3.0
40	-34.6	-2.0
50	-30.2	-1.3
63	-26.2	-0.8
80	-22.5	-0.5
100	-19.1	-0.3
125	-16.1	-0.2
160	-13.4	-0.1
200	-10.9	0.0
250	-8.6	0.0
315	-6.6	0.0
400	-4.8	0.0

Table A1. A- and C-filters for centre frequencies ranging from 8 Hz to 400 Hz.

Centre frequency (Hz)	A-weighting (dB)	C-weighting (dB)
500	-3.2	0.0
630	-1.9	0.0
800	-0.8	0.0
1,000	0.0	0.0
1,250	0.6	0.0
1,600	1.0	-0.1
2,000	1.2	-0.2
2,500	1.3	-0.3
3,150	1.2	-0.5
4,000	1.0	-0.8
5,000	0.5	-1.3
6,300	-0.1	-2.0
8,000	-1.1	-3.0
10,000	-2.5	-4.4
12,500	-4.3	-6.2
16,000	-6.6	-8.5
20,000	-9.3	-11.2

Table A2. A- and C-filters for centre frequencies ranging from 500 Hz to 20,000 Hz.

Appendix B: Surface roughness length

Surface roughness lengths for different terrain types [46].

Terrain Description	Surface Roughness Length, z_0 [m]
Very smooth, ice or mud	0.00001
Calm open sea	0.0002
Blown sea	0.0005
Snow surface	0.003
Lawn grass	0.008
Rough pasture	0.01
Fallow field	0.03
Crops	0.05
Few trees	0.1
Many trees, hedges, few buildings	0.25
Forests and woodlands	0.5
Suburbs	1.5
Centres of cities with tall buildings	3.0

Table B1. The surface roughness length of some common ground types.

Appendix C: Atmospheric absorption coefficient

The atmospheric absorption coefficient α expressed in dB/100 m for different air temperatures, relative humidity and 1/1 frequencies. Standard atmospheric pressure of 1.0 atm (101.325 kPa) applies.

Relative humidity [%]	Frequency [Hz]							
	63	125	250	500	1,000	2,000	4,000	8,000
10	0.030	0.100	0.244	0.428	0.768	1.943	6.424	22.060
30	0.011	0.042	0.154	0.454	0.924	1.504	2.953	8.396
50	0.007	0.026	0.101	0.353	0.952	1.770	2.938	6.471
70	0.005	0.019	0.074	0.276	0.866	1.922	3.226	6.106
90	0.004	0.015	0.058	0.224	0.763	1.949	3.520	6.196

Table C1. Atmospheric absorption coefficient at 40 ^{o}C.

Relative humidity [%]	Frequency [Hz]							
	63	125	250	500	1,000	2,000	4,000	8,000
10	0.036	0.095	0.181	0.339	0.868	2.868	9.695	26.280
30	0.015	0.054	0.167	0.336	0.616	1.189	3.302	11.422
50	0.009	0.035	0.124	0.356	0.703	1.170	2.468	7.417
70	0.007	0.025	0.095	0.312	0.714	1.277	2.320	6.003
90	0.005	0.020	0.077	0.270	0.732	1.381	2.361	5.397

Table C2. Atmospheric absorption coefficient at 30 ^{o}C.

Relative humidity [%]	Frequency [Hz]							
	63	125	250	500	1,000	2,000	4,000	8,000
10	0.037	0.077	0.157	0.424	1.411	4.558	11.008	17.625
30	0.019	0.061	0.142	0.251	0.501	1.414	4.899	16.869
50	0.012	0.044	0.131	0.273	0.467	0.990	2.972	10.549
70	0.009	0.033	0.112	0.279	0.498	0.905	2.312	7.777
90	0.007	0.027	0.096	0.270	0.530	0.909	2.032	6.354

Table C3. Atmospheric absorption coefficient at 20 ^oC.

Relative humidity [%]	Frequency [Hz]							
	63	125	250	500	1,000	2,000	4,000	8,000
10	0.034	0.078	0.227	0.751	2.166	4.248	5.749	6.972
30	0.022	0.055	0.105	0.227	0.678	2.363	7.737	18.858
50	0.016	0.048	0.105	0.189	0.427	1.328	4.718	15.719
70	0.012	0.041	0.104	0.193	0.366	0.972	3.313	11.864
90	0.010	0.034	0.099	0.200	0.354	0.818	2.599	9.380

Table C4. Atmospheric absorption coefficient at 10 ^oC.

Relative humidity [%]	Frequency [Hz]							
	63	125	250	500	1,000	2,000	4,000	8,000
10	0.042	0.129	0.398	0.925	1.408	1.659	1.906	2.662
30	0.022	0.047	0.116	0.372	1.271	3.620	6.932	9.566
50	0.018	0.041	0.082	0.208	0.684	2.395	7.164	14.804
70	0.015	0.039	0.076	0.161	0.465	1.625	5.609	15.479
90	0.013	0.036	0.076	0.145	0.367	1.218	4.368	13.988

Table C5. Atmospheric absorption coefficient at 0 ^oC.

Appendix D: Effective flow resistivity

The effective flow resistivity for various ground surface conditions [22].

Types of ground	Effective Flow Resistivity [kPa · s/m^2]	
	Range	Average
Concrete, painted	200,000	200,000
Concrete, depends on finish	30,000 – 100,000	65,000
Asphalt, old, sealed with dust	25,000 – 30,000	27,000
Quarry dust, hard packed	5,000 – 20,000	12,500
Asphalt, new, varies with particle size	5,000 – 15,000	10,000
Dirt, exposed, rain-packed	4,000 – 8,000	6,000
Dirt, old road, filled mesh	2,000 – 4,000	3,000
Limestone chips, ½ – 1 in. mesh	1,500 – 4,000	2,750
Dirt, roadside with <4 in. rocks	300 – 800	550
Sand, various types	40 – 906	317
Soil, various types	106 – 450	200
Grass lawn or grass field	125 – 300	200
Clay, dry (wheeled/unwheeled)	92 – 168	130
Grass field, 16.5% moisture content	75	75
Forest floor (Pine/Hemlock)	20 – 80	50
Grass field, 11.9% moisture content	41	41
Snow, various types	1.3 – 50	29

Table D1. The effective flow resistivity of some common ground type surfaces.

Appendix E: Ground attenuation derivation

Equation (3.22) for the ground attenuation of a monopole point sound source is derived below, based on [60].

The equation for the complex sound field is determined with the Helmholtz equation for the complex pressure amplitude (E1).

$$\nabla^2 p_c + k^2 p_c = 0 \tag{E1}$$

Where p_c the complex pressure amplitude [Pa]
k the wave number (see section 2.1.1) [rad/m]

The emitted sound field by a monopole point source will have a spherical symmetry, meaning it is only dependent on the radial distance from the source. Consequently, the Helmholtz equation is transformed into the following expression.

$$\frac{1}{r}\frac{\partial^2}{\partial r^2}(r p_c) + k^2 p_c = 0 \tag{E2}$$

The modified Helmholtz equation has the solution shown below, which represents the complex pressure amplitude of a sound wave propagating away from a point source.

$$p_c = S\frac{e^{ikr}}{r} \tag{E3}$$

Where S a constant [-]

In order to determine the ground effect, the sound source may be imagined as being positioned in a free field, i.e. with no surrounding boundaries. Considering the dimensions illustrated in figure 3.5, the complex pressure amplitude for the source can be expressed according to the equation below.

$$p_{source} = S\frac{e^{ikR_1}}{R_1} \tag{E4}$$

Where p_{source} the sound pressure emitted by the source [Pa]
R_1 the length of the direct sound wave (see section 3.2.2) [m]

The complex pressure amplitude at the receiver is the combined sound pressure generated by the source and that reflected by the ground surface. It may thus be further derived as to be dependent on the complex pressure amplitude for the source, which is expressed in equation (E5).

$$
\begin{aligned}
p_{receiver} &= S\frac{e^{ikR_1}}{R_1} + QS\frac{e^{ikR_2}}{R_2} \\
&= p_{source} + QS\frac{e^{ikR_2}}{R_2} \\
&= p_{source}\left[1 + Q\frac{R_1}{R_2}e^{(ikR_2 - ikR_1)}\right] \qquad \text{(E5)}
\end{aligned}
$$

Where $p_{receiver}$ the sound pressure detected at the receiver point [Pa]
R_2 the length of the reflected sound wave (see section 3.2.2) [m]

By employing (2.5), equations (E4) and (E5) may be transformed into expressions of the sound pressure level.

$$L_{p,source} = 10\log\left(\frac{1}{2}\frac{|p_{source}|^2}{{p_{ref}}^2}\right) \qquad \text{(E6)}$$

$$L_{p,receiver} = 10\log\left(\frac{1}{2}\frac{|p_{source}|^2}{{p_{ref}}^2}\right) \qquad \text{(E7)}$$

The sound pressure levels that will be experience at the receiver may thus be expressed as the sum of the levels emitted by the source and those absorbed or amplified due to interference with the ground. Furthermore the ground attenuation is the reversed sign of the resulting expression and is hence calculated with equation (3.22).

$$
\begin{aligned}
A_{ground} &= -\left[L_{p,receiver} - L_{p,source}\right] \\
&= -10\log\left(|p_{receiver}|^2 / |p_{source}|^2\right) \\
&= -10\log\left|1 + Q\frac{R_1}{R_2}e^{(ikR_2 - ikR_1)}\right|^2 \qquad \text{(3.22)}
\end{aligned}
$$

Appendix F: Effective flow resistivity in forests

The effective flow resistivity for various ground types commonly included in layers of forest floors [1].

F.1 Granular surfaces

Ground type	Effective Flow Resistivity [kPa · s/m^2]
Wet sandy loam	1,501
Compacted silt	1,477
Mineral layer beneath mixed deciduous forest	540 ± 92
Sand (moistened)	479
Loamy sand or plain	422 ± 165
Hard clay field	400
Sand (dry)	376
Bare sandy plain	366 ± 108
Dry sandy plain	259
Humus on pine forest floor	233 ± 223
Sand (dry)	134
Sand (grain diameter 0.25 – 0.33 mm)	95.9
Sand (dry)	70.9
Sand (grain diameter 0.33 – 0.50 mm)	61.2
Gravel (mean max. grain dimension 1.81 mm)	57.8

Table F1. The effective flow resistivity of granular ground surfaces.

F.2 Organic root layers

Ground type	Effective Flow Resistivity [kPa · s/m^2]
Bare loamy sand	422 ± 165
Grass root layer in loamy sand	153 ± 91
Grass root layer in loamy sand	237 ± 77
Loamy sand beneath root-zone	677 ± 93
Loamy sand with roots	114 ± 52

Table F2. The effective flow resistivity of organic root layers.

F.3 Low flow resistivity outdoor surfaces

Ground type	Effective Flow Resistivity [kPa · s/m^2]
Litter layer on mixed deciduous forest floor (0.01 – 0.05 m)	30 ± 31
Wet peat	24 ± 5
Beech forest litter layer (0.04 – 0.08 m)	22 ± 13
Snow (old)	16.4
Pine forest litter (0.06 – 0.07 m)	9 ± 5
Snow (new)	4.73
Gravel (mean max. grain dimension 9.02 mm)	1.648

Table F3. The effective flow resistivity of low flow resistivity outdoor ground surfaces.

F.4 Grassland

Ground type	Effective Flow Resistivity [kPa · s/m^2]
Loamy sand beneath lawn (no roots)	677 ± 93
Grass covered compact sandy soil	463 ± 122
Grass-covered field	300
Loamy sand beneath lawn (0.06 m thick with roots)	237 ± 77
Grass	220
Grass root-filled layer	189 ± 91
Loamy sand with roots (mixed grass overgrowth)	114 ± 52

Table F4. The effective flow resistivity of grassland.

Appendix G: Fresnel function derivation

The Fresnel function is derived below as to be dependent on the complementary error function [73].

The Fresnel function is commonly expressed with equation (3.38).

$$F_2(x) = \int_x^\infty e^{\left(iw^2\right)}\, dw = \int_x^\infty e^{-\left(i\sqrt{i}\, w\right)^2}\, dw \tag{3.38}$$

The equation may be expressed in terms of the complementary error function by employing the following relationships.

$$iw^2 = -t^2$$

$$\Longrightarrow \sqrt{i}\, w = it$$

$$\Longrightarrow -i\sqrt{i}\, w = t$$

$$\Longrightarrow bw = t \qquad \text{if} \qquad b = -i\sqrt{i}$$

$$= -i(1+i)\frac{\sqrt{2}}{2} = (1-i)\frac{\sqrt{2}}{2}$$

The imaginary part of the Fresnel function is substituted with the relations presented above.

$$F_2(x) = \int_x^\infty e^{-(bw)^2}\, dw$$

$$= \frac{1}{b}\int_x^\infty e^{-(bw)^2} dbw$$

$$= \frac{1}{b}\int_{bx}^\infty e^{-t^2} dt$$

The complementary error function is expressed with equation (G1).

$$\mathrm{erfc}(x) = \frac{2}{\sqrt{\pi}} \int_x^{\infty} e^{-t^2} dt \tag{G1}$$

By insertion of equation (G1), the Fresnel function may be simplified to the following.

$$F_2(x) = \frac{1}{b} \frac{\sqrt{\pi}}{2} \; \mathrm{erfc}(bx)$$

$$= \frac{2}{(1-i)\sqrt{2}} \frac{\sqrt{\pi}}{2} \; \mathrm{erfc}\left[(1-i)\frac{\sqrt{2}}{2} x\right]$$

$$= \frac{(1+i)}{2} \frac{\sqrt{\pi}}{\sqrt{2}} \; \mathrm{erfc}\left[(1-i)\frac{\sqrt{2}}{2} x\right]$$

Appendix H: Noise measurement results

The equivalent sound pressure level L_{eq} 90 of the emitted white noise as well as background noise, measured in 1/3 octave from 6.3 Hz to 20,000 Hz during the *initial open field* measurements.

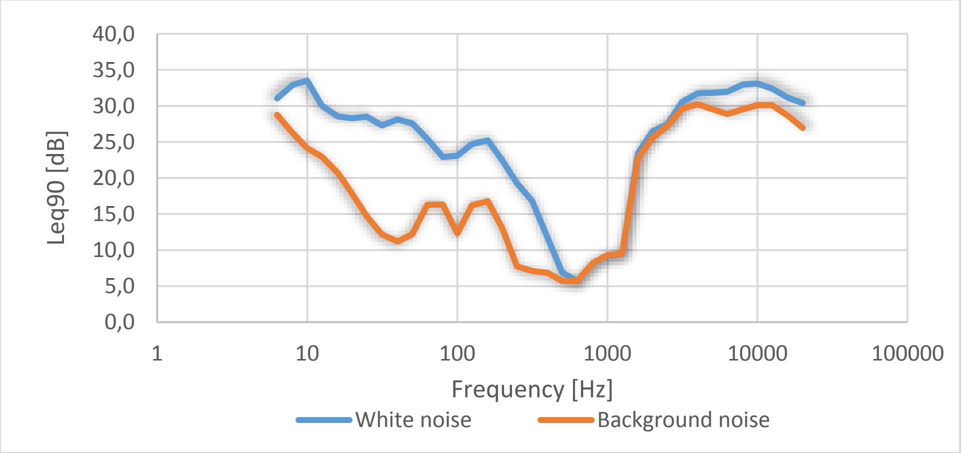

Diagram H1. White noise and background noise at 300 m (measuring point 1.2).

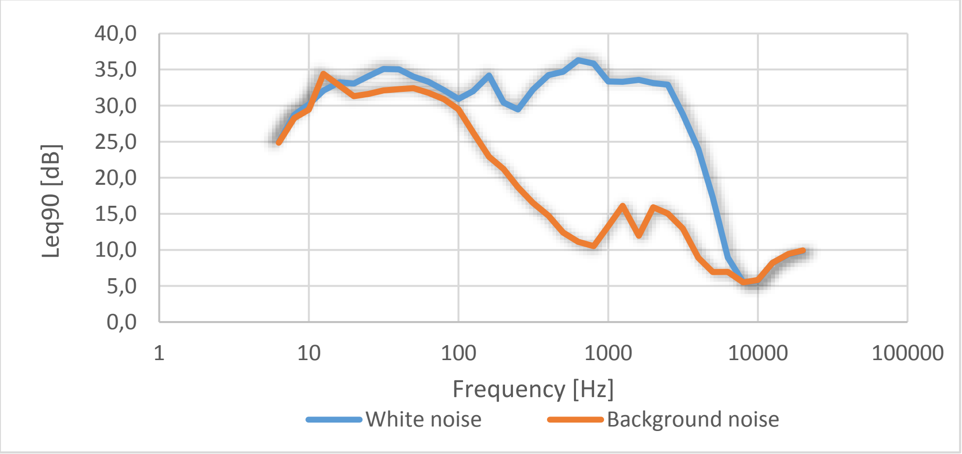

Diagram H2. White noise and background noise at 600 m (measuring point 1.3).

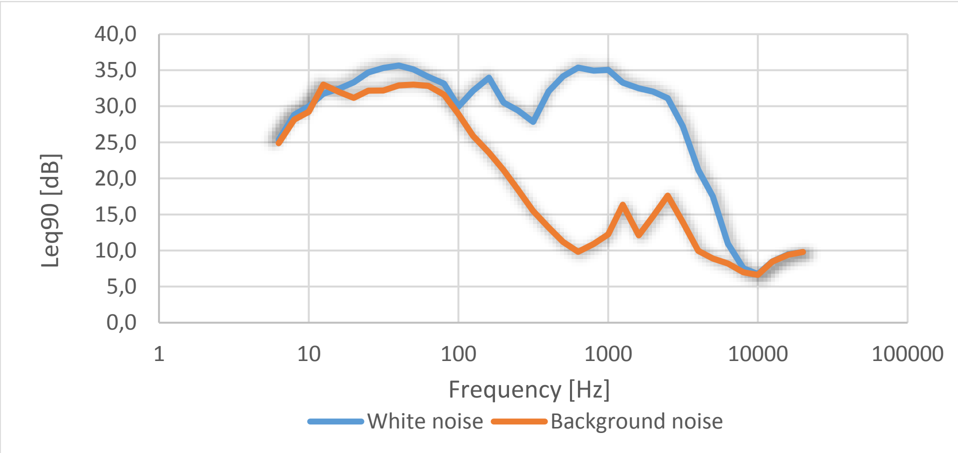

Diagram H3. White noise and background noise at 900 m (measuring point 1.4).

The equivalent sound pressure level L_{eq} 90 of the emitted white noise as well as background noise, measured in 1/3 octave from 6.3 Hz to 20,000 Hz during the *initial forest* measurements.

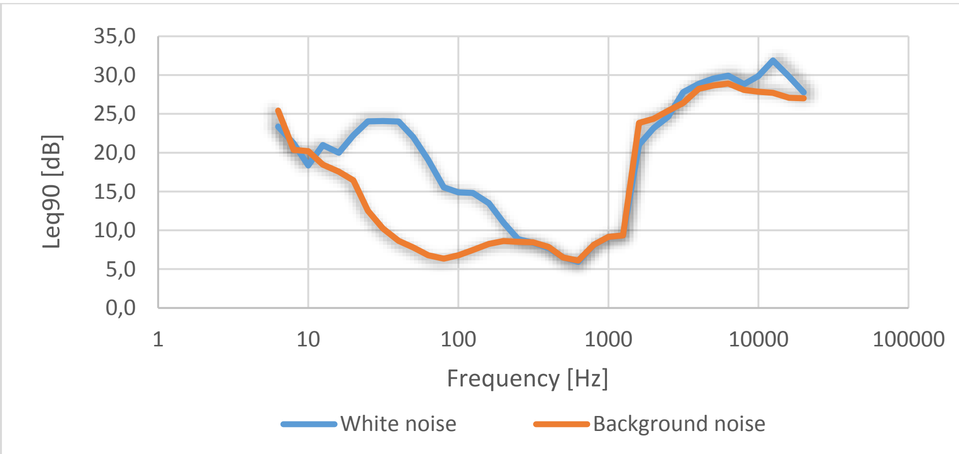

Diagram H4. White noise and background noise at 300 m (measuring point 2.2).

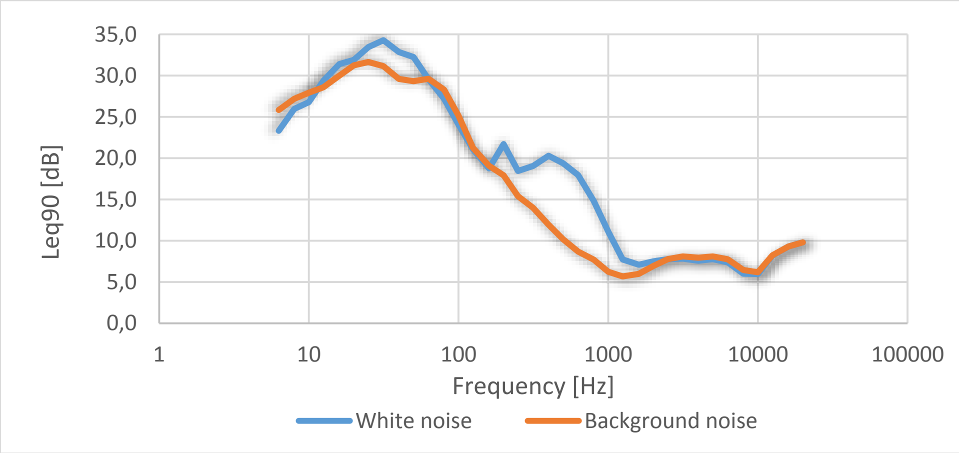

Diagram H5. White noise and background noise at 600 m (measuring point 2.3).

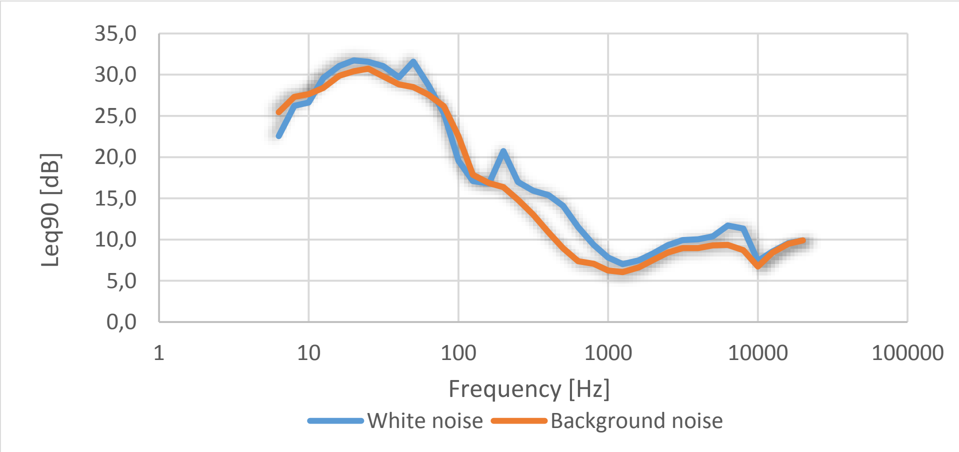

Diagram H6. White noise and background noise at 900 m (measuring point 2.4).

The equivalent sound pressure level L_{eq} 90 of the emitted white noise as well as background noise, measured in 1/3 octave from 6.3 Hz to 20,000 Hz during the *initial mixed ground* measurements.

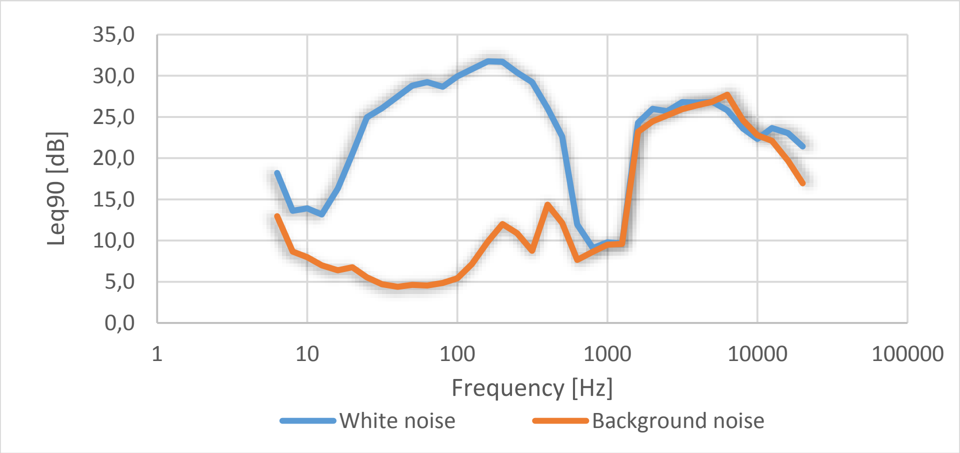

Diagram H7. White noise and background noise at 300 m (measuring point 3.2).

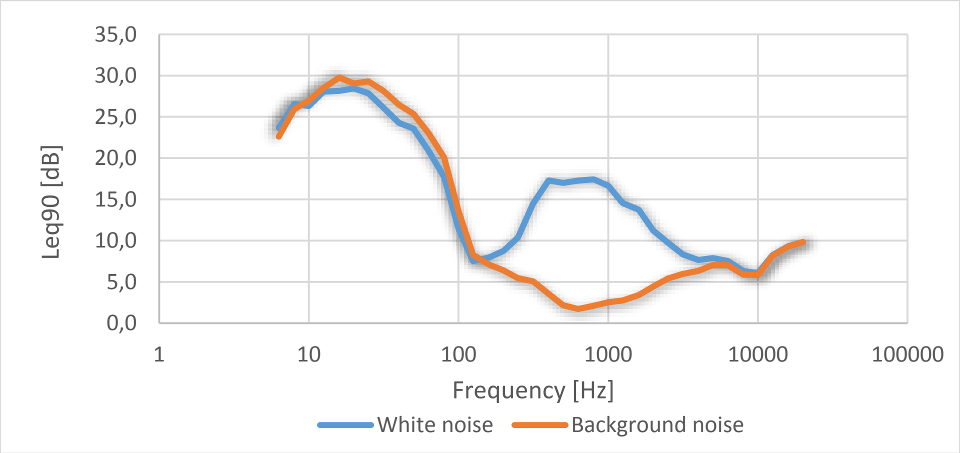

Diagram H8. White noise and background noise at 600 m (measuring point 3.3).

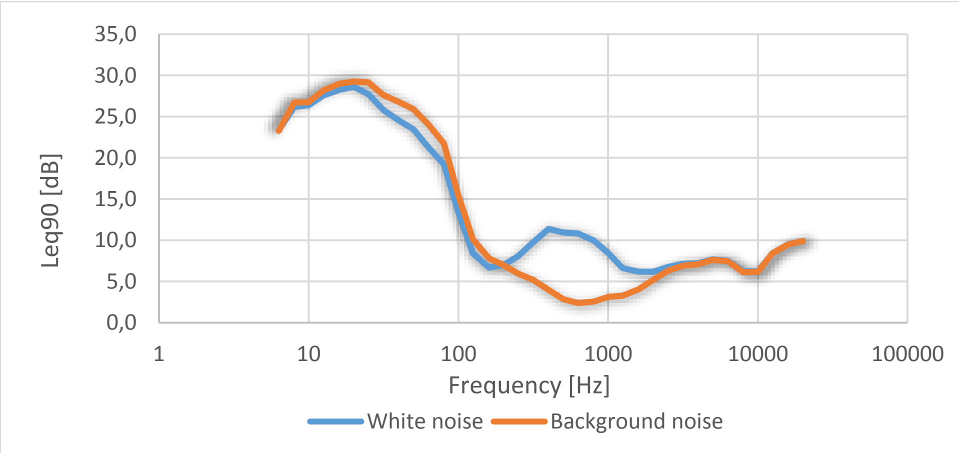

Diagram H9. White noise and background noise at 900 m (measuring point 3.4).

The equivalent sound pressure level L_{eq} 90 of the emitted white noise, measured in 1/3 octave from 6.3 Hz to 20,000 Hz during the *initial* measurements.

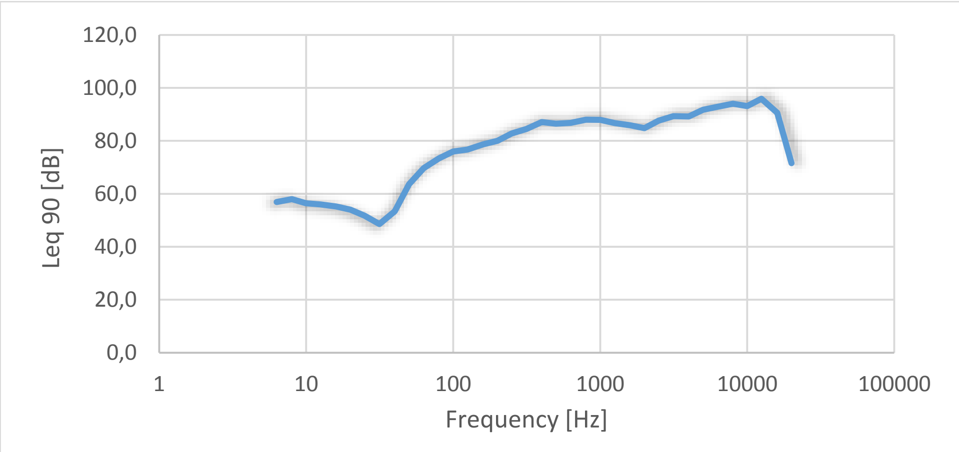

Diagram H10. The emitted white noise at 1.0 m (measuring points 1.1, 2.1 and 3.1).

The equivalent sound pressure level L_{eq} 90 of the emitted white noise as well as background noise, measured in 1/3 octave from 6.3 Hz to 20,000 Hz during the *continued forest* measurements.

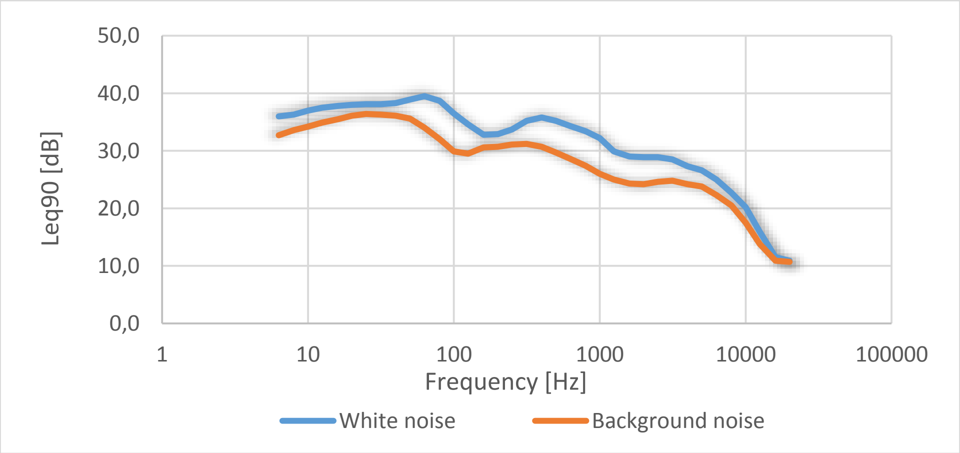

Diagram H11. White noise and background noise at 200 m (measuring point 2.2).

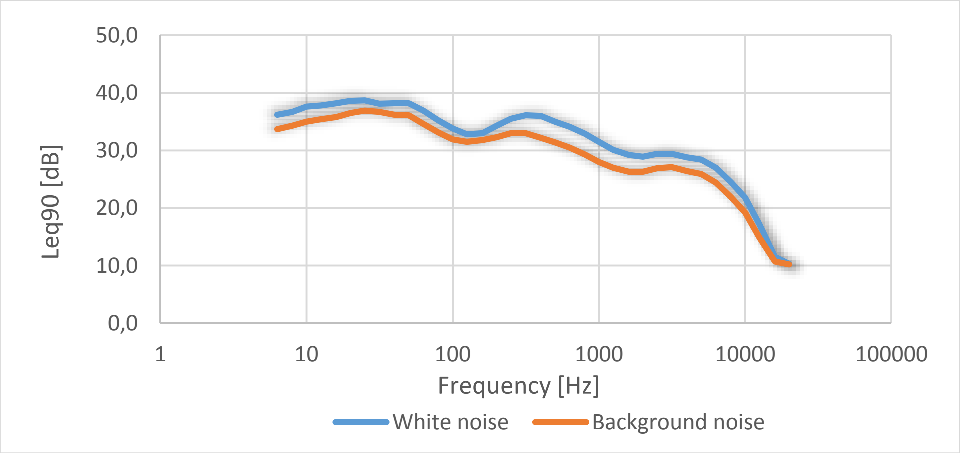

Diagram H12. White noise and background noise at 400 m (measuring point 2.3).

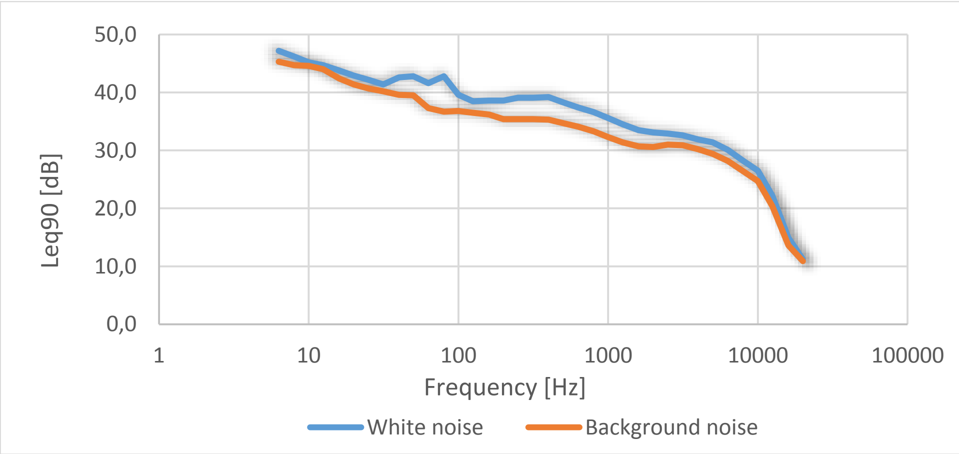

Diagram H13. White noise and background noise at 600 m (measuring point 2.4).

The equivalent sound pressure level L_{eq} 90 of the emitted white noise as well as background noise, measured in 1/3 octave from 6.3 Hz to 20,000 Hz during the *continued mixed ground* measurements.

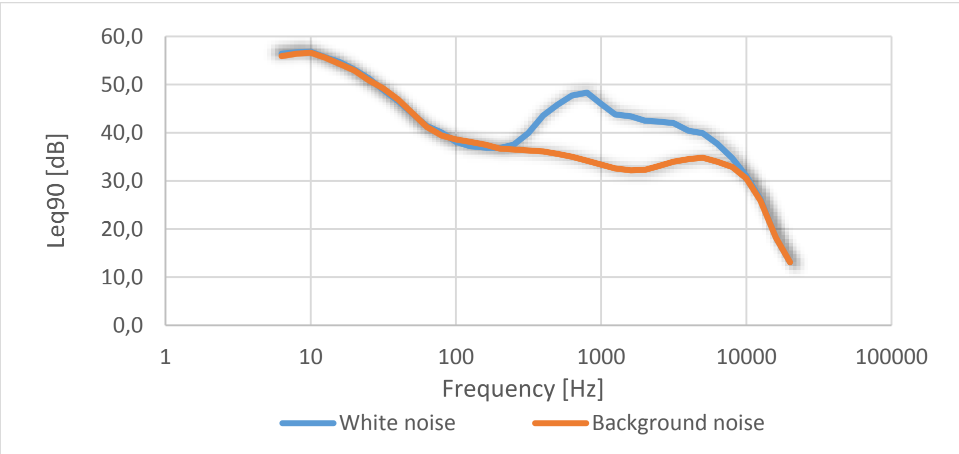

Diagram H14. White noise and background noise at 200 m (measuring point 3.2).

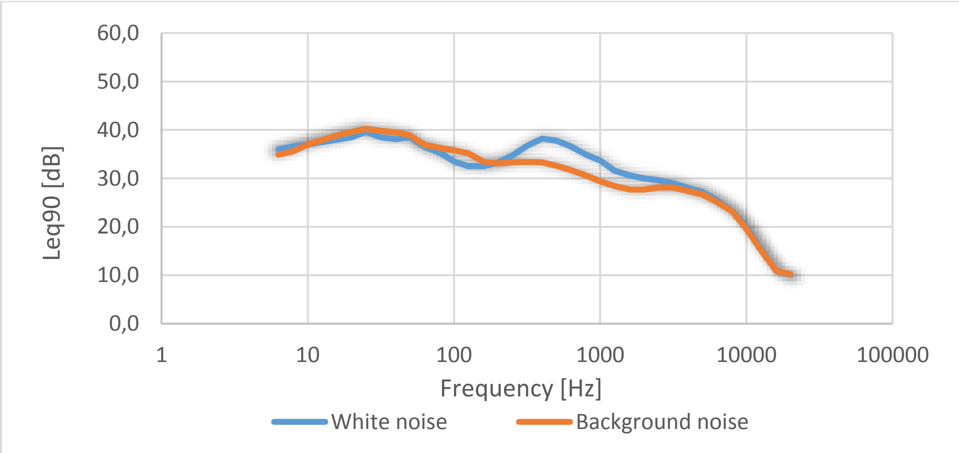

Diagram H15. White noise and background noise at 400 m (measuring point 3.3).

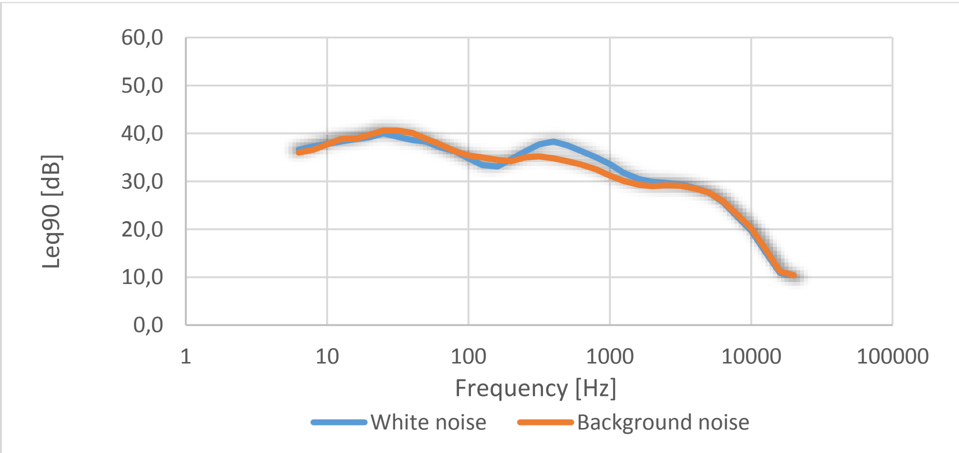

Diagram H16. White noise and background noise at 600 m (measuring point 3.4).

The equivalent sound pressure level L_{eq} 90 of the emitted white noise as well as background noise, measured in 1/3 octave from 6.3 Hz to 20,000 Hz during the *final* measurements.

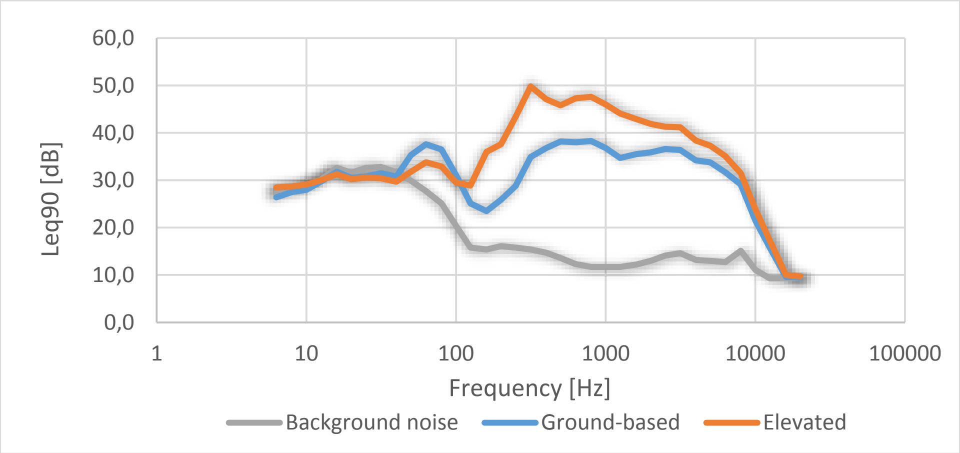

Diagram H17. White noise and background noise at 100 m (measuring point 2.2).

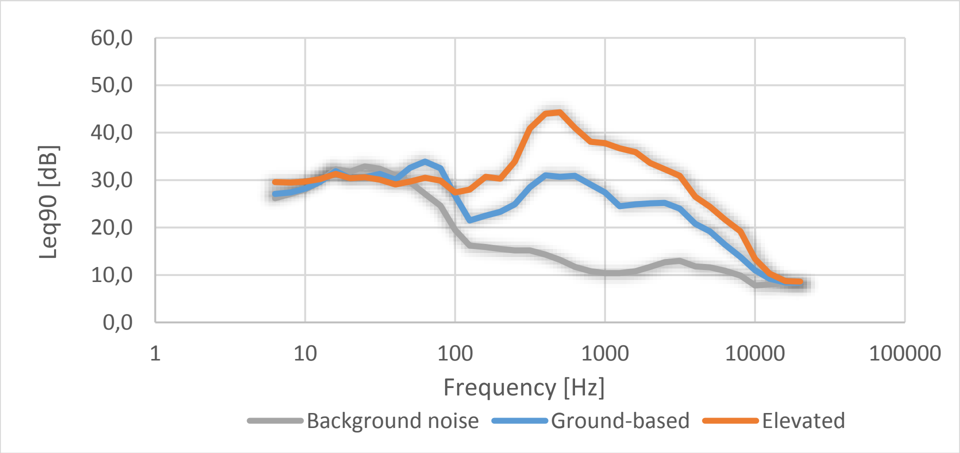

Diagram H18. White noise and background noise at 200 m (measuring point 2.3).

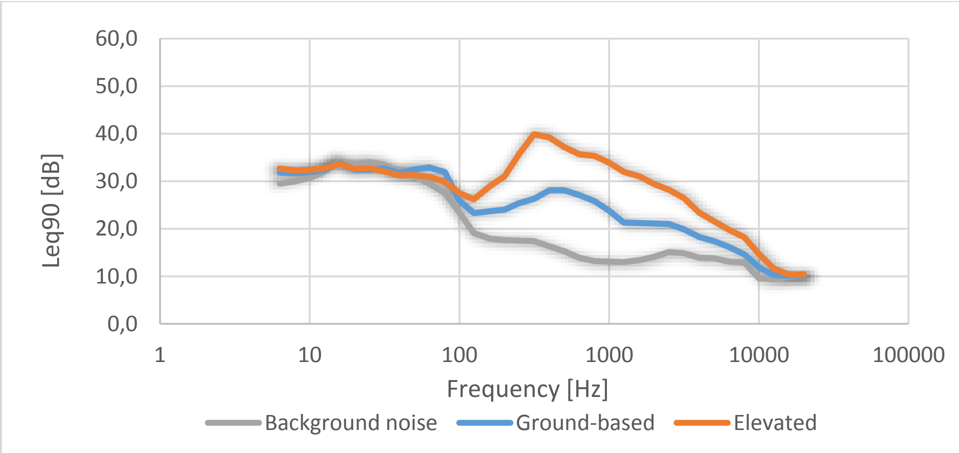

Diagram H19. White noise and background noise at 300 m (measuring point 2.4).

Appendix I: Meteorological data

Weather data for a community in close proximity to the chosen measuring site, during the *initial* measurements. The statistics were obtained from the Australian Bureau of Meteorology.

Time	Weather conditions during forest measurements (points 2.1 to 2.4) 31st of May 2014					
	Atmospheric temperature [°C]	Relative humidity [%]	Wind speed [m/s]	Wind direction [° from N]	Maximum wind speed [m/s]	Atmospheric pressure [hPa]
13.00	14.7	71	2.1	50	2.6	1,019.8
13.30	14.7	73	2.6	50	4.1	1,018.9
14.00	15.0	74	2.1	70	3.6	1,018.5
14.30	14.7	75	1.5	70	2.6	1,017.9
Average	14.8	73.3	2.1	60.0	3.2	1,018.8

Table I1. Meteorological conditions during the initial forest measurements

Time	Weather conditions during open field measurements (points 1.1 to 1.4) 2nd of June 2014					
	Atmospheric temperature [°C]	Relative humidity [%]	Wind speed [m/s]	Wind direction [° from N]	Maximum wind speed [m/s]	Atmospheric pressure [hPa]
08.00	6.1	99	2.6	210	3.1	1,019.5
08.30	8.2	99	2.1	220	2.6	1,019.5
09.00	10.1	99	2.1	220	3.1	1,019.3
09.30	12.1	96	1.5	200	2.6	1,019.3
Average	9.1	98.2	2.1	212.5	2.9	1,019.4

Table I2. Meteorological conditions during the initial open field measurements.

Time	Weather conditions during mixed ground measurements (points 3.1 to 3.4) 2nd of June 2014					
	Atmospheric temperature [^oC]	Relative humidity [%]	Wind speed [m/s]	Wind direction [^{o} from N]	Maximum wind speed [m/s]	Atmospheric pressure [hPa]
11.00	14.4	80	2.6	190	3.1	1019.4
11.30	15.1	75	1.5	230	2.6	1019.1
12.00	14.9	71	1.0	260	2.1	1018.6
12.30	14.8	75	1.5	230	2.6	1018.1
Average	14.8	75.3	1.7	227.5	2.6	1,018.8

Table I3. Meteorological conditions during the initial mixed ground measurements.

Weather data for a community in close proximity to the chosen measuring site, during the *continued* measurements. The statistics were obtained from the Australian Bureau of Meteorology.

Time	Weather conditions during mixed ground measurements (points 3.1 to 3.4) 18th of October 2014					
	Atmospheric temperature [^{o}C]	Relative humidity [%]	Wind speed [m/s]	Wind direction [^{o} from N]	Maximum wind speed [m/s]	Atmospheric pressure [hPa]
13.00	21.5	32	4.1	30	6.2	1,024.8
13.30	22.2	34	4.6	20	7.7	1,024.2
14.00	22.1	35	4.1	10	6.7	1,023.4
14.30	22.7	31	2.6	350	5.1	1,022.9
15.00	22.2	33	3.1	30	6.2	1,022.6
Average	22.1	33.0	3.7	18.0	6.4	1,023.6

Table I4. Meteorological conditions during continued mixed ground measurements.

Time	Weather conditions during forest measurements (points 2.1 to 2.4) 19th of October 2014					
	Atmospheric temperature [^{o}C]	Relative humidity [%]	Wind speed [m/s]	Wind direction [^{o} from N]	Maximum wind speed [m/s]	Atmospheric pressure [hPa]
12.30	25.2	31	4.1	360	6.2	1,021.4
13.00	25.8	27	2.6	20	4.1	1,020.9
13.30	27.3	24	3.1	20	5.7	1,020.3
14.00	29.5	18	4.1	360	7.2	1,019.8
14.30	29.9	17	4.6	360	7.7	1,019.2
Average	27.5	23.4	3.7	8.0	6.2	1,020.3

Table I5. Meteorological conditions during continued forest measurements.

Weather data for a community in close proximity to the chosen measuring site, during the *final* measurements. The statistics were obtained from the Australian Bureau of Meteorology.

Time	Weather conditions during forest measurements (points 2.1 to 2.4) 29th of October 2014					
	Atmospheric temperature [^{o}C]	Relative humidity [%]	Wind speed [m/s]	Wind direction [^{o} from N]	Maximum wind speed [m/s]	Atmospheric pressure [hPa]
Background noise measurements						
10.30	15.1	55	2.6	310	4.1	1,018.8
11.00	17.2	53	1.5	290	5.1	1,018.3
11.30	17.6	50	2.1	310	4.1	1,017.8
Average	16.6	52.7	2.1	303.3	4.4	1,018.3
Ground based measurements						
11.30	17.6	50	2.1	310	4.1	1,017.8
12.00	18.6	47	2.1	310	5.1	1,017.5
12.30	20.3	43	3.1	330	5.1	1,017.2
Average	18.8	46.7	2.4	316.7	4.8	1,017.5
Elevated measurements						
13.30	21.7	40	3.1	10	6.2	1,016.2
14.00	22.3	38	2.6	290	5.1	1,015.7
14.30	22.6	35	3.6	290	5.1	1,015.0
Average	22.2	37.7	3.1	316.7	5.5	1,015.6

Table I6. Meteorological conditions during the final forest measurements.

Appendix J: Sound attenuation factors

Sound attenuation caused by geometrical divergence, atmospheric absorption and ground effect calculated for analysis of the *initial forest* measurements.

[Hz]	Geometrical divergence [dB]			Atmospheric absorption [dB/m]			Ground attenuation [dB]		
	300 m	600 m	900 m	300 m	600 m	900 m	300 m	600 m	900 m
6.3	-60.301	-66.322	-69.844	0.000	0.001	0.001	-6.312	-6.330	-6.699
8				0.001	0.001	0.002	-6.423	-6.446	-6.960
10				0.001	0.002	0.002	-6.564	-6.593	-7.292
12.5				0.001	0.002	0.004	-6.753	-6.790	-7.735
16				0.002	0.004	0.006	-7.034	-7.082	-8.392
20				0.003	0.006	0.010	-7.373	-7.434	-9.172
25				0.005	0.010	0.015	-7.811	-7.889	-10.147
31.5				0.008	0.016	0.023	-8.385	-8.485	-11.328
40				0.013	0.025	0.038	-9.107	-9.233	-12.511
50				0.019	0.039	0.058	-9.842	-9.996	-12.900
63				0.031	0.061	0.092	-10.465	-10.639	-10.494
80				0.048	0.097	0.145	-10.324	-10.480	1.199
100				0.074	0.147	0.221	-7.888	-7.873	25.335
125				0.110	0.221	0.331	0.919	1.797	44.358
160				0.169	0.338	0.508	24.713	24.235	52.534
200				0.242	0.483	0.725	39.859	50.579	42.348
250				0.334	0.668	1.002	28.814	39.760	35.158
315				0.448	0.895	1.343	22.320	30.853	30.189
400				0.579	1.158	1.737	17.792	25.155	26.376

Table J1. Sound attenuation factors for centre frequencies ranging from 8 Hz to 400 Hz during the initial forest measurements.

[Hz]	Geometrical divergence [dB]			Atmospheric absorption [dB/m]			Ground attenuation [dB]		
	300 m	600 m	900 m	300 m	600 m	900 m	300 m	600 m	900 m
500	-60.301	-66.322	-69.844	0.710	1.420	2.130	14.540	21.327	23.470
630				0.855	1.710	2.565	11.714	18.152	20.844
800				1.026	2.052	3.078	9.137	15.351	18.376
1,000				1.228	2.456	3.684	6.928	12.998	16.210
1,250				1.505	3.010	4.516	4.847	10.804	14.128
1,600				1.965	3.929	5.894	2.658	8.498	11.887
2,000				2.607	5.215	7.822	0.772	6.488	9.900
2,500				3.597	7.194	10.791	-1.015	4.535	7.941
3,150				5.198	10.395	15.593	-2.725	2.567	5.938
4,000				7.825	15.649	23.474	-4.264	0.599	3.900
5,000				11.675	23.350	35.026	-5.356	-1.154	2.036
6,300				17.867	35.734	53.601	-5.882	-2.840	0.163
8,000				27.872	55.745	83.617	-5.188	-4.360	-1.677
10,000				42.166	84.333	126.499	-1.883	-5.440	-3.256
12,500				63.346	126.691	190.037	17.497	-5.951	-4.615
16,000				97.839	195.677	293.516	-2.976	-5.249	-5.685
20,000				141.864	283.728	425.593	-5.701	-1.928	-5.957

Table J2. Sound attenuation factors for centre frequencies ranging from 500 Hz to 20,000 Hz during the initial forest measurements.

Sound attenuation caused by geometrical divergence, atmospheric absorption and ground effect calculated for analysis of the *initial mixed ground* measurements.

[Hz]	Geometrical divergence [dB]			Atmospheric absorption [dB/m]			Ground attenuation [dB]		
	300 m	600 m	900 m	300 m	600 m	900 m	300 m	600 m	900 m
6.3	-60.301	-66.322	-69.844	0.000	0.001	0.001	-6.104	-5.923	-6.592
8				0.000	0.001	0.001	-6.137	-5.879	-6.809
10				0.001	0.002	0.002	-6.180	-5.821	-7.084
12.5				0.001	0.002	0.004	-6.237	-5.746	-7.450
16				0.002	0.004	0.006	-6.322	-5.641	-7.992
20				0.003	0.006	0.009	-6.423	-5.542	-8.629
25				0.005	0.010	0.014	-6.552	-5.500	-9.409
31.5				0.008	0.015	0.023	-6.713	-5.703	-10.309
40				0.012	0.024	0.037	-6.905	-6.607	-11.076
50				0.019	0.038	0.057	-7.088	-8.442	-11.057
63				0.030	0.060	0.090	-7.235	-10.823	-9.772
80				0.047	0.095	0.142	-7.249	-11.570	-6.411
100				0.072	0.144	0.216	-6.983	-6.354	-2.087
125				0.108	0.216	0.325	-6.203	-6.357	9.203
160				0.166	0.332	0.499	-4.243	-4.936	11.235
200				0.238	0.477	0.715	-0.700	-3.975	16.202
250				0.331	0.661	0.992	5.767	-2.855	19.907
315				0.445	0.891	1.336	11.292	-0.843	21.333
400				0.579	1.158	1.737	9.592	2.895	21.932

Table J3. Sound attenuation factors for centre frequencies ranging from 8 Hz to 400 Hz during the initial mixed ground measurements.

[Hz]	Geometrical divergence [dB]			Atmospheric absorption [dB/m]			Ground attenuation [dB]		
	300 m	600 m	900 m	300 m	600 m	900 m	300 m	600 m	900 m
500	-60.301	-66.322	-69.844	0.712	1.425	2.137	14.686	8.933	22.421
630				0.859	1.719	2.578	19.952	19.416	21.118
800				1.031	2.063	3.094	10.736	28.255	18.679
1,000				1.232	2.463	3.695	9.076	22.284	16.414
1,250				1.504	3.008	4.512	6.595	16.740	14.239
1,600				1.953	3.905	5.858	3.852	12.232	11.923
2,000				2.578	5.157	7.735	1.430	8.999	9.892
2,500				3.541	7.082	10.622	-0.488	6.243	7.908
3,150				5.097	10.194	15.291	-2.332	3.721	5.893
4,000				7.651	15.302	22.954	-4.020	1.372	3.852
5,000				11.397	22.794	34.192	-5.186	-0.623	1.991
6,300				17.426	34.853	52.279	-5.808	-2.482	0.124
8,000				27.184	54.367	81.551	-5.176	-4.127	-1.708
10,000				41.155	82.311	123.466	-1.957	-5.291	-3.279
12,500				61.925	123.851	185.776	16.207	-5.868	-4.630
16,000				95.924	191.848	287.772	-2.838	-5.233	-5.693
20,000				139.618	279.237	418.855	-5.665	-2.000	-5.958

Table J4. Sound attenuation factors for centre frequencies ranging from 500 Hz to 20,000 Hz during the initial mixed ground measurements.

Sound attenuation caused by geometrical divergence, atmospheric absorption and ground effect calculated for analysis of the *continued forest* measurements.

[Hz]	Geometrical divergence [dB]			Atmospheric absorption [dB/m]			Ground attenuation [dB]		
	200 m	400 m	600 m	200 m	400 m	600 m	200 m	400 m	600 m
6.3	-56.867	-62.887	-66.409	0.000	0.001	0.001	-6.254	-6.280	-6.344
8				0.001	0.001	0.002	-6.339	-6.372	-6.460
10				0.001	0.002	0.003	-6.445	-6.486	-6.604
12.5				0.002	0.003	0.005	-6.584	-6.636	-6.792
16				0.003	0.005	0.008	-6.786	-6.852	-7.065
20				0.004	0.008	0.013	-7.022	-7.105	-7.383
25				0.007	0.013	0.020	-7.315	-7.417	-7.774
31.5				0.010	0.021	0.031	-7.679	-7.803	-8.253
40				0.017	0.033	0.050	-8.095	-8.240	-8.776
50				0.026	0.051	0.077	-8.445	-8.598	-9.154
63				0.040	0.080	0.120	-8.566	-8.687	-9.060
80				0.062	0.124	0.186	-7.888	-7.858	-7.413
100				0.092	0.185	0.277	-5.295	-4.817	-1.913
125				0.135	0.269	0.404	2.209	4.162	15.918
160				0.197	0.395	0.592	25.272	29.529	38.297
200				0.268	0.536	0.804	34.400	42.934	46.088
250				0.350	0.699	1.049	24.802	34.186	37.549
315				0.441	0.882	1.324	18.757	26.648	30.100
400				0.541	1.082	1.623	14.410	21.447	24.918

Table J5. Sound attenuation factors for centre frequencies ranging from 8 Hz to 400 Hz during the continued forest measurements.

[Hz]	Geometrical divergence [dB]			Atmospheric absorption [dB/m]			Ground attenuation [dB]		
	200 m	400 m	600 m	200 m	400 m	600 m	200 m	400 m	600 m
500	-56.867	-62.887	-66.409	0.641	1.282	1.923	11.238	17.823	21.296
630				0.762	1.523	2.285	8.464	14.755	18.226
800				0.924	1.848	2.772	5.928	12.013	15.480
1,000				1.139	2.279	3.418	3.762	9.696	13.154
1,250				1.458	2.917	4.375	1.741	7.530	10.975
1,600				2.009	4.018	6.027	-0.345	5.257	8.677
2,000				2.793	5.586	8.379	-2.081	3.288	6.670
2,500				4.006	8.012	12.017	-3.628	1.393	4.716
3,150				5.963	11.926	17.888	-4.927	-0.480	2.745
4,000				9.148	18.297	27.445	-5.730	-2.287	0.772
5,000				13.752	27.503	41.255	-5.580	-3.797	-0.990
6,300				20.989	41.979	62.968	-3.485	-5.069	-2.690
8,000				32.274	64.549	96.823	6.111	-5.850	-4.235
10,000				47.579	95.159	142.738	1.070	-5.681	-5.355
12,500				68.674	137.349	206.023	-5.656	-3.692	-5.937
16,000				99.603	199.206	298.809	0.500	6.154	-5.394
20,000				134.174	268.347	402.521	-3.997	0.920	-2.464

Table J6. Sound attenuation factors for centre frequencies ranging from 500 Hz to 20,000 Hz during the continued forest measurements.

Sound attenuation caused by geometrical divergence, atmospheric absorption and ground effect calculated for analysis of the *continued mixed ground* measurements.

[Hz]	Geometrical divergence [dB]			Atmospheric absorption [dB/m]			Ground attenuation [dB]		
	200 m	400 m	600 m	200 m	400 m	600 m	200 m	400 m	600 m
6.3	-56.813	-62.834	-66.356	0.000	0.001	0.001	-6.085	-5.947	-6.546
8				0.001	0.001	0.002	-6.111	-5.918	-6.715
10				0.001	0.002	0.003	-6.144	-5.884	-6.915
12.5				0.001	0.003	0.004	-6.188	-5.843	-7.156
16				0.002	0.005	0.007	-6.253	-5.797	-7.464
20				0.004	0.007	0.011	-6.331	-5.775	-7.750
25				0.006	0.011	0.017	-6.429	-5.823	-7.963
31.5				0.009	0.018	0.027	-6.553	-6.065	-7.910
40				0.014	0.028	0.043	-6.699	-6.752	-7.049
50				0.022	0.044	0.066	-6.837	-7.977	-4.360
63				0.034	0.068	0.102	-6.946	-9.587	3.481
80				0.053	0.106	0.160	-6.949	-10.401	10.745
100				0.079	0.159	0.238	-6.728	-8.447	19.786
125				0.116	0.231	0.347	-6.086	-6.443	19.423
160				0.169	0.339	0.508	-4.459	-5.544	18.535
200				0.230	0.461	0.691	-1.431	-4.380	19.083
250				0.301	0.602	0.902	4.732	-3.221	18.988
315				0.380	0.761	1.141	16.218	-1.649	18.027
400				0.467	0.935	1.402	9.036	1.108	17.142

Table J7. Sound attenuation factors for centre frequencies ranging from 8 Hz to 400 Hz during the continued mixed ground measurements.

[Hz]	Geometrical divergence [dB]			Atmospheric absorption [dB/m]			Ground attenuation [dB]		
	200 m	400 m	600 m	200 m	400 m	600 m	200 m	400 m	600 m
500				0.556	1.111	1.667	11.049	5.496	16.846
630				0.663	1.325	1.988	20.702	13.255	16.169
800				0.808	1.615	2.423	7.663	25.246	14.375
1,000				1.001	2.002	3.002	5.895	19.119	12.407
1,250				1.288	2.576	3.863	3.551	13.437	10.435
1,600				1.784	3.567	5.351	0.764	8.960	8.283
2,000				2.490	4.980	7.470	-1.339	5.773	6.368
2,500				3.583	7.167	10.750	-3.082	3.076	4.482
3,150	-56.813	-62.834	-66.356	5.349	10.697	16.046	-4.513	0.644	2.564
4,000				8.224	16.449	24.673	-5.573	-1.555	0.633
5,000				12.385	24.770	37.155	-5.406	-3.319	-1.097
6,300				18.940	37.879	56.819	-3.392	-4.775	-2.771
8,000				29.189	58.378	87.567	6.322	-5.684	-4.295
10,000				43.148	86.297	129.445	0.954	-5.603	-5.395
12,500				62.500	125.000	187.501	-5.618	-3.598	-5.950
16,000				91.109	182.218	273.327	1.211	6.404	-5.348
20,000				123.421	246.841	370.262	-4.236	0.751	-2.248

Table J8. Sound attenuation factors for centre frequencies ranging from 500 Hz to 20,000 Hz during the continued mixed ground measurements.

Sound attenuation caused by geometrical divergence, atmospheric absorption and ground effect calculated for analysis of the *final ground based* measurements.

[Hz]	Geometrical divergence [dB]			Atmospheric absorption [dB/m]			Ground attenuation [dB]		
	100 m	200 m	300 m	100 m	200 m	300 m	100 m	200 m	300 m
6.3				0.000	0.000	0.000	-6.175	-6.258	-6.321
8				0.000	0.000	0.001	-6.230	-6.345	-6.431
10				0.000	0.001	0.001	-6.299	-6.453	-6.569
12.5				0.001	0.001	0.002	-6.387	-6.594	-6.750
16				0.001	0.002	0.003	-6.514	-6.799	-7.015
20				0.001	0.003	0.004	-6.658	-7.039	-7.326
25				0.002	0.004	0.007	-6.833	-7.337	-7.715
31.5				0.004	0.007	0.011	-7.042	-7.706	-8.198
40				0.006	0.011	0.017	-7.268	-8.126	-8.747
50	-50.794	-56.815	-60.337	0.009	0.017	0.026	-7.434	-8.476	-9.193
63				0.014	0.027	0.041	-7.437	-8.581	-9.267
80				0.021	0.043	0.064	-6.948	-7.847	-8.043
100				0.032	0.064	0.096	-5.400	-5.104	-3.600
125				0.048	0.095	0.143	-1.374	2.814	9.870
160				0.071	0.142	0.213	10.523	26.300	37.541
200				0.099	0.198	0.297	25.862	33.643	36.636
250				0.132	0.265	0.397	18.810	24.384	27.755
315				0.172	0.343	0.515	12.748	18.474	21.897
400				0.215	0.430	0.645	8.468	14.194	17.624

Table J9. Sound attenuation factors for centre frequencies ranging from 8 Hz to 400 Hz during the final ground based measurements.

[Hz]	Geometrical divergence [dB]			Atmospheric absorption [dB/m]			Ground attenuation [dB]		
	100 m	200 m	300 m	100 m	200 m	300 m	100 m	200 m	300 m
500	-50.794	-56.815	-60.337	0.258	0.516	0.774	5.375	11.058	14.481
630				0.308	0.616	0.923	2.703	8.306	11.714
800				0.371	0.742	1.113	0.322	5.785	9.167
1,000				0.452	0.903	1.355	-1.622	3.628	6.973
1,250				0.568	1.136	1.703	-3.295	1.615	4.899
1,600				0.766	1.532	2.298	-4.741	-0.462	2.713
2,000				1.047	2.094	3.141	-5.493	-2.188	0.827
2,500				1.482	2.964	4.445	-5.319	-3.720	-0.962
3,150				2.185	4.370	6.555	-3.106	-4.994	-2.677
4,000				3.336	6.671	10.007	7.283	-5.752	-4.224
5,000				5.012	10.025	15.037	0.561	-5.523	-5.330
6,300				7.684	15.368	23.051	-5.568	-3.230	-5.879
8,000				11.936	23.871	35.807	2.005	7.661	-5.236
10,000				17.876	35.752	53.627	-4.358	0.212	-2.061
12,500				26.403	52.806	79.209	5.883	-5.752	15.180
16,000				39.649	79.299	118.948	-3.077	1.999	-2.740
20,000				55.542	111.083	166.625	-4.393	-4.598	-5.759

Table J10. Sound attenuation factors for centre frequencies ranging from 500 Hz to 20,000 Hz during the final ground based measurements.

Sound attenuation caused by geometrical divergence, atmospheric absorption and ground effect calculated for analysis of the *final elevated* measurements.

[Hz]	Geometrical divergence [dB]			Atmospheric absorption [dB/m]			Ground attenuation [dB]		
	103 m	202 m	301 m	103 m	202 m	301 m	103 m	202 m	301 m
6.3	-51.112	-56.921	-60.402	0.000	0.000	0.000	-5.981	-6.062	-6.105
8				0.000	0.001	0.001	-5.965	-6.060	-6.112
10				0.000	0.001	0.001	-5.939	-6.050	-6.110
12.5				0.001	0.001	0.002	-5.894	-6.023	-6.091
16				0.001	0.002	0.003	-5.811	-5.963	-6.033
20				0.002	0.003	0.005	-5.687	-5.862	-5.925
25				0.003	0.005	0.007	-5.490	-5.691	-5.732
31.5				0.004	0.008	0.012	-5.163	-5.399	-5.393
40				0.006	0.012	0.019	-4.614	-4.909	-4.827
50				0.010	0.019	0.029	-3.780	-4.198	-4.047
63				0.015	0.030	0.045	-2.350	-3.101	-2.963
80				0.024	0.047	0.071	0.299	-2.030	-1.649
100				0.036	0.071	0.106	5.386	0.259	0.816
125				0.054	0.105	0.157	15.523	3.996	4.332
160				0.081	0.158	0.235	2.479	11.030	10.412
200				0.112	0.219	0.328	-2.472	7.145	10.852
250				0.151	0.294	0.439	-4.350	1.009	4.226
315				0.195	0.381	0.569	-2.920	-2.615	-0.190
400				0.245	0.478	0.714	6.248	-4.344	-3.053

Table J11. Sound attenuation factors for centre frequencies ranging from 8 Hz to 400 Hz during the final elevated measurements.

[Hz]	Geometrical divergence [dB]			Atmospheric absorption [dB/m]			Ground attenuation [dB]		
	103 m	202 m	301 m	103 m	202 m	301 m	103 m	202 m	301 m
500	-51.112	-56.921	-60.402	0.294	0.573	0.856	-1.599	-3.791	-4.571
630				0.349	0.682	1.018	-2.214	1.491	-4.700
800				0.420	0.819	1.223	0.094	3.436	-2.008
1,000				0.508	0.992	1.481	0.676	-4.288	9.760
1,250				0.636	1.241	1.853	-3.210	0.452	-1.105
1,600				0.853	1.665	2.486	-2.969	-3.607	-4.744
2,000				1.160	2.265	3.381	-0.164	8.555	12.444
2,500				1.635	3.192	4.766	-0.926	-2.539	-5.028
3,150				2.404	4.692	7.005	1.541	-2.984	1.940
4,000				3.661	7.145	10.669	-2.666	9.414	13.670
5,000				5.492	10.721	16.006	-3.347	-4.623	13.843
6,300				8.409	16.414	24.508	-2.969	-4.389	-3.416
8,000				13.050	25.473	38.033	-2.658	9.203	13.719
10,000				19.530	38.121	56.916	0.572	8.838	13.319
12,500				28.823	56.260	84.000	-3.699	-2.998	-5.130
16,000				43.237	84.396	126.009	-1.766	7.401	11.536
20,000				60.494	118.080	176.300	-3.387	6.378	10.260

Table J12. Sound attenuation factors for centre frequencies ranging from 500 Hz to 20,000 Hz during the continued elevated measurements.

Appendix K: ISO 9613-2 ground attenuation

Formulas for calculating the ground attenuation each of the three surface regions identified between the sound source and receiver, according to the ISO 9613-2 prediction method [38].

Nominal midband frequency [Hz]	A_s or A_r [dB]	A_m [dB]
63	-1.5	$-3q$
125	$-1.5 + G \times a'(h)$	$-3q(1 - G_m)$
250	$-1.5 + G \times b'(h)$	
500	$-1.5 + G \times c'(h)$	
1000	$-1.5 + G \times d'(h)$	
2000	$-1.5(1 - G)$	
4000	$-1.5(1 - G)$	
8000	$-1.5(1 - G)$	

NOTES

$$a'(h) = 1.5 + 3.0 \times e^{-0.12(h-5)^2}\left(1 - e^{-d_p/50}\right) + 5.7 \times e^{-0.09h^2}\left(1 - e^{-2.8\times10^{-6}\times d_p{}^2}\right)$$
$$b'(h) = 1.5 + 8.6 \times e^{-0.09h^2}\left(1 - e^{-d_p/50}\right)$$
$$c'(h) = 1.5 + 14.0 \times e^{-0.46h^2}\left(1 - e^{-d_p/50}\right)$$
$$d(h) = 1.5 + 5.0 \times e^{-0.9h^2}\left(1 - e^{-d_p/50}\right)$$

1) For calculating A_s, take $G = G_s$ and $h = h_s$. For calculating A_r, take $G = G_r$ and $h = h_r$.

2) $q = 0$ when $d_p \leq 30(h_s + h_r)$

$$q = 1 - \frac{30(h_s + h_r)}{d_p} \text{ when } d_p > 30(h_s + h_r)$$

Table K1. Ground attenuation calculation formulas in the ISO 9613-2 model.

Appendix L: Nord2000 scattering zones

Scattering zone attenuation table, used to calculate ΔL (h’, α, R’) within the level correction due to scattering equation (5.19) [24].

R’	h’ = 0.01			h’ = 0.1			h’ = 1		
	α = 0	α = 0.2	α = 0.4	α = 0	α = 0.2	α = 0.4	α = 0	α = 0.2	α = 0.4
0.0625	6.0	6.0	6.0	6.0	6.0	6.0	6.0	6.0	6.0
0.125	0.0	0.0	0.0	0.0	0.0	0.0	0.0	0.0	0.0
0.25	– 7.5	– 7.5	– 7.5	– 6.0	– 7.0	– 7.5	– 6.0	– 7.0	– 7.5
0.5	– 14.0	– 14.25	– 14.5	– 12.5	– 13.5	– 14.5	– 12.5	– 13.0	– 14.0
0.75	– 18.0	– 18.8	– 19.5	– 17.3	– 18.0	– 19.0	– 16.0	– 16.8	– 17.7
1	– 21.5	– 22.5	– 23.5	– 20.5	– 21.6	–22.8	– 19.3	– 20.5	– 21.3
1.5	– 26.3	– 27.5	– 29.5	– 25.5	– 27.2	– 29.0	– 24.0	– 25.5	– 26.3
2	– 31.0	– 32.5	– 34.5	– 30.0	– 32.0	– 33.3	– 27.5	– 29.5	– 30.8
3	– 40.0	– 42.5	– 45.5	– 37.5	– 40.5	– 42.9	– 34.2	– 36.0	– 37.8
4	– 49.5	– 52.5	– 56.3	– 45.5	– 49.5	– 52.5	– 40.4	– 42.8	– 45.5
6	– 67.0	– 72.5	– 78.0	– 62.0	– 67.0	– 72.0	– 52.5	– 56.2	– 60.0
10	– 102.5	– 113.0	– 122.5	– 94.7	– 103.7	– 112.0	– 78.8	– 84.0	– 89.7

Tri-cubic interpolation is performed according to the following steps:

1) From $\Delta L\,(h'_i, \alpha_j, R'_k)$ interpolate in h’ for each (α_j, R'_k) to get $\Delta L\,(h', \alpha_j, R'_k)$.
2) From $\Delta L\,(h', \alpha_j, R'_k)$ interpolate in α for each R'_k to get $\Delta L\,(h', \alpha, R'_k)$.
3) From $\Delta L\,(h', \alpha, R'_k)$ interpolate in R’ to get ΔL (h’, α, R’).

Table L1. Calculation of scattering zones in the Nord2000 model.

Appendix M: Distribution of labour

M.1 Distribution of work between final thesis students

During the course of a thesis project it important that all work is distributed equally between each student involved in the venture. The thesis presented in this report was however conducted by a single student and all tasks were thus performed by that individual alone.

M.2 Assumed timetable and actual outcomes

The management of a final thesis is much facilitated by construction of a timetable. Abiding to such a schedule may however prove difficult as the project progresses. Some part of the project included in the plan may for instance require more time than was initially expected. The thesis students may also encounter work tasks not anticipated during the planning of the project. These factors can cause a delay of the project, how much depends of the extent of the obstacle.

Table M1 below shows the timetable made at the beginning of this project. As may be seen, the table merely include mayor parts of the project, all of which were explained in section 1.3.

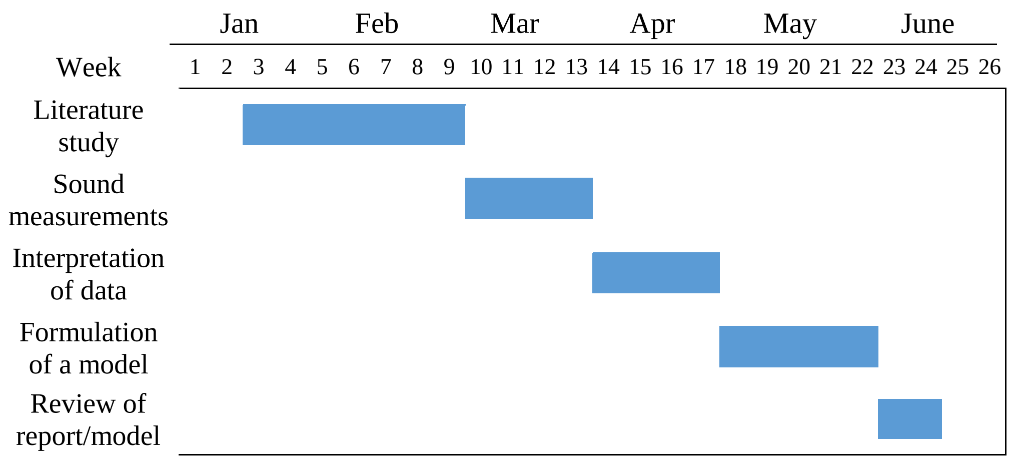

Table M1. Assumed timetable of project.

The initial timeframe of the entire project was 20 weeks, although an additional two week of work was included at the end of the schedule for unexpected tasks such as completion of the report as well as a detailed review of the calculation model. Due to the large scale of the literature study, this part of the project was projected to cover a total of 7 weeks. All attenuation factors, such as air absorption and ground effect, were also to be implemented in Excel during this period in order to simplify the development of the model. The time required for noise measurements was difficult to plan at an early stage, since neither a suitable location nor the necessary equipment had been located at that stage. It was hoped that a total of 11 days of measurements could be performed, however this would be subject to equipment availability. Interpretation of data was expected to take roughly 4 weeks, while assembling of all formulas and development of a model interface was to be completed in 5 weeks.

Implementation of the initial timetable proved much more difficult than was expected. As may be seen in table M2 below the project was severely delayed, for which the reason were many.

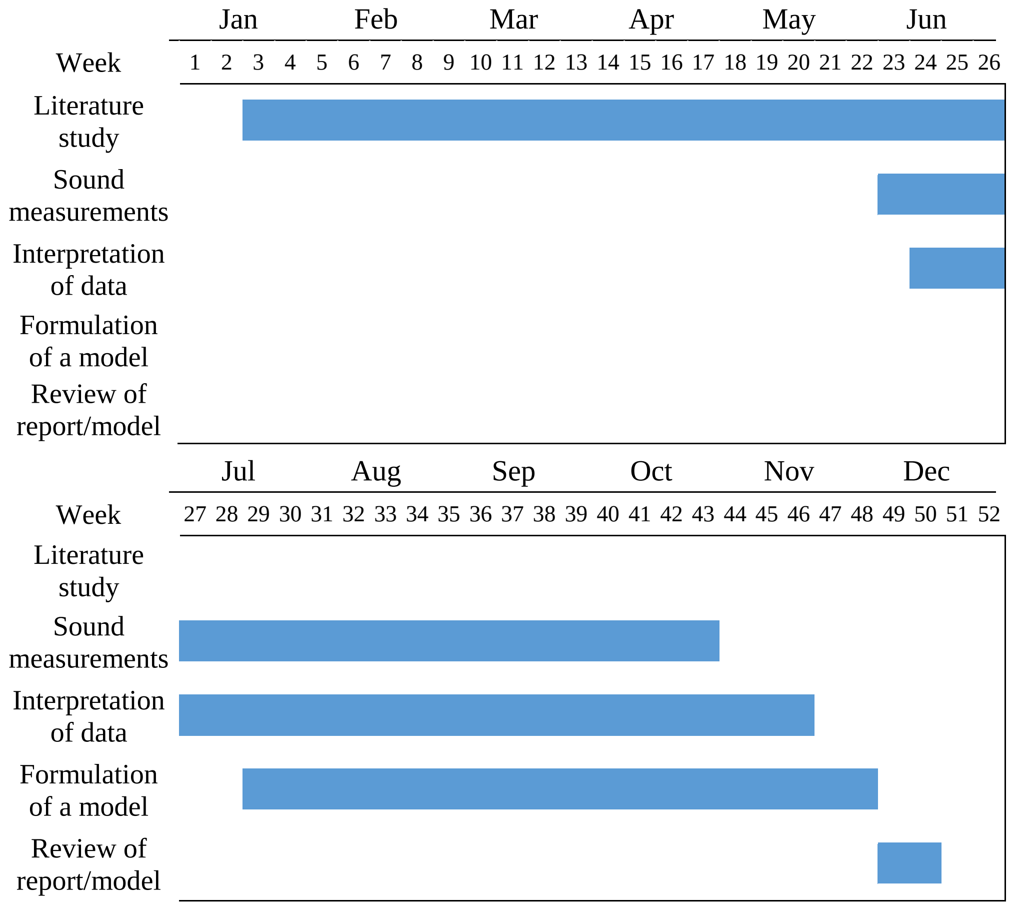

Table M2. Actual timetable of project.

A major issue was locating and organizing various permits for a site that fulfilled all requirements for noise testing. Finding a suitable site had not been included in the initial schedule and this element therefore resulted in a major delay of the project. All sound measuring equipment necessary for the project was kindly lent out by Marshall Day, an acoustic consultancy in Melbourne. Noise measurement excursions were thus dependent on the availability of this equipment, which also caused some delays. Furthermore, organizing the use of a lift, which could both be transported to a remote site and provide sufficient height, proved to be a difficult and lengthy process not anticipated in the initial timetable.

Since the sound measurements were performed over a long period, the interpretation of data and construction of a calculation model were commenced before all measurement had been conducted. Both these part also proved more time demanding than expected.

The literature study became a much more extensive part of the project than was anticipated. As the project progressed many areas of acoustics that had previously not been considered were deemed necessary for the work and thus comprised in the project. An example includes implementation of noise restrictions.

Appendix N: Model interface

An overview of the noise prediction model interface may be viewed in figures N1 and N2 on the following pages.

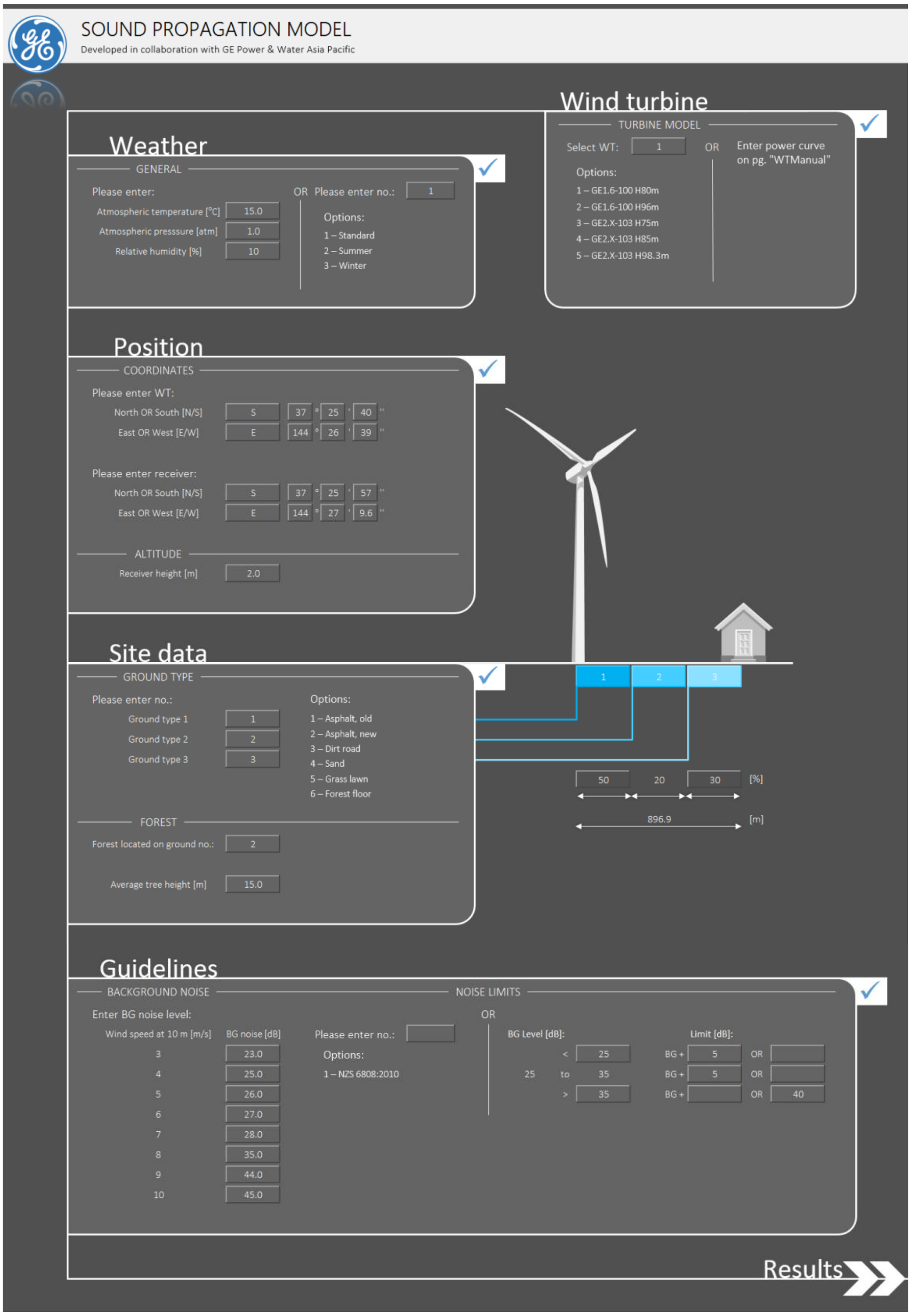

Figure N1. The data input interface of the developed calculation model.

Figure N2. The result interface of the developed calculation model.